DETERMINATION OF AMERICAN PETROLEUM INSTITUTE GRAVITY OF PETROLEUM IN THE ROCK USING PYROLYSIS

by

Dhrupad Raghuveer Beti

A thesis submitted to the faculty of
The University of Utah
in partial fulfillment of the requirements for the degree of

Master of Science

in

Petroleum Engineering

Department of Chemical Engineering

The University of Utah

August 2016

The University of Utah Graduate School

STATEMENT OF THESIS APPROVAL

The thesis of **Dhrupad Raghuveer Beti**

has been approved by the following supervisory committee members:

David J. Thul	, Chair	**2/23/16** Date Approved
John McLennan	, Member	**2/23/16** Date Approved
Terry Ring	, Member	**2/23/16** Date Approved

and by **Milind Deo** , Chair/Dean of

the Department/College/School of **Chemical Engineering**

and by David B. Kieda, Dean of The Graduate School.

ABSTRACT

Oil and gas industry is one of the most crucial industries powering the modern world. Billions of dollars have been invested into the science of petroleum extraction. Yet, due to the constraints of sample collection, very few techniques for in-situ petroleum quality assignment exist. This study develops a method of economic and efficient characterization of in-situ petroleum. The pyrolysis machine HAWK™ is used to build a temperature-based method to understand the hydrocarbon molecules using their boiling points. A set of experiments and simulations were performed on a suite of rocks to build a novel technology to predict American Petroleum Institute (API) gravity of petroleum in the rocks. Simulations of the experiments were also performed. These simulations were used to understand and highlight different relationships between oil densities and their boiling points. In this study, while a correlation between density and boiling point of hydrocarbon molecules was observed, prediction of API gravity strictly with boiling point data turned out to be inadequate. Fortunately, the refractive index was found to be the parameter bridging the gap between experimental values of boiling points of residual petroleum in the rock and density.

TABLE OF CONTENTS

LIST OF FIGURES

Figures

LIST OF TABLES

Tables

NOMENCLATURE

FID - Flame Ionization Detector

FTIR - Fourier Transform Infrared Spectroscopy

HI - Hydrogen Index

IR - Infrared

IS1 - Incremental S1

MS - Mass Spectroscopy

OI - Oxygen Index

POPI - Pyrolytic Oil Productivity Index

PI - Production Index

S1 - Free Petroleum Content (mg of HC/g of rock)

S1_1 - Free Petroleum Released at 50°C (mg of HC/g of Rock)

S1_2 - Free Petroleum Released at 100°C (mg of HC/g of Rock)

S1_3 - Free Petroleum Released at 150°C (mg of HC/g of Rock)

S1_4 - Free Petroleum Released at 200°C (mg of HC/g of Rock)

S1_5 - Free Petroleum Released at 250°C (mg of HC/g of Rock)

S1_6 - Free Petroleum Released at 300°C (mg of HC/g of Rock)

S2 - Kerogen Content (mg of HC/g of rock)

S3 - Carbon Dioxide and Carbon Monoxide Released During Pyrolysis (mg of CO2 or CO /g of rock)

S4 - Residual Carbon Dioxide and Carbon Monoxide Released During Oxidation (mg of CO2 or CO /g of rock)

S5 - Mineral Carbon Dioxide and Carbon Monoxide Released During Oxidation (mg of CO2 or CO /g of rock)

Tα- Summation of Product of Temperature and Molar Flow Values (°C)

TGA - Thermal Gravimetric Analysis

T max - Maximum temperature of S2 release (°C)

Tmean - Mean Temperature Value of a Normal Distribution Fit (°C)

TOC - Total Organic Carbon (%)

V_1 - Molar flow (Kmol/min) of ProMax Simulation Result at 50°C

V_2 - Molar flow (Kmol/min) of ProMax Simulation Result at 50°C

V_3 - Molar flow (Kmol/min) of ProMax Simulation Result at 510°C

V_4 - Molar flow (Kmol/min) of ProMax Simulation Result at 200°C

V_5 - Molar flow (Kmol/min) of ProMax Simulation Result at 250°C

V_6 - Molar flow (Kmol/min) of ProMax Simulation Result at 300°C

ACKNOWLEDGEMENTS

First of all, I am extremely grateful to David J. Thul for acting as my primary adviser, chair of my supervisory committee, and for employing me as a graduate research assistant at EGI. I thank him for his research advice, and his encouragement throughout my research. I would like to thank Dr. Raymond Levey and EGI for employing me throughout my graduate school. I would like to especially thank Dr. John McLennan for his advice and support throughout my academic, research, and personal life for the last two years. I thank Dr. Terry Ring for enlightening me with all his guidance in my research and personal life. I thank him for introducing me to all the chemical engineering tools and software used in this work. I especially thank him for all his enthusiasm and interest in helping me with my research. I thank Dr. Palash Panja for all his timely personal and academic advice and help in my research. I thank Kali Blevins for all her insight and help on the programing side of this research. I am thankful to all the faculty and staff of the Petroleum Engineering program for their support. I thank Robert Cox, Dina, Ding, Shae, and Richard for helping me in my experimentations. I would like to thank David Weldon for helping in the maintenance of the HAWK. I would like to thank my colleagues and classmates Abdul, Bill, Nikolaja, Rand, Manas, and Andrew for making the school and workplace friendly and productive. I would like to thank both Jessica Page and Kali for their help in editing my thesis. Lastly, I would like to thank my family for all their love, support, and encouragement in my life so far.

CHAPTER 1

INTRODUCTION

Oil and gas has long proven to be one of the most crucial parts of the energy sector. Since its discovery in the 19th century, the utility of this commodity has changed drastically. Operators have gone from primary production in the early days to present-day enhanced oil recovery and well stimulation practices like hydraulic fracturing. With a continuing global increase in petroleum consumption, mainly driven by growing economies and global population increase, efficient extraction of oil and gas is critical for global stability. Despite growing demand and increase in consumption, oil and gas prices have shown to be volatile. This volatility, consequently, has affected the capital-intensive exploration activity of energy companies. The increase in production of oil and gas has mainly been a function of new and advanced technology used to tap the resources. However, these technologies are often expensive, and economic justification of using advanced technology is largely dictated by the oil and gas market prices. When market price is low and expensive technology is required to tap the resources, an efficient exploration and production strategy is key. This thesis is an attempt to better understand petroleum systems in-situ by analyzing the source and reservoir rock, using a novel, effective, and economical technology based on advancements in petroleum geochemistry. Utilizing this technology will enable petroleum engineers and geologist to find and extract oil and gas efficiently. This technology is equally applicable and useful for academia and practical industrial application.

1.1. Objectives

Hydrocarbon generation potential, free petroleum content, kerogen content, total organic carbon, and thermal maturity are some of the key parameters analyzed in a rock by petroleum geochemists to understand the petroleum system. Source rock pyrolysis is a basic method used to produce these parameters. HAWK ™ (Hydrocarbon Analysis With Kinetics) is a third-generation instrument used to perform anhydrous pyrolysis, and all the pyrolysis experiments in this work were performed using the HAWK ™. The primary objective of this work is developing a novel incremental pyrolysis method to analyze rocks for petroleum, by using the HAWK ™ instrument. Incremental pyrolysis of a source or reservoir rock results in a release of petroleum compounds. The fractional production of these hydrocarbons as a result of thermal distillation is processed numerically to predict the American Petroleum Institute (API) gravity of the oil that is present in the rock matrix.

CHAPTER 2

PETROLEUM GEOCHEMISTRY AND PYROLYSIS

Traditionally, petroleum geochemists have studied the origin, generation, migration, and accumulation of oil and gas from a geological standpoint. According to Bordenave (1993), it was not until the last few decades that advanced studies have been performed in the area of petroleum systems analysis. A petroleum geochemist's area of research is mainly focused on petroleum systems analysis. The essential parameters to understanding a petroleum system are obtained by performing compositional analysis of petroleum, source rock analysis, evaluation of hydrocarbon generation potential, biomarkers analysis, and analyzing free petroleum and kerogen in the rock. There are several experimental methods and techniques used to obtain data in order to perform a petroleum system analysis, some of the widely used techniques are solvent extraction, gas chromatography of oils and gases, as well as anhydrous and hydrous pyrolysis.

2.1. Petroleum Systems

Magoon and Dow (1994) state that petroleum systems can be explained through a collection of elements and processes. These elements are source rock, reservoir rock, seal rock or cap rock and overburden rock, and the processes include generation, migration, and accumulation of petroleum. While these processes occur, the elements must coexist in time and space to have an effective petroleum system.

2.2. Source Rock Pyrolysis

Anhydrous pyrolysis, most commonly referred to as source rock pyrolysis in petroleum geology is one of the essential techniques used to determine the kerogen content, kerogen type, source rock maturity, total organic carbon (TOC), and free petroleum content in source and reservoir rocks. The instruments used by petroleum geochemists to perform pyrolysis are HAWK ™ (Hydrocarbon Analysis With Kinetics), Rock-Eval®, and SRA™. The principles and methodology of source rock pyrolysis are explained in the following section.

2.2.1. Principle

The use of pyrolysis and oxidation to understand source rock, kerogen, and petroleum were first introduced by Espitalié et al. (1977). The working principle and applications of Rock-Eval ® were later discussed in studies such as (Espitalié et al. 1985, 1986a, 1986b; Bordenave 1993; Lafargue et al. 1998). Over the ensuing decades, anhydrous pyrolysis instruments have undergone many technical improvements. The latest version, HAWK ™, is a third-generation pyrolysis instrument. Although some technological and engineering advancements been made in the functionality and operation of the HAWK™, the basic principles are the same as Rock-Eval®. The process flow schematic of the HAWK™ is shown in Figure 2.1. Three primary parameters are measured with this instrument: the concentration of organic compounds using a flame ionization detector (FID), and the concentrations of carbon dioxide and carbon monoxide using two infrared (IR) detectors. These parameters are measured as a function of carrier gas, time, and temperature at atmospheric pressure conditions. Pyrolysis and oxidation are the two generic functional modes used in these instruments. In general, samples are pyrolyzed prior to oxidation, pyrolysis is performed in inert atmosphere, and oxidation is performed in oxidizing atmosphere. There are several temperature profiles used in all the three instruments; one of the most commonly used and widely accepted methods is PyroS3650_TOC750 (shown in Figure 2.2). This method has two parts,

at first, in pyrolysis, the oven temperature profile is at 100°C with an initial purge time of 5 minutes, then the sample is introduced in the oven and is subjected to a 3-minute initial pyrolysis isotherm followed by a temperature increase at a rate of 25°C/min to a maximum of 600°C. The second part of the method is oxidation, where the oven temperature profile starts from 300°C and increases at a rate of 25°C/min to a maximum of 750°C followed by a final 5-minute isotherm at 750°C.

In pyrolysis mode, as shown in Figure 2.1, Helium gas (or any inert gas) is sent in as a carrier gas at a flow rate of 100 ml/min; the gas passes through the pedestal and then sweeps the sample gas through the sample crucible which is placed in the oven. This gas is then sent to an FID to detect the quantity of sample ionised in the hydrogen flame. Simultaneously, a split flow rate of 40 ml/min is continuously sampled and sent to a moisture trap, followed by a filter, and then to infrared detectors to detect the amount of carbon dioxide and carbon monoxide present in the sample. In oxidation mode, intending to create an oxidizing environment, air is sent in as carrier gas at a flow rate of 250 ml/min. Now that the sample has already undergone pyrolysis, only two of the IR detectors are used in the oxidation mode. The two way split is again used to sweep a portion of gas at a flow rate of 50 ml/min as exhaust from the oven. This gas is sent to the IR detectors to detect the concentrations of carbon dioxide and carbon monoxide, respectively.

2.2.2. Methodology

In Espitalié et al. (1977, 1985a, 1985b, 1986), the raw signals from three detectors are recorded and a set of parameters are calculated. The measurement of these parameters from the FID and IR detectors are a function of temperature and time. These parameters are then arranged in plots, templates, and used in formulas to understand the organic compounds (oil, kerogen) in the rock.

As shown in Figure 2.3, the FID signal is studied in two sections, S1 and S2. The first peak, which is the area under the curve of the FID signal from 100°C to 300 °C for an initial isotherm

time of 3 minutes is considered to be S1. Conventionally, this peak is considered indicative of the quantity of free petroleum present in the rock sample at the time of analysis. The second peak, S2, is measured from 300 °C to 650 °C as the sample is heated at a rate of 25 °C/min. This is considered as an indication of the kerogen content of the sample. Both S1 and S2 have units of milligrams of hydrocarbons per gram of rock (mg of HC/g of rock). The signals from the carbon dioxide and carbon monoxide IR cells are recorded as S3, S4, and S5, respectively (Figure 2.3). The CO_2 and CO released in the pyrolysis stage are a result of decomposition of organic matter and are indicated by S3. CO_2 and CO released during oxidation are a result of decomposition of inorganic matter and are indicated by S4 and S5, respectively. The temperature at which maximum generation of the peak S2 (kerogen content) is achieved is denoted as Tmax; this is an indication of the maturity of kerogen in the sample; maturity of the source rock increases with increase in the value of Tmax. A set of standards with known quantities of S1, S2, S3, S4, S5, and Tmax are used to calibrate and calculate the values of every new unknown sample.

TOC (total organic carbon) analysis is performed in two ways; the first method is combustion of organic matter in the presence of air at 1500°C (Leco induction oven) and the second is using Rock-Eval pyrolysis or source rock pyrolysis. In each method and instrument, TOC is calculated in weight percent and it is a function of free petroleum content, kerogen content, and carbon content inferred by release of CO2 and CO at the time of oxidation (Bordenave 1993, 235-245). TOC is calculated using the following equation.

$$TOC\ (wt\ \%) = [0.085(S1 + S2)] + [0.10(S4)] \quad . \quad (1)$$

S1, S2, and S4 are measured in parts per thousand (mg/g). According to Jarvie and Baker, (1984) the first part of equation (1) involving S1 and S2 accounts for the percent of carbon released as a result of thermal decomposition of petroleum and kerogen. The second term accounts for any carbon remaining after pyrolysis, which results in conversion to carbon dioxide and carbon monoxide.

Espitalié et al. (1977, 1985, 1986a, 1986b) have developed a set of interpretive parameters called HI (hydrogen index), OI (oxygen index), and PI (production index). Hydrogen index is the ratio of kerogen content to total organic carbon, given as follows

$$HI = S2/TOC, \text{ mg of HC/g of TOC} \quad (2)$$

By dividing the kerogen content by the total organic carbon in equation (2), organic carbon is removed from the kerogen content, resulting in an estimation of hydrogen associated with the unconverted petroleum (note that S1 is not included) in the sample. The oxygen index is defined as the ratio of S3 to TOC.

$$OI = S3/TOC, \text{ mg of } CO_2/\text{g of TOC} \quad (3)$$

Similar to the hydrogen index, the estimation of oxygen is inferred by an attempt to cancel out the organic carbon content from the S3. In addition, the production index, PI, is defined as the ratio of the amount of free petroleum divided by the total amount of hydrocarbon (includes mature and immature). PI is usually used as an indication of thermal maturity; the value of PI increases with an increase in maturity of the rock. This value lies between zero and one and has no units, as shown in equation (4).

$$PI = S1 / (S1+S2) \quad (4)$$

In Bordenave (1993, 251-255), the type of kerogen and the thermal maturity of the source rock are inferred by two important plots. The type of kerogen is determined by the HI versus OI plot, as shown in Figure 2.4. The type of kerogen is a function of depositional conditions of the source rock. The depositional conditions are indicated by hydrogen and oxygen content of a sample (Figure 2.4). The thermal maturity of the source is determined by plotting HI versus Tmax, as shown in Figure 2.5. For all kerogen types, with an increase in maturity, the Tmax value increases, and the HI value decreases.

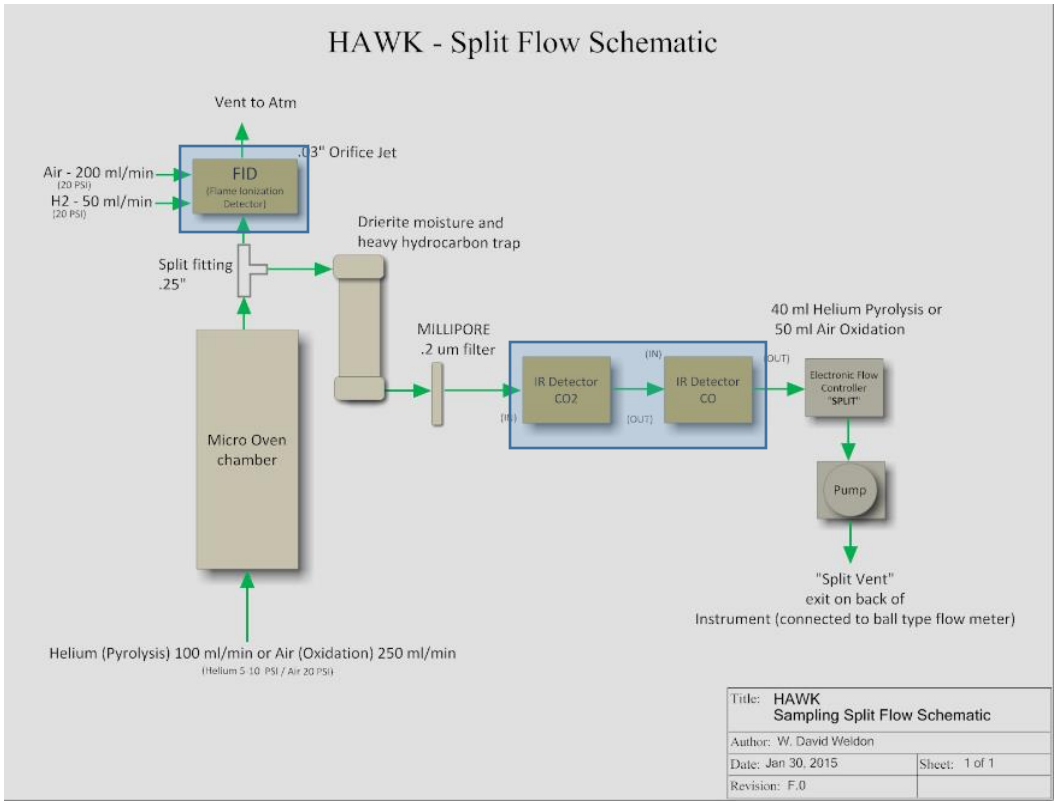

Figure 2.1: Process flow of HAWK ™, showing the conditions of the micro oven in pyrolysis versus oxidation, and gas flow schematic - modified from HAWK Workstation manual.

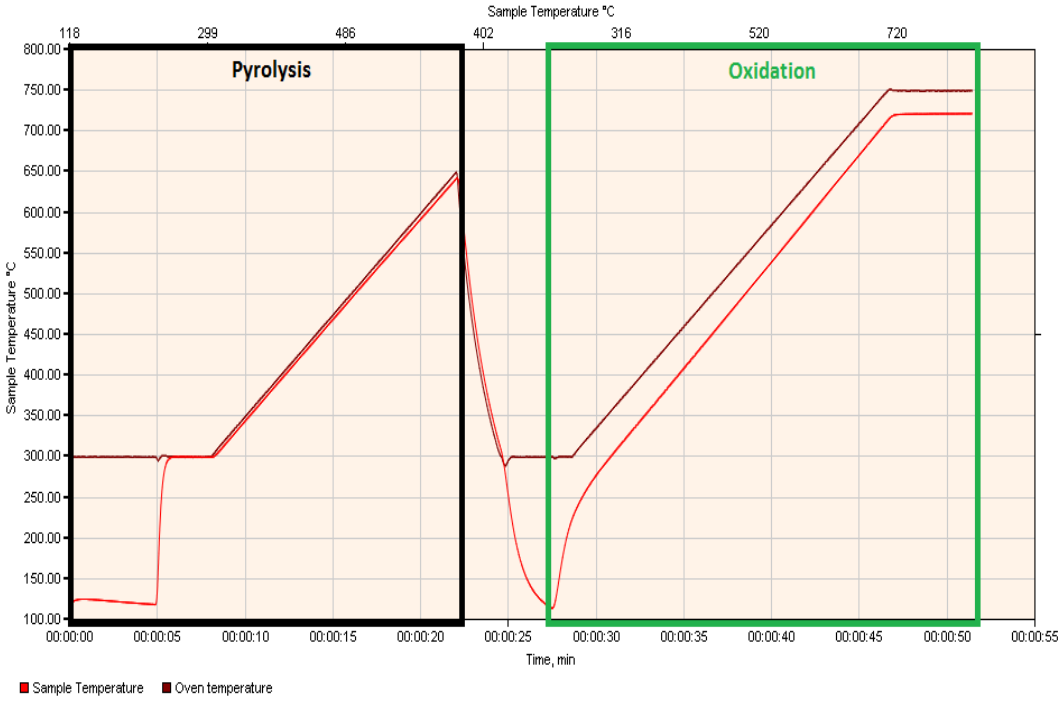

Figure 2.2: Method PyroS3650_TOC750 showing the oven and sample temperature profile versus time for pyrolysis and oxidation - modified from Hawk software.

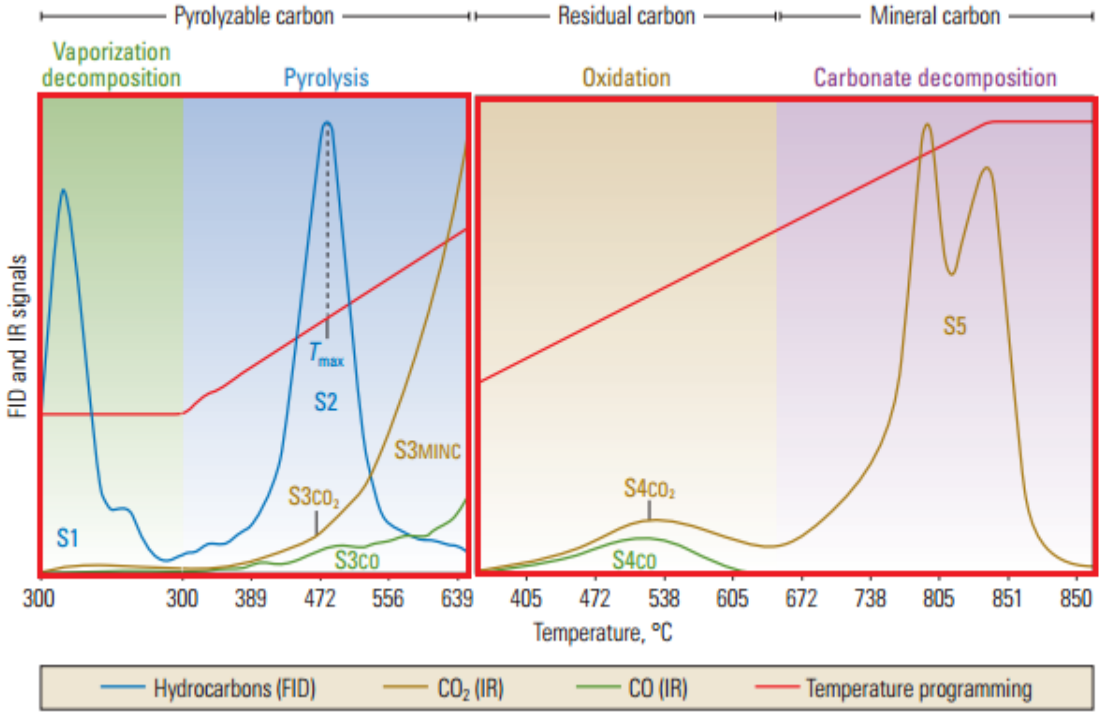

Figure 2.3: FID and IR signals of a sample in the temperature method PyroS3650_TOC750, showing the assigned S1, S2, S3, S4, and S5 parameters as a function of temperature - modified from SLB (2011).

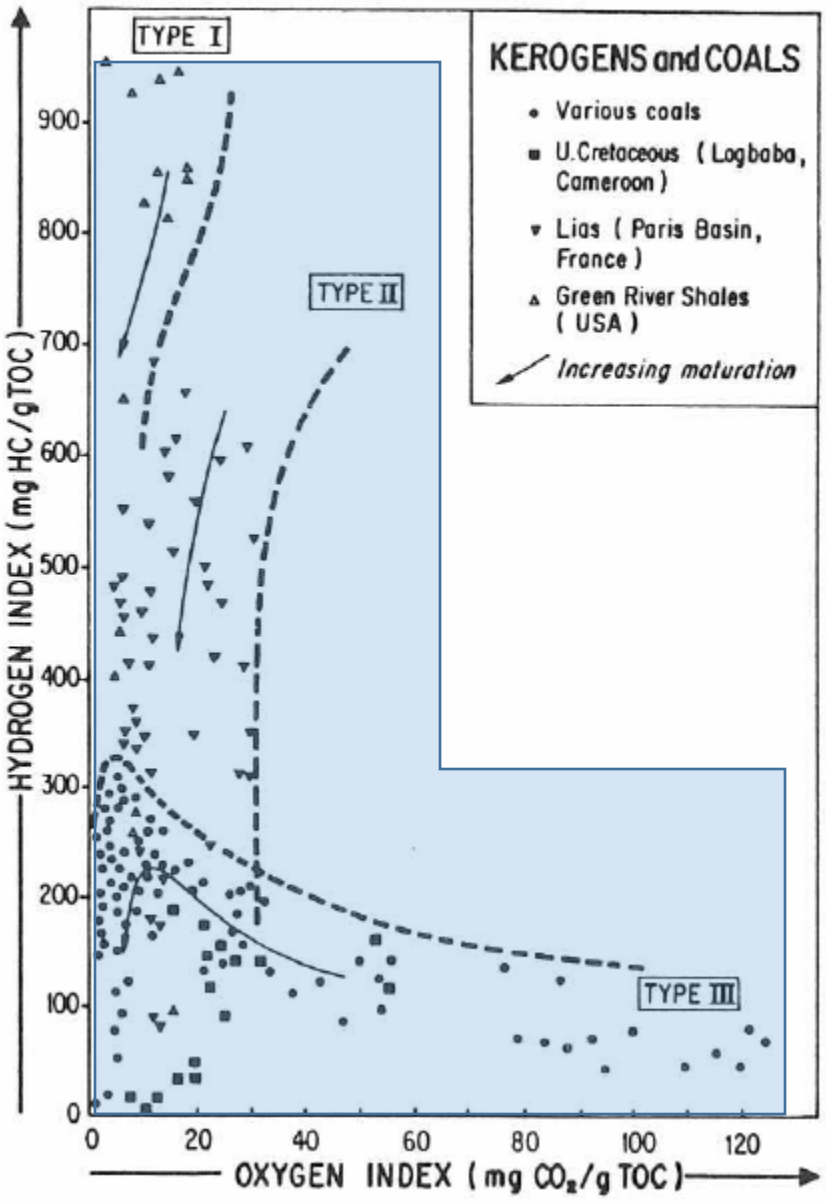

Figure 2.4: Van Krevelen diagram, plotting HI versus OI with different areas showing kerogen types – modified from Bordenave (1993).

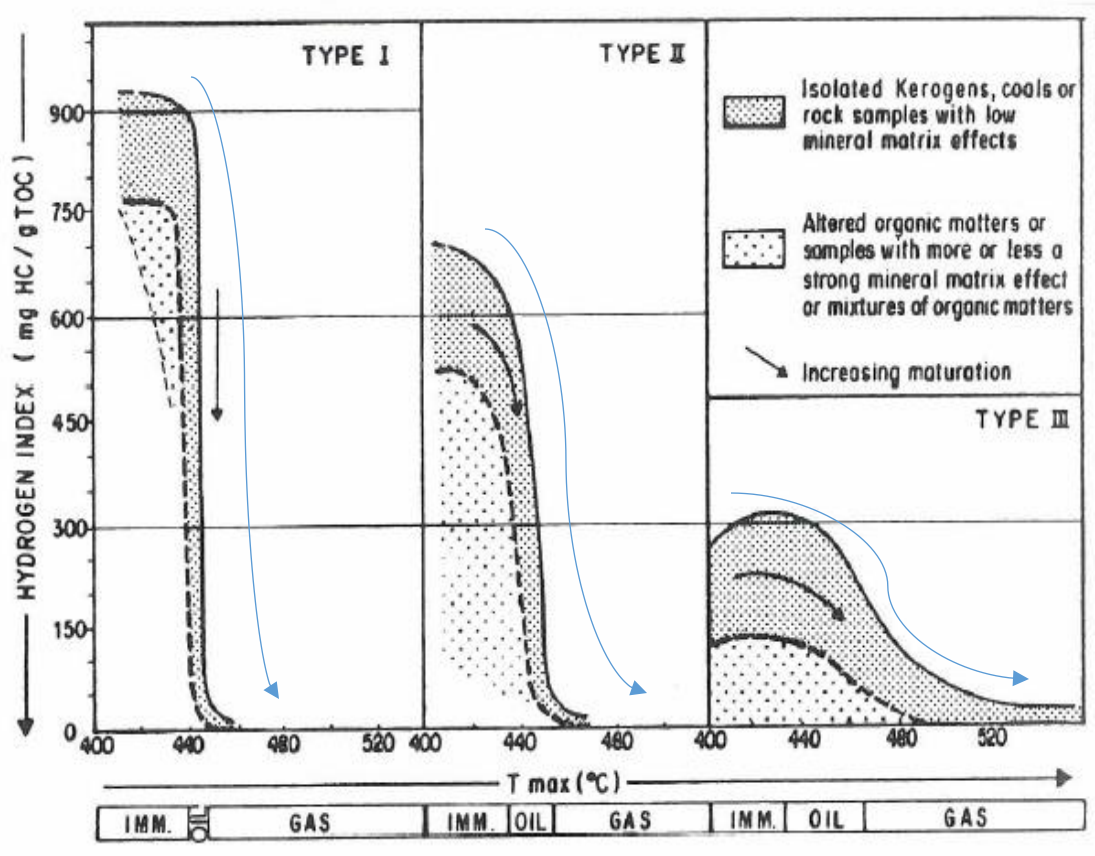

Figure 2.5 Van Krevelen diagram, plotting HI versus OI of kerogen types I, II, and III – modified from Bordenave (1993).

CHAPTER 3

API GRAVITY THROUGH SOURCE ROCK PYROLYSIS

API gravity is a function of specific gravity and hence a function of density. Average boiling point of oil is a function of density to a certain extent (James 2006).

$$API\ Gravity = \left(\frac{141.5}{specific\ gravity^{\frac{15.6}{15.6}°C}}\right) - 131 \quad (5)$$

One of the primary goals of this work is to build a relationship between experimentally acquired boiling points of the oil present in a rock in order to find the API gravity of petroleum. Source rock pyrolysis is used to determine the boiling points. After a number of tests performed with various temperature profiles on the HAWK ™, the most convenient and feasible temperature method was selected (explained in Chapter 4). This method is the first of its kind. It is designed to measure the fraction of petroleum evaporating at or below 300°C. As mentioned in Chapter 2, conventionally, the FID signal measured at the temperature range of 100°C - 300°C is considered free petroleum (S1). The method described here incorporates a temperature profile starting from 50°C to 300°C, with incremental steps allowing thermal distillation of the sample. The fractions of sample evaporated at different temperature plateaus (isotherms) is analyzed to build an average boiling point - API gravity relationship.

Changing the temperature profile of the method to perform source rock pyrolysis is not a conventional practice. Every time an experiment of this sort is performed, the functionality of oven temperature control in the pyrolysis machines must be altered. Therefore, all the experimentation in this work were performed by altering functions of the machine. Very few similar studies have

been performed in the past; amongst them are some patents (Jones and Mark 1999; Jones et al. 2004; Jones and Halpern 2008, 2009, 2014). In the first patent (Jones and Mark 1999), a pyrolytic oil productivity index (POPI) was created to characterize the reservoir rock. The pyrolytic oil productive index is calculated using an oven temperature profile of an initial temperature isotherm of 180°C, followed by an increase in temperature untill 600°C at a rate of 25°C per minute (shown in Figure 3.1). The FID signal is recorded as a function of temperature and assigned three different parameters (light volatile hydrocarbons, thermally distilled hydrocarbons, and thermally cracked hydrocarbons). These parameters are then used to calculate the pyrolytic oil productive index. This technique has been used to infer the location of bits during directional drilling. Cuttings from different locations were analyzed to check for oil content to estimate the location of the drill bit in the reservoir rock. Later, the method with the same temperature profile (POPI) was used in predicting reservoir rock and oil characteristics (Jones et al. 2004). In the past few years, the POPI method was used to perform compositional modeling, to determine the volume of organic matter, and to determine the total organic content (Jones and Halpern 2008, 2009, 2014).. None of the above-mentioned studies are similar to the method or experimentation performed in this work.

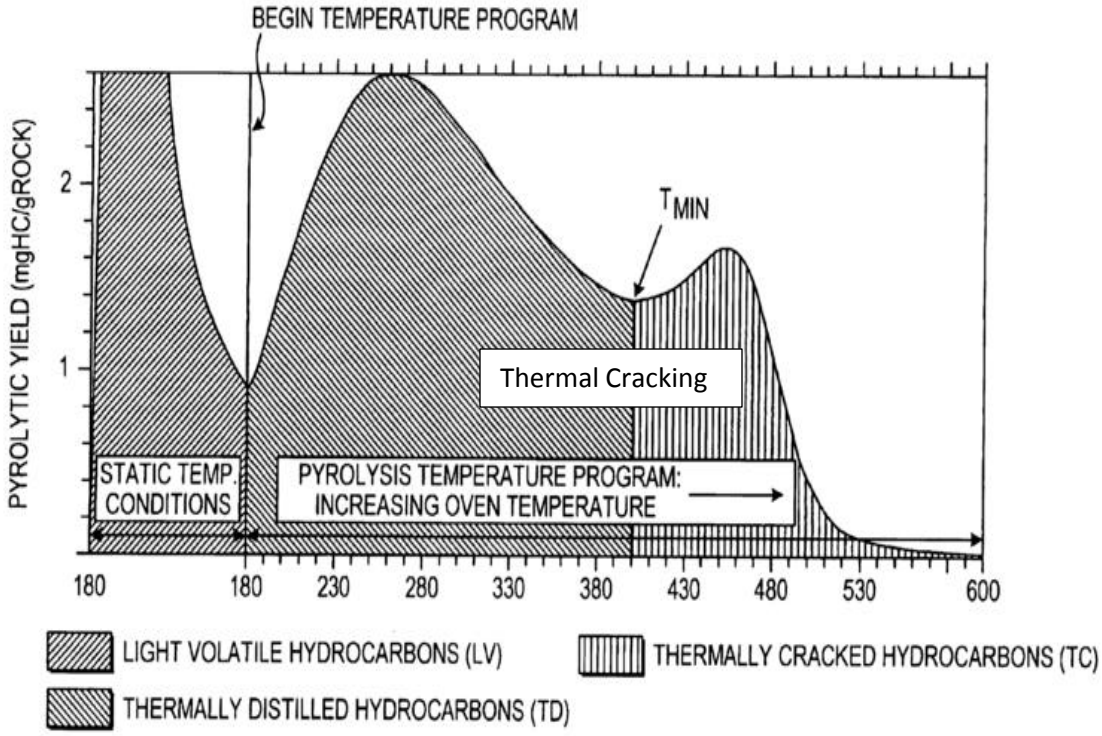

Figure 3.1: POPI temperature profile, light volatile, thermally distilled and thermally cracked hydrocarbons, indicated as a function of pyrolytic yield and temperature (°C) in the POPI method – modified from (Jones and Mark 1999).

CHAPTER 4

EXPERIMENTATION AND SIMULATIONS

This chapter is a discussion of the experimentation and simulations performed, in order to develop an analytical tool to predict the API gravity. After a number of trial and error experiments, a suitable HAWK temperature profile (Incremental S1 method) was selected.

4.1. Experimentation to Development of the IS1 Method

There were several experiments performed on the HAWK™ by altering the temperature method. This section is a discussion of a series of experiments performed to develop the IS1 method.

In the initial stages of research, the degrees of freedom to control the oven temperature method HAWK™ were limited. Hence, some of the first few experiments performed on the HAWK™ were merely an alteration of the conventional pyrolysis temperature method (PyroS3650_TOC750) mentioned in Chapter 2. The pyrogram of a sample with an initial pyrolysis isotherm of 2 minutes at 300°C is shown in Figure 4.1a. Likewise, the pyrogram of the same sample with an initial pyrolysis isotherm of 5 minutes at 300°C is shown in the Figure 4.1b. The temperature method used to produce the pyrograms in Figure 4.1a is Figure 4.1b are similar to the conventional method with the exception of the initial pyrolysis isotherm time. The initial pyrolysis isotherm in the conventional pyrolysis temperature method (PyroS3650_TOC750) is 3 minutes. It was observed from Figure 4.1b, that the 5 minute isotherm gives the sample enough time to completely evaporate the hydrocarbons molecules with boiling points less than or equal to 300°C. Hence all the further experiments were conducted with a pyrolysis isotherm of 5 minutes.

In order to measure the fractions of petroleum as a function of boiling point, a clear segregation of the FID signal with respect to the boiling points is essential. Consequently, using an optimum rate of change in temperature with respect to time between the isotherms is important. A sample with S1 value of 4 mg of HC / gram of rock was selected. This sample was experimented at five different temperature rates (200°C/min, 150ºC/min, 100°C/min, 50°C/min, 10°C/min) between the isotherms of 180°C and 300°C and are shown in Figures 4.2a, 4.2b, 4.2c, 4.2d, and 4.2e. The optimum temperature rate was observed to be 200°C/min, because with the rate of 200°C/min there was a maximum release of FID signal in limited time when compared to the other temperature rates. Experiments with temperature rate of 250°C/min or higher were not possible because of the oven control limitations.

By this point, it is established that the IS1 method should consist of 5 minute pyrolysis isotherms, and have a temperature rate of 200°C/min between the isotherms. The next set of experiments were aimed towards selection of isotherm temperatures. Thereafter, two new temperature methods were created on the HAWK™, the first one with a temperature range of 50°C to 150°C with 5 minute isotherms at 50°C, 100°C, and 150°C shown in Figure 4.3a and the second one with a temperature range of 50°C to 300°C with 5 minute isotherms at 50°C, 150°C, and 300°C shown in Figure 4.3b. A sample with known quantities of free petroleum was analyzed using the first temperature method (Figure 4.3a), and FID signal indicating the release of hydrocarbon molecules with a boiling point range of 50°C to 150°C was recorded. Then, using the same sample, having lost its hydrocarbons between boiling point ranges of 50°C to 150°C, was immediately analyzed using the second method (Figure 4.3b); here it is observed that the sample had no FID signal between 50°C to 150°C. There was only one FID signal peak observed at 300°C. This is an indication that sample evaporated all of its hydrocarbon (between boiling point ranges of 50°C to 150°C) in the first experiment, and the second experiment released the hydrocarbon molecules remaining after the first experiment.

To check the FID signal behavior on the HAWK™, a crude oil sample was analyzed in the HAWK™ oven. It was observed that the sample evaporated hydrocarbons at 10, 3 minute isotherms, between the temperatures of 50°C to 360°C (pyrogram shown in Figure 4.4a). Another crude oil sample was analyzed in the HAWK™ oven; this time, the isotherms between the temperature range of 50°C to 300°C were not at a constant 3 or 5 minute time frame; instead the temperature was increased whenever the FID signal was reduced. In other words, the temperature was increased after all the hydrocarbon molecules had evaporated at that particular temperature (pyrogram shown in Figure 4.4b). This provides information on the time required to evaporate hydrocarbons at different temperatures. Although this was useful information, it is difficult to control the oven as a function of the FID signal. Hence, using a specific number of isotherms at equal temperature intervals was opted for further experimentations.

Later on, in order to understand the relationship of the boiling point and the FID signal, four oils with different known values of API gravity were added to a pulverized source rock which did not contain any free petroleum. The API gravity of these oils were 56, 35, 25, and 18. These artificial samples were analyzed using a method with 6, 5 minute isotherms at 50°C, 100°C, 150°C, 200°C, 250°C, and 300°C, respectively, shown in Figure 4.5a, 4.5b, 4.5c, and 4.5d. It was observed that with the decrease in the API gravity of oil, there was a shift of the FID signal from lower temperatures to the higher temperatures. Because there was a clear distinction of the FID signal peaks at the six temperature isotherms, this particular temperature method (named IS1) is suited best to measure the fractions of hydrocarbon molecules in a sample.

One of the major concerns was to check if the particle size of the sample would affect the FID signal. To rule this out, samples with high TOC content and with two different particle sizes (0.5mm-0.4mm and 0.1mm-0.074mm) were analyzed on the HAWK™ with the IS1 temperature method. The pyrograms of these samples are shown the Figure 4.6a and Figure 4.6b. From these

pyrograms, it was observed that the particle size had little or no effect on the FID signal. Hence, it can be hypothesized that the particle size will have no significant impact on the FID signal.

4.2. Procedure and Working

As shown in Figure 4.7, the IS1 (Incremental S1) method consists of 6, 5 minute isotherms at 50°C, 100°C, 150°C, 200°C, 250°C, and 300°C, respectively, with a temperature rate of 200°C/min at every 50° interval (from 50°C to 100°C, 100°C to 150°C, and so on until 300°C). This is followed by a 50°C/min increase in temperature followed by a 5 minute isotherm at 650°C. As mentioned in Chapter 2, there are three detectors in the HAWK. Only the FID detector is used in this method.

After subjecting the sample in the oven to a programed IS1 temperature method, the sample releases fractions of petroleum and kerogen at different temperatures. The quantities of these evaporated fractions at these discrete temperatures are measured by the FID signal, based on the amount of sample ionized in a hydrogen flame. This FID signal, recorded as a function of temperature and time, is assigned seven different peaks S1_1, S1_2, S1_3 S1_4 S1_5, S1_6, and S2, as shown in Figure 4.8. As mentioned in the earlier chapter, in the conventional pyrolysis method, the S2 is considered the FID signal measured from 300°C to 650°C, and the conventional temperature increase rate is 25°C/min. In the IS1 method, although the temperature range over which the S2 is measured is the same as the conventional method, the rate of temperature increase in the IS1 method is twice (50°C/min) that of the conventional method (Pyro3650_TOC750). This increase in temperature rate in IS1 method is intended to achieve a faster, less time-consuming experiment. The fraction of sample ionized in the hydrogen flame between 300°C and 650°C was originally considered to be kerogen by Espitalié et al. (1977). Assuming that kerogen is released in this temperature range, it is reasonable to speculate that the change in the temperature rates might have an effect on kinetics, and in turn may alter the FID signal. When a new sample is analyzed, a calibration with known parameters is used. For example, a standard with a known S2 value (9.02

mg of HC/gm of rock) for a known (75 milligrams) sample weight is analyzed on the HAWK, and the area under the curve for S2 is calculated from the raw FID signal and that area is given a corresponding S2 value (9.02 mg of HC/ gm of rock). Thereafter, every unknown sample with a specific area under the FID signal curve S2 is calculated with the known calibration. The same known S2 calibration is used to calculate the quantity of sample ionized during the S1 peak or S1_1 to S1_6 peaks. Hence, to avoid any errors in the calculations of the values S1, S1_1 to S1_6 and S2 of a new sample, understanding the effect of temperature rate change in S2 is crucial. On the other hand, it is essential to confirm FID signal peaks of a sample measured at IS1 temperatures (Incremental S1 signature), which is an indication of hydrocarbons evaporating at their respective boiling points. In order to use the IS1 method as a standard method for experimentation on the HAWK, there are two major concerns that need to be addressed: first that any calibration errors caused by the increase in temperature rate and second, that hydrocarbon molecules evaporate at their corresponding boiling point temperatures in the HAWK™ between the temperatures of 50°C to 300°C.

4.2.1 Experimentation on the S2 Temperature Rates

In order to check if the increase in the temperature rate affects the area under the S2 FID signal curve, source rocks with a range of maturities from various basins were chosen from the sample library. The maturity of these rocks range in Tmax values from 417°C to 479°C. The typical range of Tmax values is from 420°C for an immature rock to 460°C to a mature rock (Tissot et al. 1980; Bordenave 1993, 409-410). A set of seven samples (varying in maturity) were analyzed at both temperature rates (50°C/min and 25°C/min). The data are shown in Appendix A. Figure 4.9 is a plot showing S2 measured at a temperature rate of 50°C/min versus S2 measured at a temperature rate of 25°C/min. It is evident from the graph that there is negligible difference in the S2 values from both temperature rates. On plotting S2 at 50°C/min versus S2 at 25°C/min, a straight

line with an R^2 value of 0.99 was observed. In Figure 4.10, on plotting Tmax values at 50°C/min versus Tmax values at 25°C/min, there is a slight variation in the Tmax from the maturity temperatures of 430°C to 455°C. However, a straight line was again observed with an R^2 value of 0.99. Based on these experiments, it can be concluded that a change in S2 temperature rate will likely have little or no effect on the S2 value. Hence, using a faster, less time-consuming temperature rate in the IS1 method is hypothesized to not affect the calculations.

4.2.2 Evaluation of Hydrocarbon Molecules Evaporating at 50°C to 300°C

Thermal Gravimetric Analysis (TGA) with mass spectrometry (MS) was performed in order to check if the hydrocarbon molecules are vaporized at respective IS1 temperatures. The TGA includes an oven, two gas inlets, and two highly weight-sensitive cantilever rods; one of which holds a reference sample and the other of which holds an unknown sample (TA Instruments, 2016). Conventionally, TGA is used to observe the weight loss of a sample within an oxidizing or reducing atmosphere with varying temperature. The exhaust gas from the TGA oven can be connected to a mass spectrometer or a gas chromatograph. In the experiments performed for this work, the sample was introduced into the oven in an inert atmosphere with the IS1 temperature profile emulating the HAWK IS1 experimental conditions. The only difference is that the exhaust gas from the oven is connected to a mass spectrometer whereas in the HAWK, it is connected to the FID detector. The weight loss of a pulverized reservoir rock sample at different IS1 temperatures can be associated with the loss of hydrocarbon molecules from the rock. The weight loss of a sandstone sample containing a 31.9 API gravity oil is shown in Figure 4.11. From Figure 4.11, it can be noted that the temperatures ranges at the peaks S1_2, S1_3, S1_4, S1_5 have weight loss of 0.75%, 1.25%, 1.20%, 0.80%, respectively. The composition of this oil is given in Table 4.1. It is evident that approximately 67% of this oil has carbon chain lengths from C5 to C17. According to Hayney

(2014), the boiling point of these hydrocarbon molecules lies between 50°C and 300°C. Now, intending to prove that the peaks S1_1 to S1_6 indicate evaporation of hydrocarbon molecules, results from the mass spectra should represent carbon chain lengths at their respective boiling point range (In the IS1 range). In mass spectrometry, the sample that is being tested (in this case vaporized hydrocarbon molecules) is bombarded with an electron beam to ionize the sample and then indicate the mass and charge of the fragmented molecules in relative abundance. By plotting relative abundance versus mass-to-charge, the fragmented molecules and their concentration is inferred (Sparkman et al. 2011). In Figure 4.12, Ion current (A) versus Mass (amu) is plotted and each color is associated with each cycle (scan for amu at one particular time frame). The mass spectrometry data given in Figure 4.12 with the lines C1, C13, C23, C33, and C43 indicate the MS signal of the baseline, S1_2, S1_3, S1_4, S1_5, respectively. This figure shows a decreasing trend of the ion charge between the amu values from 50 to 100 as the cycle value increases (increase in IS1 temperature). This is an indication of the relative decrease in the mass of the fragmented molecules with increasing chain length - which is expected. Hence, this experiment proved that the hydrocarbon molecules evaporate according to their boiling points at the programmed IS1 temperatures.

4.3. IS1 method simulations on ProMax and experiments on HAWK

After the final processes of accumulation and preservation occur in a petroleum system of a basin, petroleum engineers attempt to produce the crude oil or gas from the reservoir rock (conventional or unconventional). The oil and gas being produced in-situ go through a pressure and temperature regime. By the time crude oil or gas reaches the surface at stock tank conditions (14.696 psi and 60°F; 101.3 KPa and 16 °C), the original phase of the petroleum may change (Dake 1978, 37-41). Similarly, core or cuttings samples are extracted from the high pressure and temperature conditions (reservoir conditions). By the time these samples are exposed to

atmospheric pressure and temperature conditions and pulverized to be analyzed in the HAWK or any pyrolysis machine, the residual oil in the rock will end up emulating the properties of the oil that could be produced out of that particular formation.

Since the oil in the rock is incrementally being vaporized by pyrolysis with the IS1 method, to have a comprehensive understanding of vaporizing hydrocarbon molecules in the IS1 method, a number of simulations on oils were performed. These simulations were performed on oils with API gravities ranging from 20 to 70 and were taken from all over the world. ProMax was the software used to perform these simulations, with the oil composition data also taken from the oil library in the ProMax software. A total of 192 oil samples with known API gravities are tabulated in Appendix B. A six-stage, two-phase separation using the Peng-Robinson equation of state was performed on these oils emulating the incremental pyrolysis occurring in the IS1 method from 50 °C to 300 °C in the HAWK. The separator conditions are provided in Table 4.2. The regular rock samples analyzed on the HAWK for pyrolysis are at room temperature. Hence, the initial separator (VSSL-100) is added to the simulation so as to achieve the same input conditions as the real-time IS1 method experiment. Figure 4.13 shows the ProMax simulation at IS1 temperatures (50 °C to 300 °C). The molar flow of vapor phase in kmol/min of all the simulations at different temperatures is plotted in Appendix C. Some of the results from the simulations showed higher than expected quantities of petroleum vaporized above 300°C, hence there likely occurred a loss of volatile hydrocarbon above the temperature range aimed at measuring of API gravity. Such outliers were excluded from the data. The average molar flow in vapor phase (kmol/min) of different groups of API gravity oils at different temperatures is provided in Table 4.3. Note that there is a decreasing pattern to the values of the molar flow when comparing higher API gravity to the lower ones. It is evident from the results of the ProMax simulations (Table 4.3) that depending on the density of the oil, a certain portion of oil vaporizes at temperatures greater than 300°C. In the HAWK experiments of IS1 method, oil vaporizing between temperatures 50°C to 300°C is measured for characterization.

This is because, usually unlike the produced crude oil, the residual oil in the rock samples may coexist with bitumen and kerogen. When producing from a reservoir, only the petroleum flows through the wellbore because bitumen and kerogen are immobile (Tissot & Welte, 1978). Considering the ProMax simulations data, the FID signal above 300°C in a regular pyrolysis method accounts for heavy petroleum molecules, bitumen, and kerogen. Yet based on the studies by Espitalié et al. (1977, 1985a, 1985b, 1986) the area under the FID signal curve between 300°C to 650°C is considered kerogen. In order to validate this, a sandstone reservoir rock (upper Navajo sandstone) sample was analyzed using the HAWK instrument with the IS1 method shown in Figure 4.14. The FID signature of the sample shown in Figure 4.14 has no bitumen or kerogen in it. Yet there exists an FID signal at temperatures between 300°C to 650°C. Both the simulations and sandstone sample pyrolysis on IS1 method establish that not all organic compounds that vaporize or crack above 300°C during pyrolysis is kerogen. Considering this fact, oil simulations on ProMax were performed between 50°C and 300°C. These temperatures are appropriate for characterizing the oil based on boiling points as this range (50°C - 300°C) acts as a good operating temperature range in the HAWK. By using the 50°C - 300°C range in the HAWK, it can be stated that the measured quantity of sample vaporizing at their corresponding boiling points is nothing but oil (note that any contamination of drilling mud and other oil-based lubricants is excluded). Consequently, the simulated oil data of known API gravity of oil are used as a reference (in Chapter 5) to build a representation scale, which provides a relationship to calculate the API gravity of a sample with known values of S1_1 to S1_6, measured with the IS1 method on HAWK. The results of the normalized molar flow values of vapor phase at different IS1 temperatures of the simulations excluding outliers are given in Appendix C. The raw results of the HAWK experiments performed with IS1 method on a set sample are provided in Appendix D. Further details on the samples selected to perform the HAWK experiments will be discussed in the next chapter.

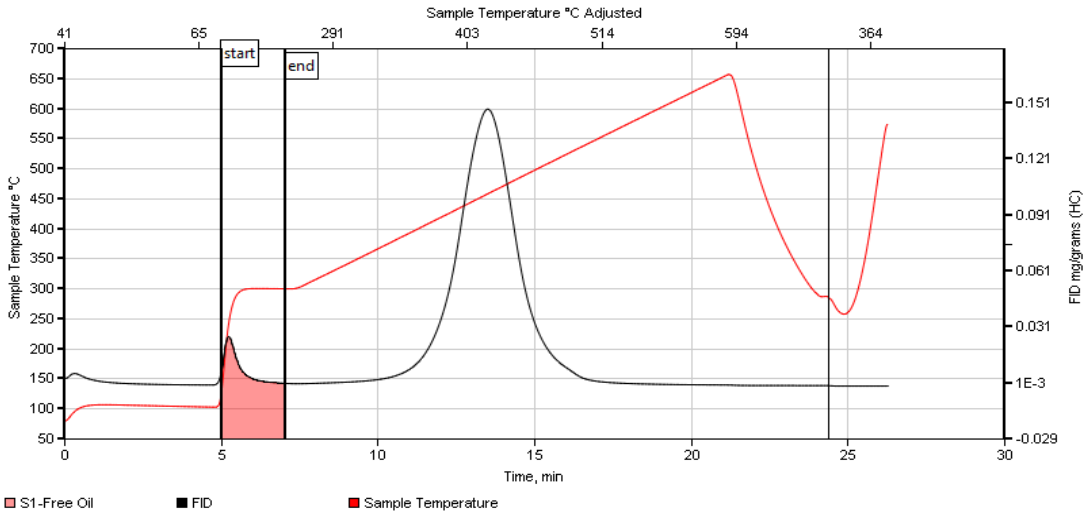

(a)

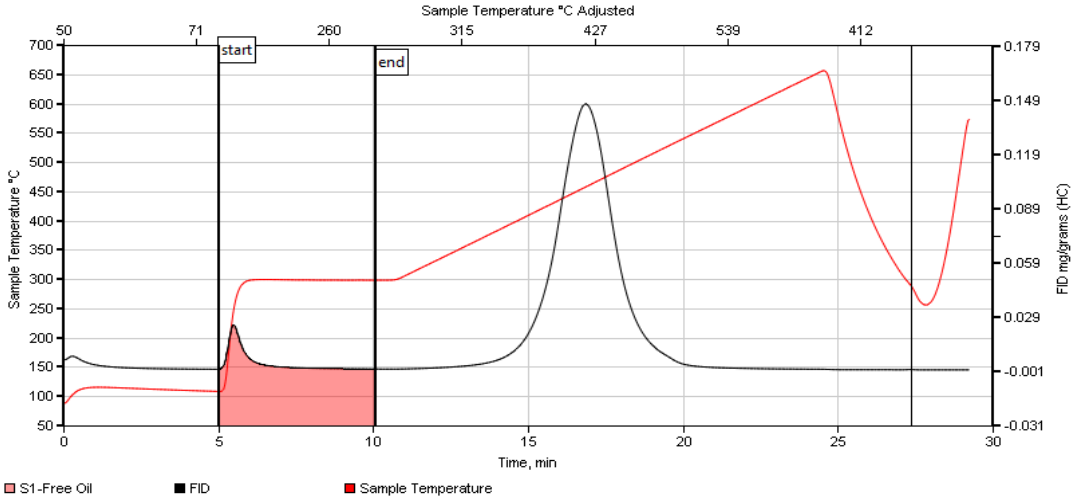

(b)

Figure 4.1: FID signal of a sample measured as a function of time and temperature using the conventional temperature method with an exception of initial pyrolysis isotherm (a) (2 minutes), indicating nonaccurate measurement of S1, and (b) (5 minutes), Indicating accurate measurement of S1 by allowing the FID signal to coincide with the base line.

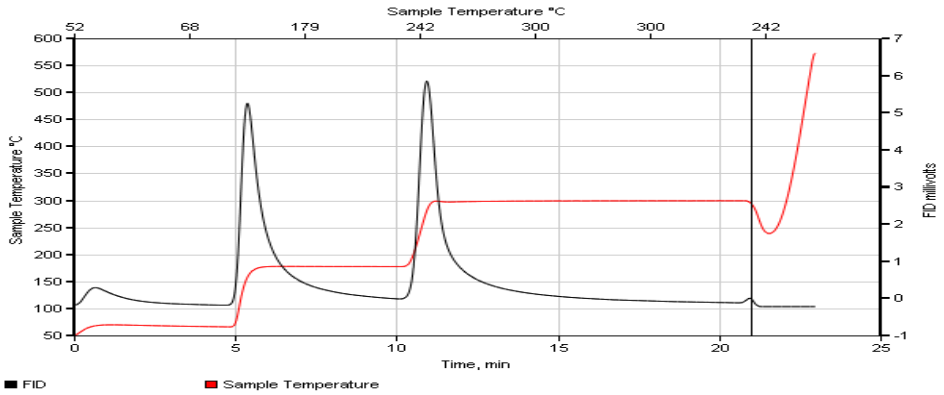

(a)

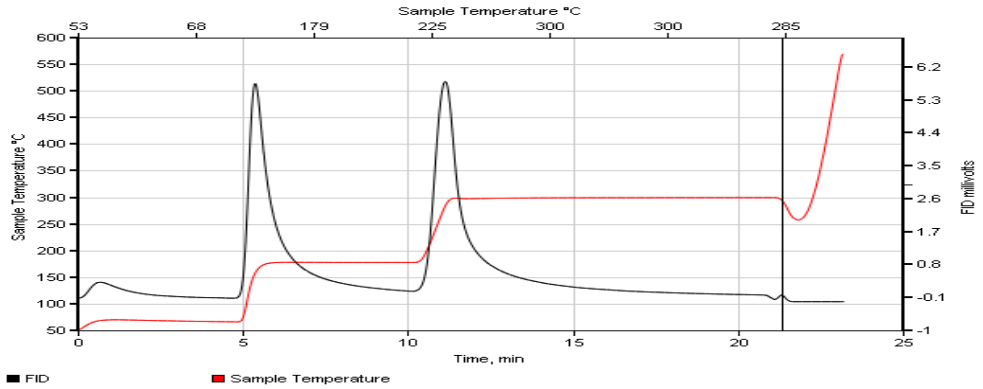

(b)

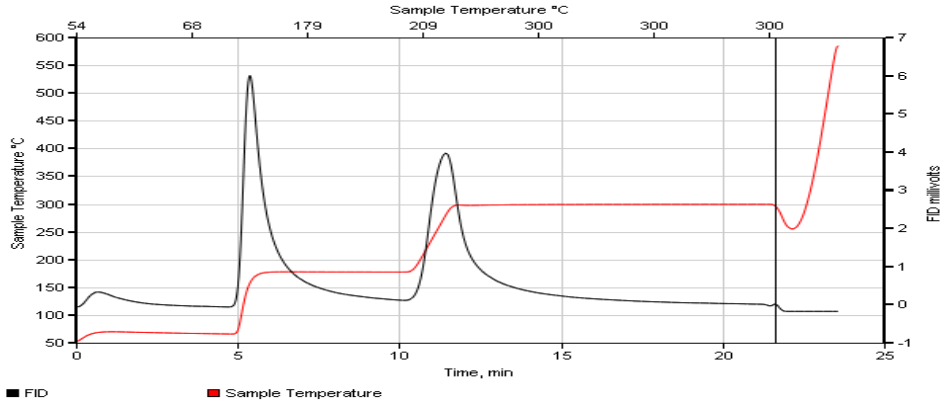

(c)

Figure 4.1 Continued

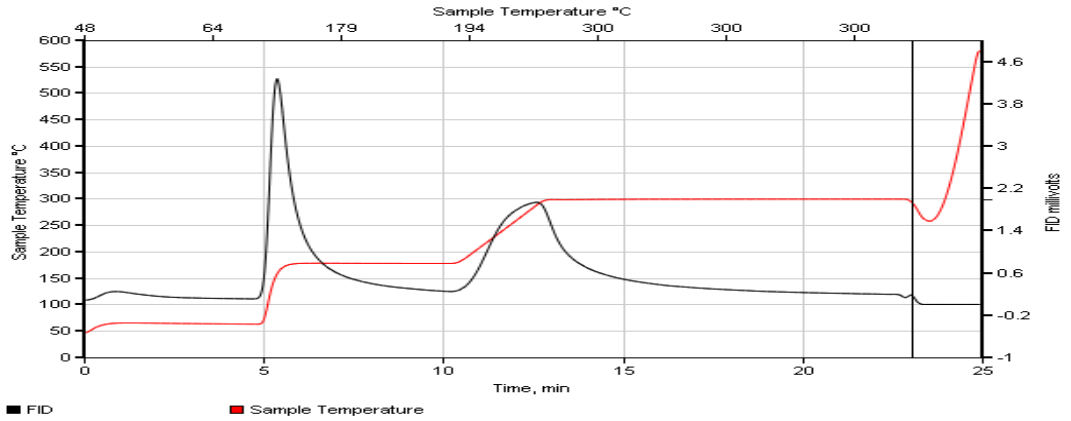

(d)

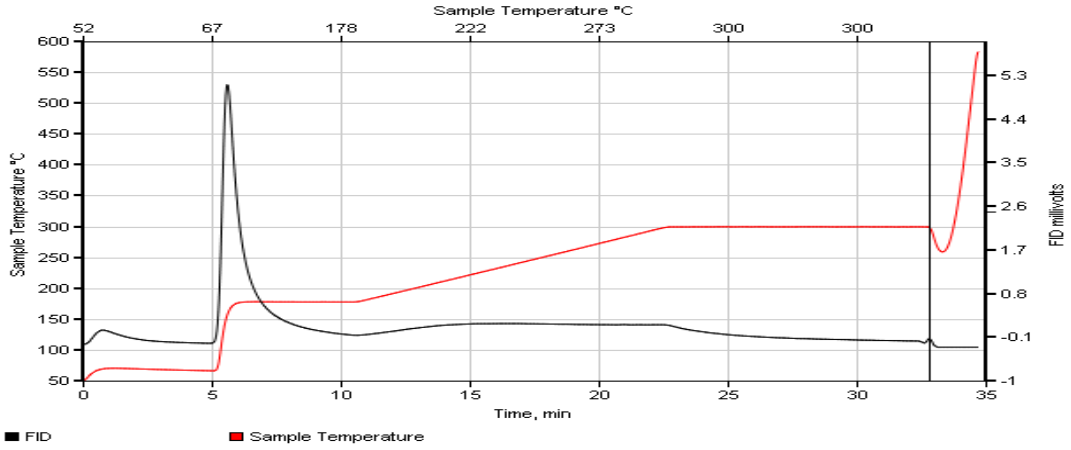

(e)

Figure 4.2: FID signal of a sample measured as a function of time and temperature with a temperature rate of (a) 200°C/min between the 180°C and 300°C showing a narrow FID signal peak. (b) 150°C/min between the 180°C and 300°C showing slightly wider FID signal peak. (c): 100°C/min between the 180°C and 300°C showing wider FID signal peak. (d) 50°C/min between the 180°C and 300°C showing slow release of hydrocarbons with wide FID signal peak. (e) 10°C/min between the 180°C and 300°C showing a very slow release of hydrocarbons with nearly flat FID signal peak.

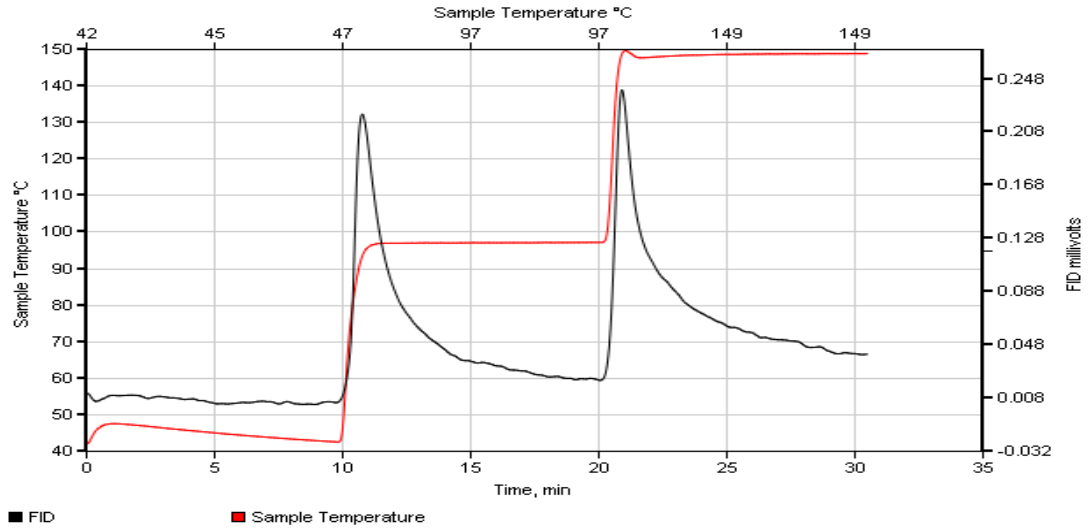

(a)

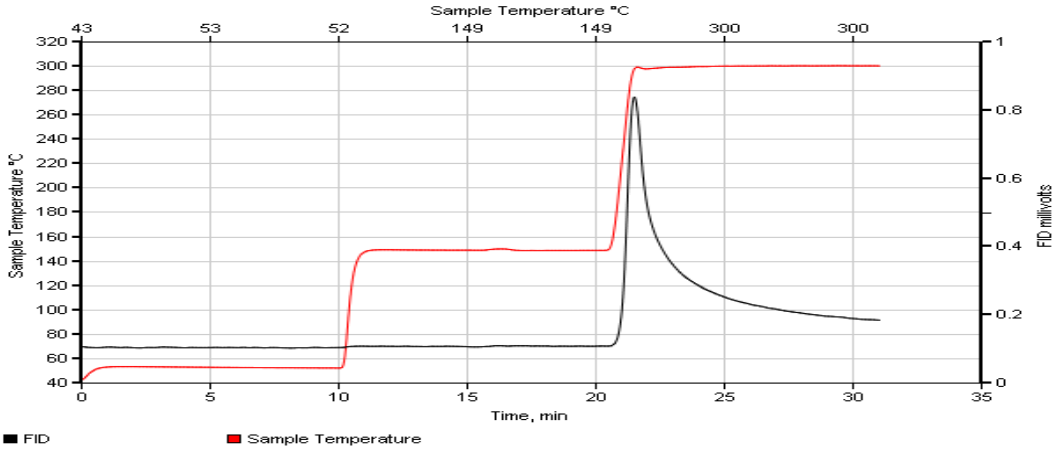

(b)

Figure 4.3: The recorded FID signal of a sample between the temperatures (a) 50°C and 150°C, indicating the volatile hydrocarbons at two FID peaks. (b) 150°C and 300°C, experimented after vaporizing the hydrocarbons between the temperatures 50°C and 150°C (Figure 4.3a), indicating the volatile hydrocarbons at temperatures more than 150°C.

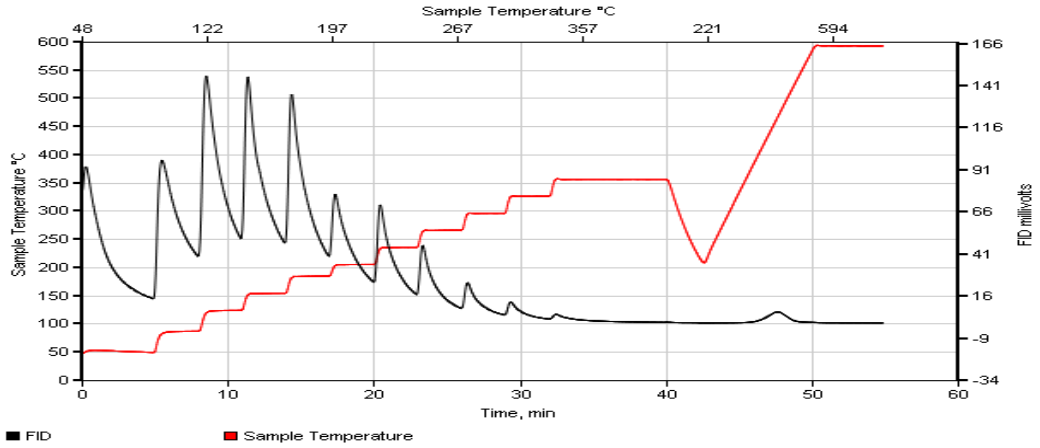

(a)

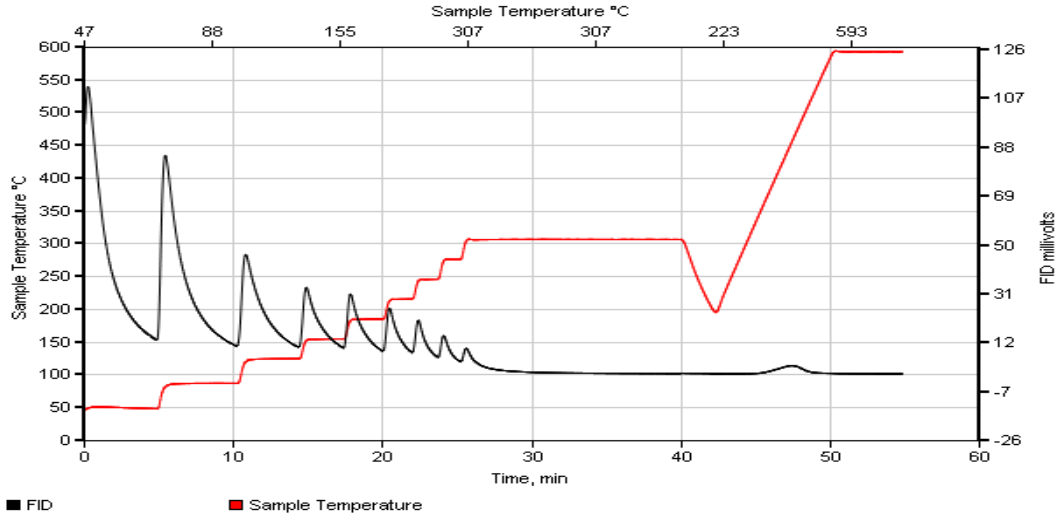

(b)

Figure 4.4: The FID signal of a random crude oil measured in (a) three minute isotherms at ten different temperatures between 50° and 300°C, indicating the different quantity of volatile hydrocarbons distributed in specific temperature range. (b) isotherms varying time at ten different temperatures between 50° and 300°C, indicating the different quantity of volatile hydrocarbons distributed in specific temperature range.

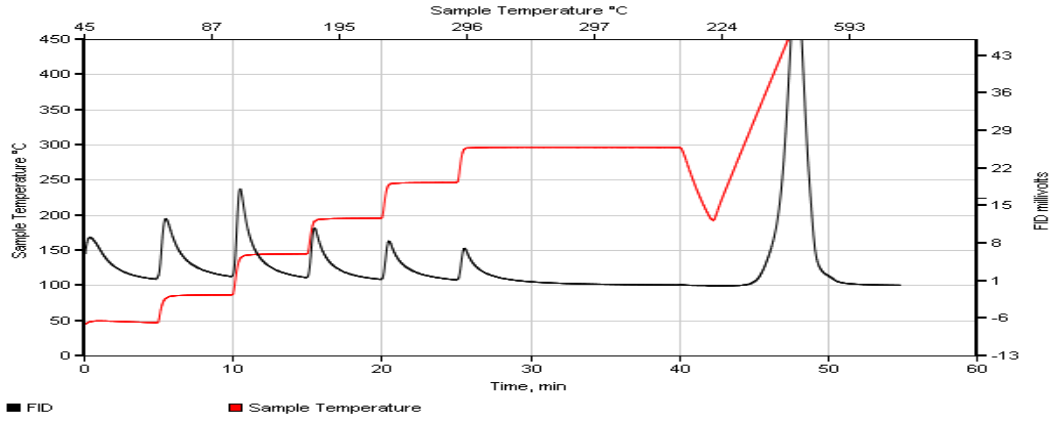

(a)

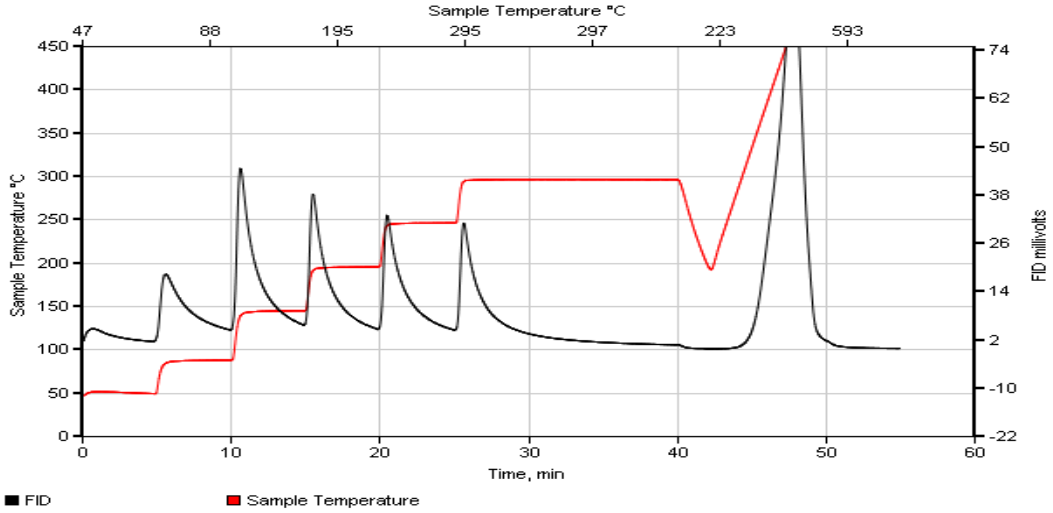

(b)

Figure 4.5: FID signal of an engineered sample containing an oil of (a) API gravity 56, showing the Incremental S1 signature with the highest fraction of petroleum released at 150°C. (b) API gravity 35, showing the Incremental S1 signature with the highest fraction of petroleum released at 150°C and decrease in fraction of petroleum at 50° and 100°C when compared to sample with 56 API gravity of oil. (c) API gravity 25, showing the Incremental S1 signature with the highest fraction of petroleum released at 250°C. (d) API gravity 18, showing the Incremental S1 signature with the highest fraction of petroleum released at 300°C.

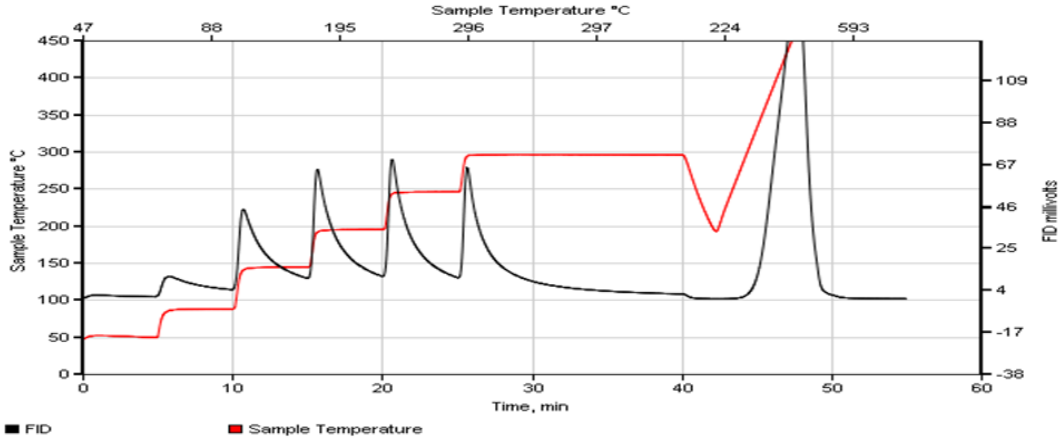

(c)

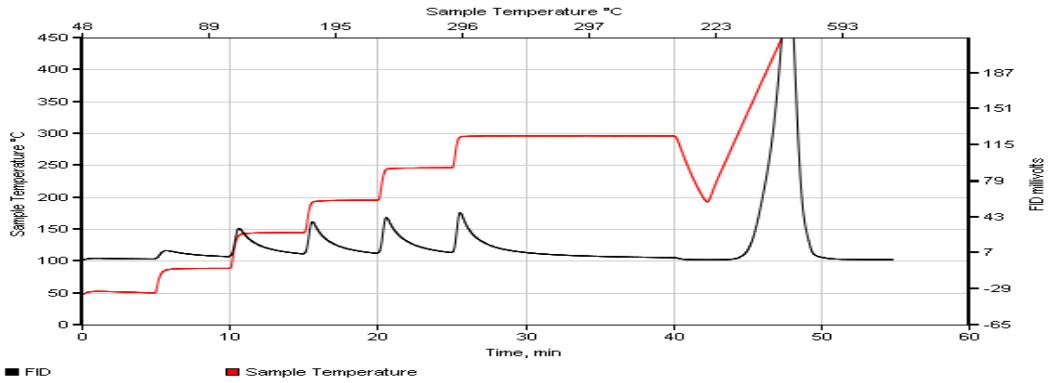

(d)

Figure 4.5 continued

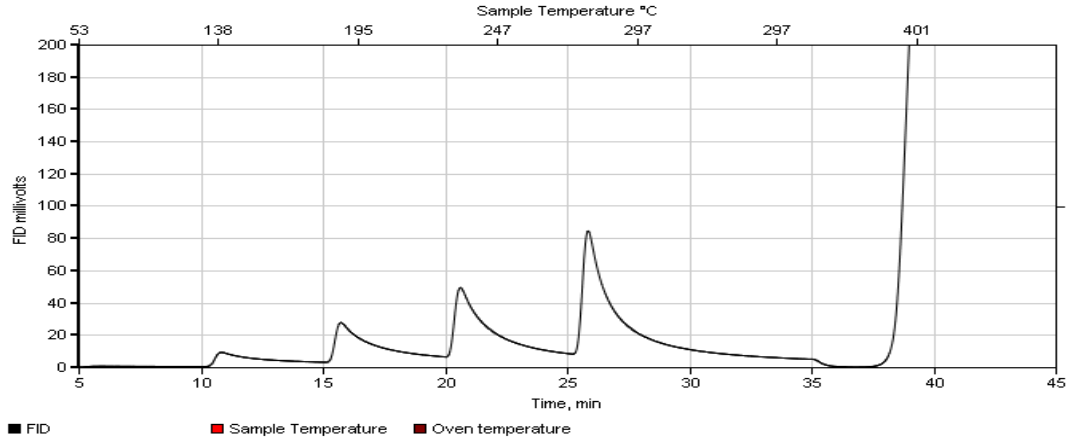

(a)

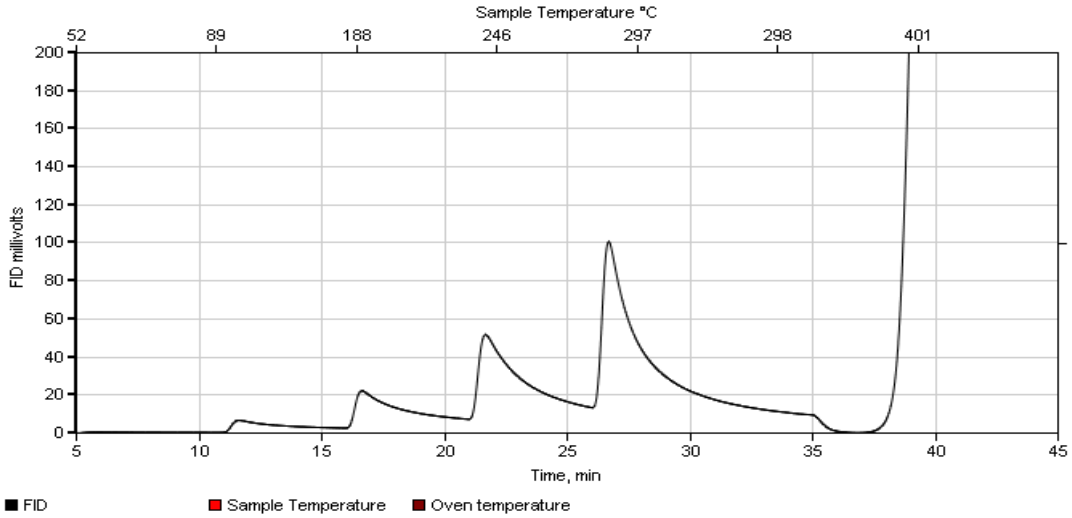

(b)

Figure 4.6: FID signal showing the incremental S1 signature of a sample with particle size (a) between 0.1mm to 0.074mm. (b) between 0.5mm-0.4mm.

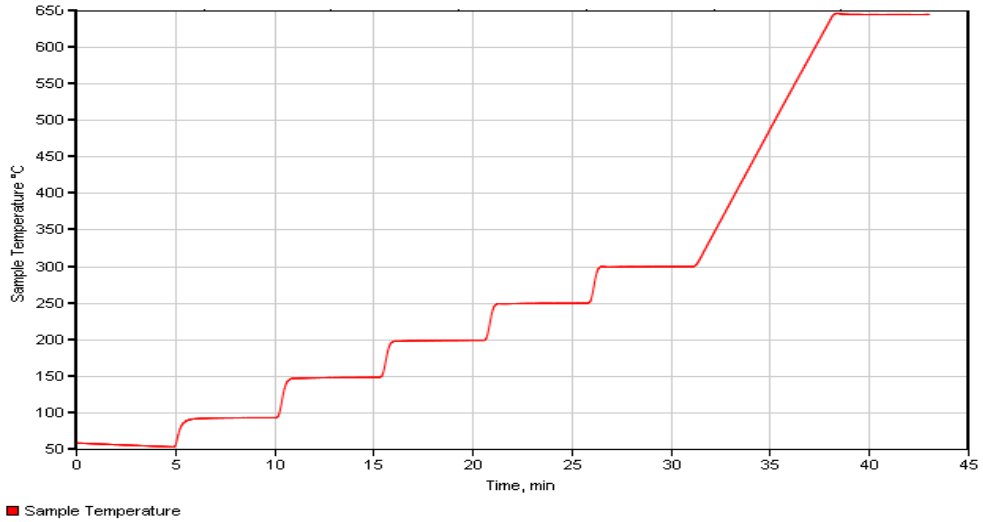

Figure 4.7: Incremental SI temperature profile (IS1 method), showing six temperature isotherms at 50°C, 100°C, 150°C, 200°C, 250°C, and 300°C with temperature rate of 200°C per minute between every isotherm, followed by an increase in temperature of 50°C per minute until a final temperature five minute isotherm 650°C.

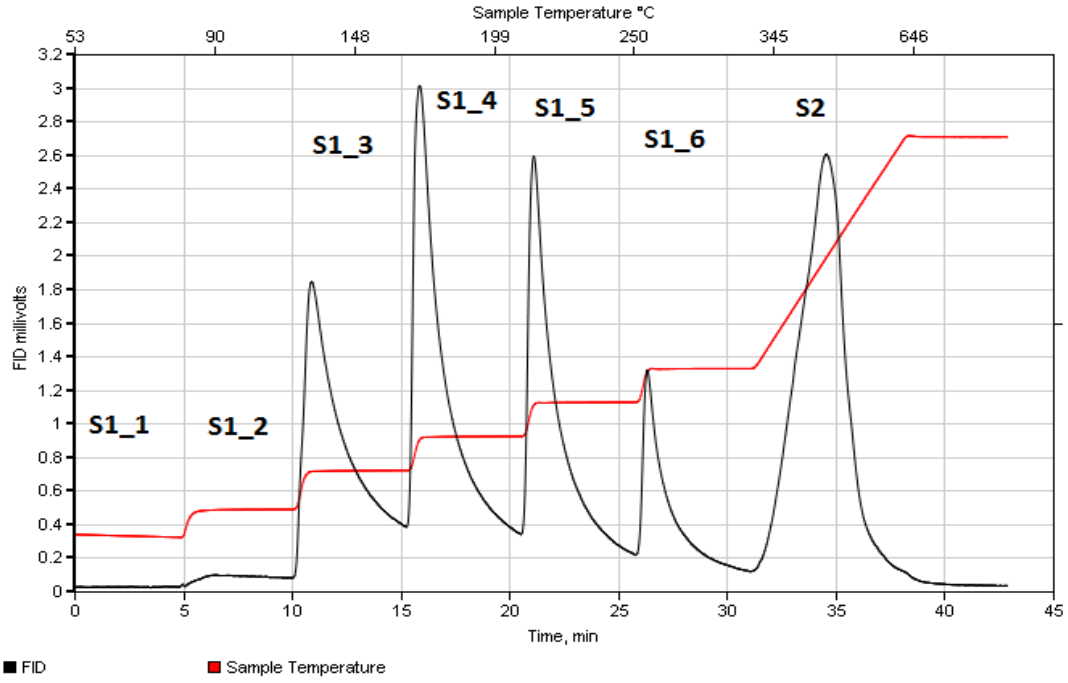

Figure 4.8: Raw FID signal of a sample experimented on IS1 method, showing the different assigned incremental S1 values (S1_1, S1_2, S1_3, S1_4, S1_5, and S1_6) and S2 as a function of temperature and time.

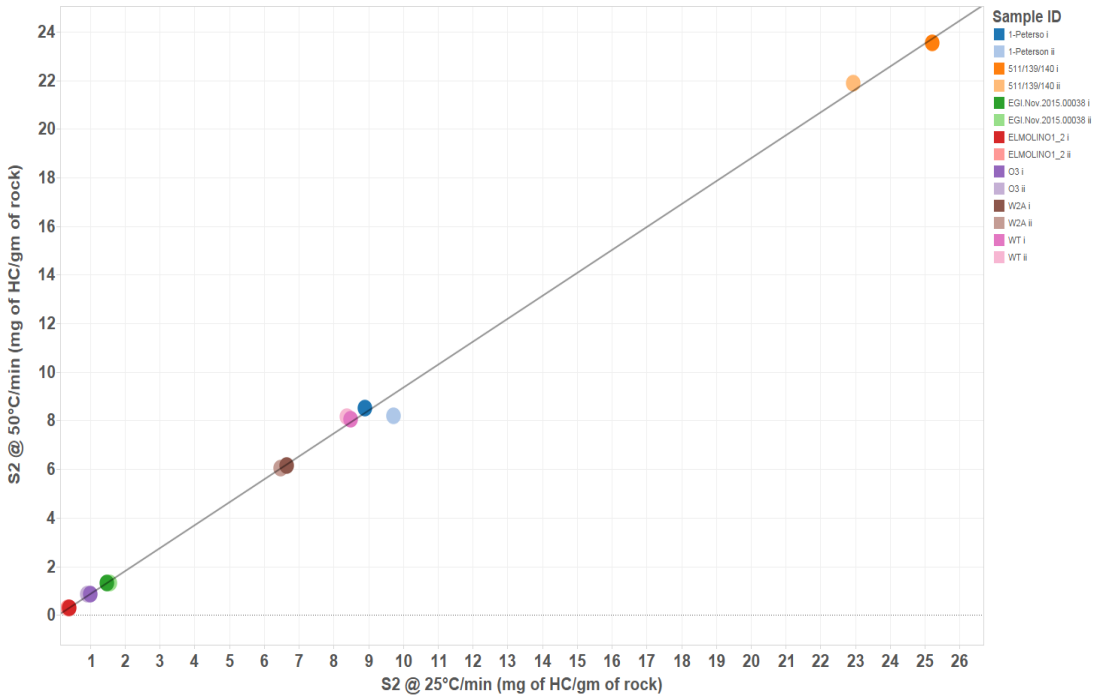

Figure 4.9: Plot of data correlating to a straight line with R^2 value of 0.99, showing S2 values of samples with varying in maturity experimented and measured at 50°C/min versus S2 values of samples with varying in maturity experimented and measured at 25°C/min (mg of HC/gm of rock).

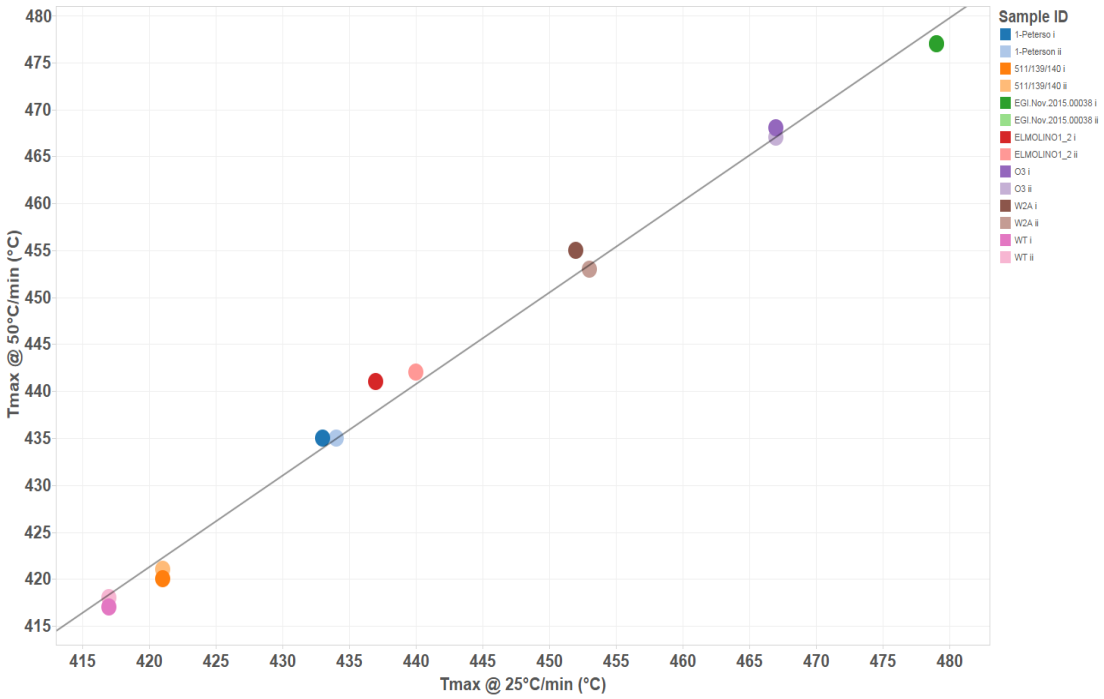

Figure 4.10: Plot of data correlating to a straight line with R^2 value of 0.99, showing Tmax values of samples with varying in maturity experimented and measured at 50°C/min versus Tmax values of samples with varying in maturity experimented and measured at 25°C/min (°C); with a slight variation in data between the temperature range of 430°C to 460°C.

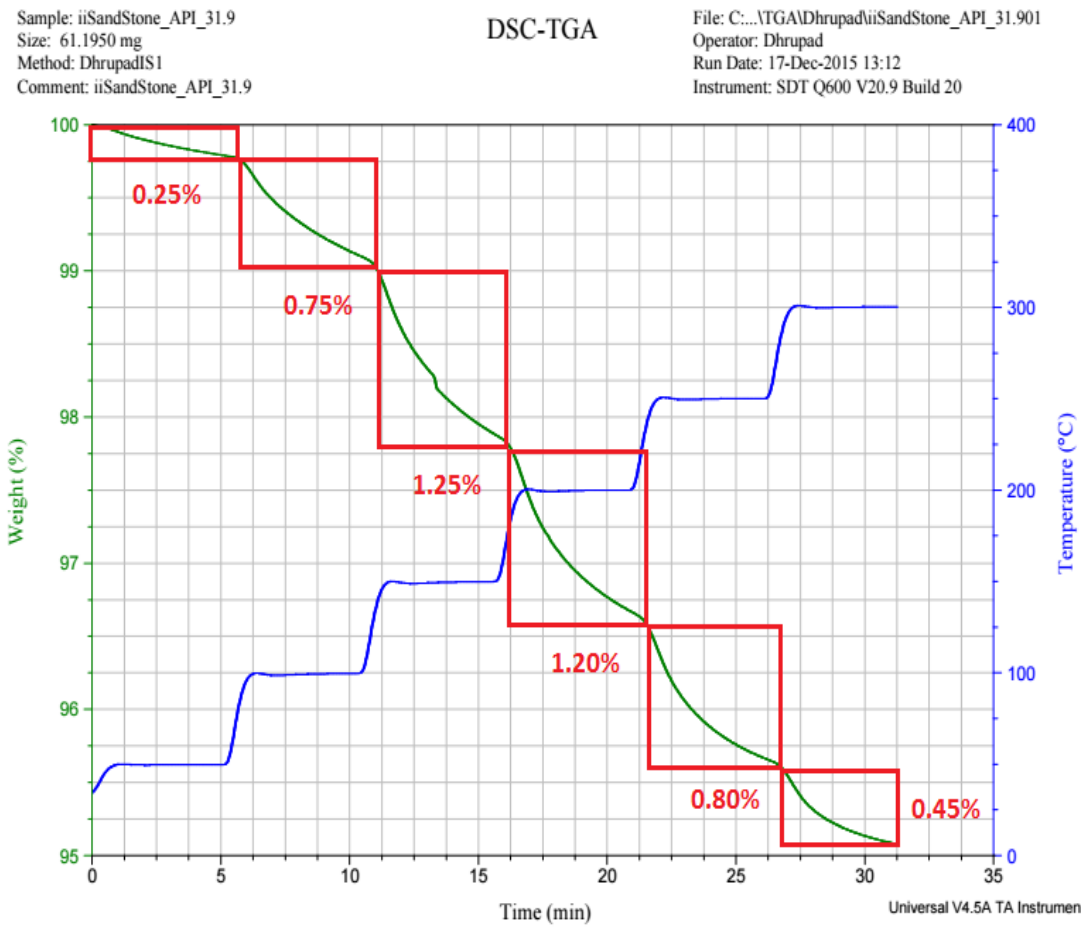

Figure 4.11: Percent weight loss of a rock sample as a function of temperature and time, indicating the quantity of hydrocarbon lost or vaporized in a TGA data when experimented on IS1 method.

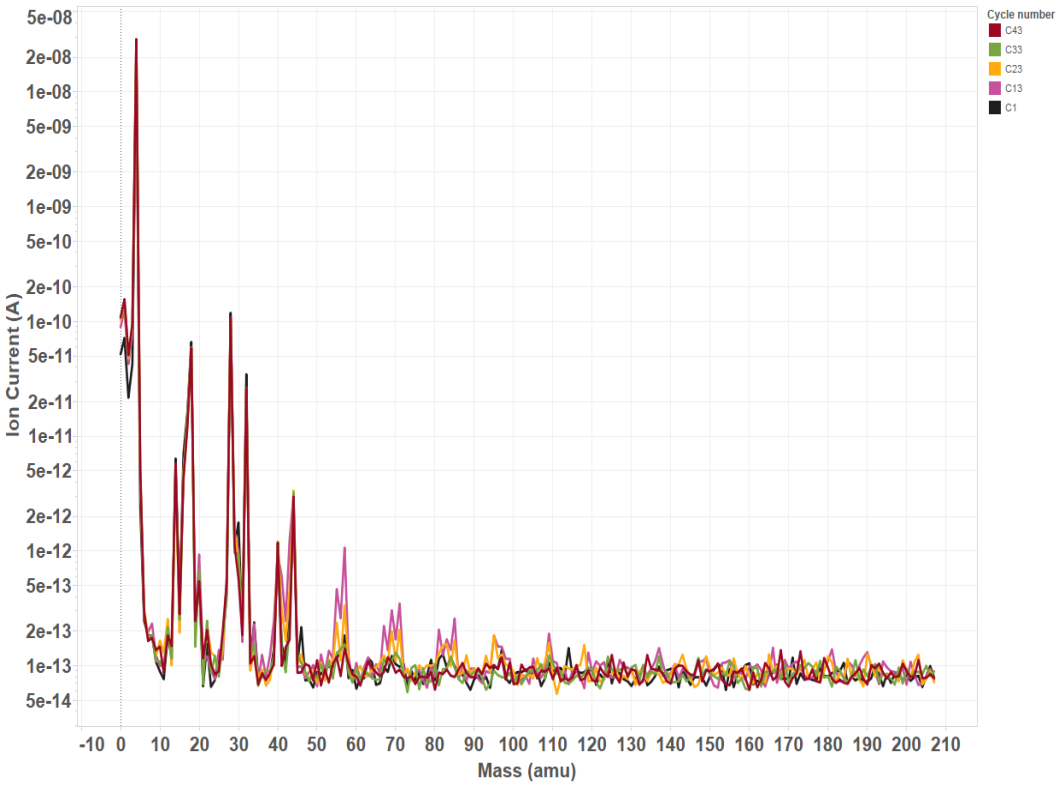

Figure 4.12: Ion current (A) versus Mass (amu) - Mass Spectrometer data of the sandstone sample with the oil API gravity 31.9, showing the release of different fragmented hydrocarbon molecules at different incremental temperatures indicated by different color.

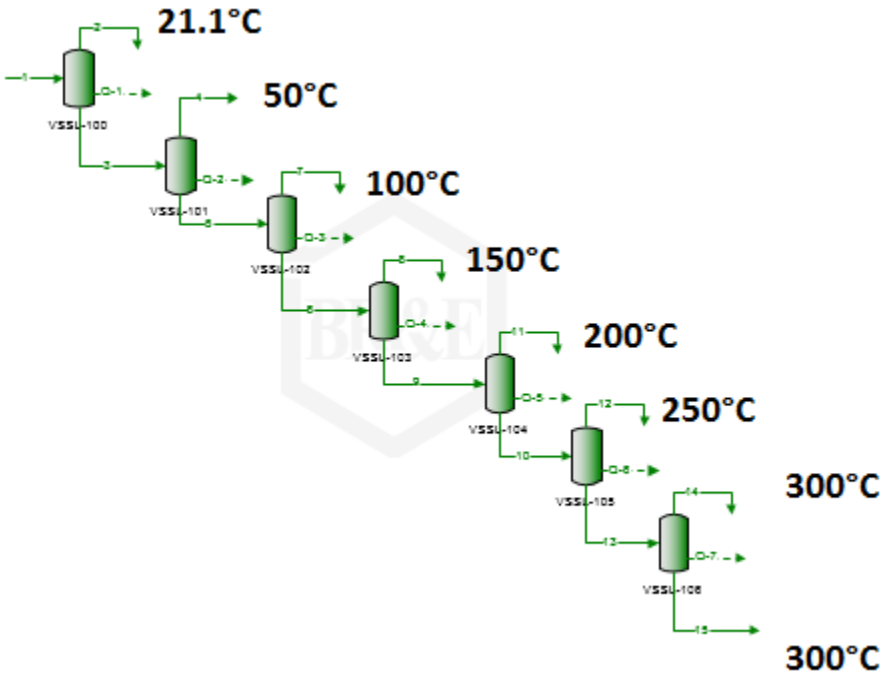

Figure 4.13: Schematic of the ProMax two phase separation at IS1 temperatures.

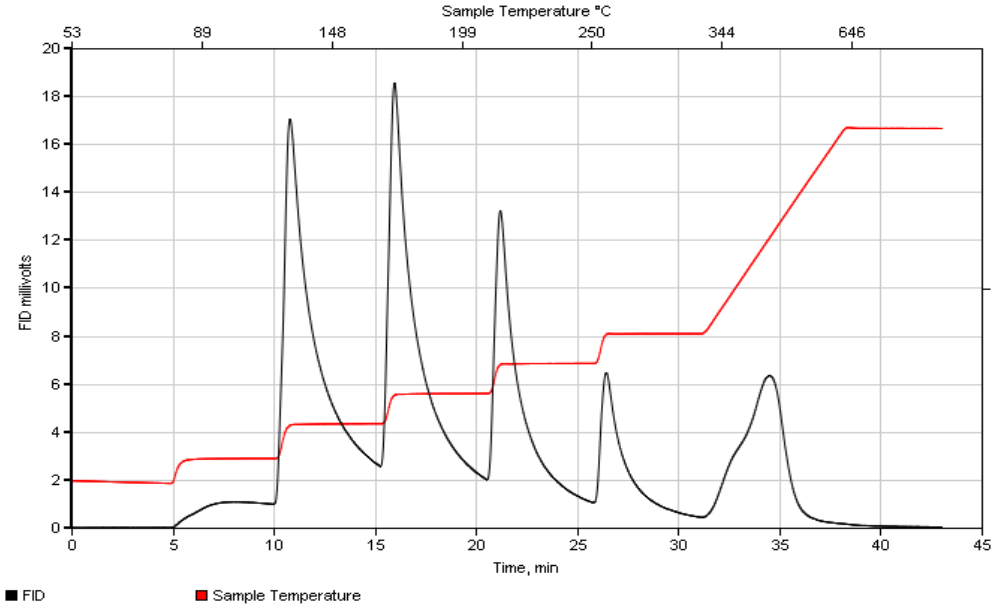

Figure 4.14: Incremental S1 signature of sandstone reservoir rock containing only oil, showing the FID signal at temperatures more than 300°C, which is conventionally measured as S2.

Table 4.1: Composition of the oil (API 31.9) in the sandstone sample experimented on the TGA.

API 31.9 Oil Carbon Number Estimation			
Carbon #	Avg. Ret. Time	Total Area	Area %
C5	1.78	7091.09	12.26%
C6	2.22	2240.24	3.87%
C7	2.45	1714.18	2.96%
C8	2.83	2242.69	3.88%
C9	3.05	2929.36	5.07%
C10	3.70	3187.62	5.51%
C11	4.53	3214.15	5.56%
C12	5.67	2382.79	4.12%
C13	6.60	3148.60	5.44%
C14	7.61	3211.59	5.55%
C15	8.27	3377.31	5.84%
C16	8.95	2155.16	3.73%
C17	9.83	1891.02	3.27%
C18	10.37	2138.98	3.70%
C19	11.24	1802.33	3.12%
C20	11.98	1558.75	2.70%
C21	12.65	1344.58	2.33%
C22	13.15	1153.97	2.00%
C23	13.71	1146.93	1.98%
C24	14.31	1216.17	2.10%
C25	14.80	1145.14	1.98%
C26	15.29	1140.84	1.97%

Table 4.1 Continued			
Carbon #	Avg. Ret. Time	Total Area	Area %
C27	15.77	1135.58	1.96%
C28	16.16	1012.95	1.75%
C29	16.65	955.85	1.65%
C30	17.09	759.14	1.31%
C31	17.44	623.96	1.08%
C32	17.85	437.20	0.76%
C33	18.28	425.45	0.74%
C34	18.86	617.23	1.07%
C35	19.52	269.03	0.47%
C36	20.20	156.90	0.27%
Total		57826.76	

Table 4.2: Separators conditions of ProMax simulations.

Separator	Pressure (Pascals)	Phase Separation Temperature (°C)
VSSL-100	101325	21.1
VSSL-101	101325	50
VSSL-102	101325	100
VSSL-103	101325	150
VSSL-104	101325	200
VSSL-105	101325	250
VSSL-106	101325	300

Table 4.3: Average molar flow (kmol/min) of vapor phase of different group of API gravity oils at different temperatures.

API group	Ave. Molar flow (Kmol/ min) 50°C	Ave. Molar flow (Kmol/min) 100°C	Ave. Molar flow (Kmol/min) 150°C	Ave. Molar flow (Kmol/ min) 200°C	Ave. Molar flow (Kmol/ min) 250°C	Ave. Molar flow (Kmol/min) 300°C	Ave. Molar flow (Kmol/min) >300 ° C
API Gravity (20-25)	0	0	2.44	9.14	13.21	14.37	62.76
API Gravity (26-30)	0	2.55	16.9	13.64	12.21	12.1	46.6
API Gravity (31-35)	0.2	3.8	15.95	15.38	13.09	12.42	38.89
APIGravity (36-40)	0.18	5.64	22.62	16.87	13.1	11.66	30.01
API Gravity (41-45)	0.24	8.95	26.74	18.87	13.97	10.61	20.62
API Gravity (46-50)	0	16.3	25.58	18.78	13.27	10.44	15.61
API Gravity (51-55)	0	25.94	41.54	15.14	7.09	4.52	5.74
API Gravity (56-60)	0	44.2	28	14.42	9.09	3.16	1.12
API Gravity (60+)	0.3	56.9	31	6	4	1.6	0.3

CHAPTER 5

DATA PROCESSING AND INTERPRETATION

In the previous chapter, it was established that the molar flow values from ProMax simulations of a suite of oils with known API gravity were used to build a relationship between known HAWK values (S1_1, S1_2, S1_3, S1_4, S1_5 S1_6) from the IS1 experiment, and the unknown API gravity. This chapter is a discussion on the iterative process used to build this relationship and the possible advantages and drawbacks of each iteration.

5.1. HAWK data processing

Prior to interpretation, the raw FID signal at different IS1 temperatures from the HAWK has to be processed. The data processing involves calculating the area under the curve and normalizing the area with the total IS1 values. There are two kind of samples used on the IS1 experimentations of the HAWK. Table 5.1 provides information about the samples used in the experimentation of the HAWK. Note that samples are taken from three different producing wells, in two basins. These samples represent all the three major reservoir types (sandstone, carbonate, and shale). Some artificial samples are prepared by adding oil of known API gravity to sandstone and carbonate rock. Attempts to saturate shale with oil were not successful as the porosity and permeability are naturally low in such rocks (Table 5.2).

One of the major concerns in reliability and accuracy of resulting data from the experiment was that the lithology of the rock may affect the boiling points of the hydrocarbon molecules in the oven (during incremental pyrolysis). This was addressed by experimenting with different lithology

mixtures containing the same oil artificially added to the mineral matrix. The sandstone and carbonate samples containing the same oil had similar results when normalized (See Appendix D and Appendix E). The sandstone samples had a higher FID signal in the raw data because the sandstone absorbed a larger quantity of oil by the virtue of its high relative pore space when compared to the carbonate rock. Apart from these samples, a set of four source rock samples were also tested on the HAWK using the IS1 method (Appendix E). The raw result (FID signal) was taken as an output from the HAWK and processed to find the area under the curve of the FID signal at different IS1 temperatures using a software called "R". The area under the curve is calculated using the calibration with known area under the curve, as mentioned in Chapter 4. The graphical output of the software "R" is given in Figure 5.1. These data were taken and further normalized with the IS1 values (S1_1, to S1_6) to get the final results as provided in Appendix E.

5.2. Interpretation

The most straightforward method of building a relationship between API gravity and boiling points is by plotting the summation of the product of the molar flow values, IS1 temperature, and API gravity.

$$T\alpha = (V\_1*50)+(V\_2*100)+(V\_3*150)+(V\_4*200)+(V\_5*250)+(V\_6*300) \quad (5)$$

where

$T\alpha$ = Average temperature of a sample in degrees celsius (°C)

V_1 = Molar flow (Kmol/min) at 50°C

V_2 = Molar flow (Kmol/min) at 100°C

V_3 = Molar flow (Kmol/min) at 150°C

V_4 = Molar flow (Kmol/min) at 200°C

V_5 = Molar flow (Kmol/min) at 250°C

V_6 = Molar flow (Kmol/min) at 300°C

The values of V_1 to V_6 are obtained from the results of ProMax simulations. Plotting API gravity versus Tα, the best fit trend line was a straight line with an R^2 value of 0.74 (as shown in Figure 5.2). A trend of the normal distribution with varying mean and standard deviation in the simulation results (see Appendix C) was observed. In trying to understand the distribution of different API gravity oils, the results from the simulations were fit on a normal distribution using the MathCad software[1]. Plotting the API gravity versus Tmean (from the best fit normal distribution), the best fit trend line was of a straight line with an R^2 value of 0.70 (as shown in Figure 5.3). Note that in both the plots (Figures 5.2 and 5.3), there is not a unique temperature value associated for API gravity values between 30 and 50. Attempts to predict the API gravity of the oil by analyzing a particular sample on HAWK (IS1) and plotting API gravity versus Tα and API gravity versus Tmean were unsuccessful.

Lastly, to observe the ratio of hydrocarbon molecules vaporizing at IS1 temperatures, a ternary plot was created. The values S-heavy (Sh), S-medium (Sm), and S-lights (Sl) were calculated and denote the amount the sample vaporized at 50°C+100°C, 150°C+200°C, and 250°C+300°C temperatures, respectively. Appendix F provides the values of Sh, Sm, and Sl of the ProMax simulations results. The ternary plot of Sh, Sm, and Sl is shown in Figure 5.4a and 5.4b. It can be observed from the ternary plot that although it follows a trend from heavy oils (having more Sh and Sm) to light oils (having more of Sl and Sm), there is no clear segregation in the area occupied by samples of API gravity ranging from 30 to 50. The IS1 experimental results from the HAWK for ternary plots are provided in Appendix G. The ternary plots of these data are shown in Figure 5.5a, 5.5b, and 5.6. From Figure 5.5a and 5.5b, it is evident that the ternary plot is also not an accurate method to predict API gravity from the boiling points.

[1] Calculation performed by Dr. Terry A. Ring and communicated via private communication.

After examining the three interpretative relationships (API gravity V/S Tα, API gravity V/S Tmean, and ternary plot of Sh, Sm, and Sl), though there is some correlation between boiling points and API gravity, prediction of API gravity strictly by measuring boiling points of hydrocarbon molecules in the sample between the range of 50° to 300° HAWK (IS1 method) is not possible. This is because boiling point of hydrocarbon molecules is a function of the strength and number of bonds that are associated with the molecules. Every crude oil contains a specific ratio of paraffinic, naphthenic, and aromatic compounds. They can be estimated using FTIR techniques (fourier transform infra-red)[2]. However, that alone would not address the problem. For example, within an aromatic compound, a single aromatic ring structure has a lower boiling point when compared to a compound with more than one aromatic ring structure, yet both fall in the same classification as aromatic compounds (Tissot and Welte, 1978, 333-368). Due to a wide variety of different combinations of hydrocarbon molecules (paraffinic, naphthenic, and aromatic) in a particular rock sample from residual oil in core or cuttings, simply measuring the boiling points of the sample will not provide a unique solution to the density of the oil. In addition to the use of boiling points, another parameter that is a function of density should be used in order to accurately predict the API gravity of oil in the rock. From the *Handbook of Physics and Chemistry* (Haynes, 2014), it was evident that the refractive index has a direct correlation with the density. Figure 5.7 shows the density of some of the most commonly found petroleum molecules plotted against refractive index and boiling points. The increasing size of the data points is a function of carbon chain length (carbon number) and the color of the data points is indicative of the type of structure the molecule is associated with (paraffinic, naphthenic, and aromatic). It is clear from the plot in Figure 5.7 that the boiling point is a function of carbon number and refractive index is a function of density. Hence, previously in all the three temperature and density (API gravity) relationships

[2] CalTech FTIR. 2016. Surface FTIR. *The Molecular Materials Research Center*, (http://mmrc.caltech.edu/FTIR/FTIR.html).

that were built, the solution was always nonunique. The density and boiling point plot in Figure 5.7 supports this argument. For example, the data points in the ternary plot 5.5a and 5.5b are plotted not far from each other, yet the density of the oil was measured to be different. The molecules with varying density might have the same boiling point range, like how octane, cyclooctane, and ethylbenzene all fall in the boiling point range of 100°C-150°C, but vary in density. In such cases, refractive index can be used in association with the boiling point to accurately come up with the density of an oil, and in turn API gravity. Therefore, by using the FTIR before and after pyrolysis (by IS1 method) of the rock sample (core or cuttings), refractive index of an oil residing within the sample can be calculated. The required operating procedure followed experimentally to predict API gravity of petroleum in the rock includes performing an FTIR test on the sample followed by IS1 experiment and then use the sample to perform an FTIR test again. In this way, the refractive index of rock, bitumen, and kerogen will be canceled out as background interference values and just the refractivity of the oil will be measured. After attaining the refractive index of the oil and the IS1 values, a ternary plot can then be created with the IS1 values and a fourth parameter of refractive index can be added in the ternary plot. Using the FTIR in combination with IS1 is still going to be a fast and simple operating procedure. In this way, the initial objectives to build a robust and cost-effective analytical technique to predict the API gravity of oil in the rock remain the same and are achievable. In conclusion, with the information provided above, it can be stated that a correlative relationship between boiling point and density can be bridged by using refractive index as an additional parameter in the interpretations.

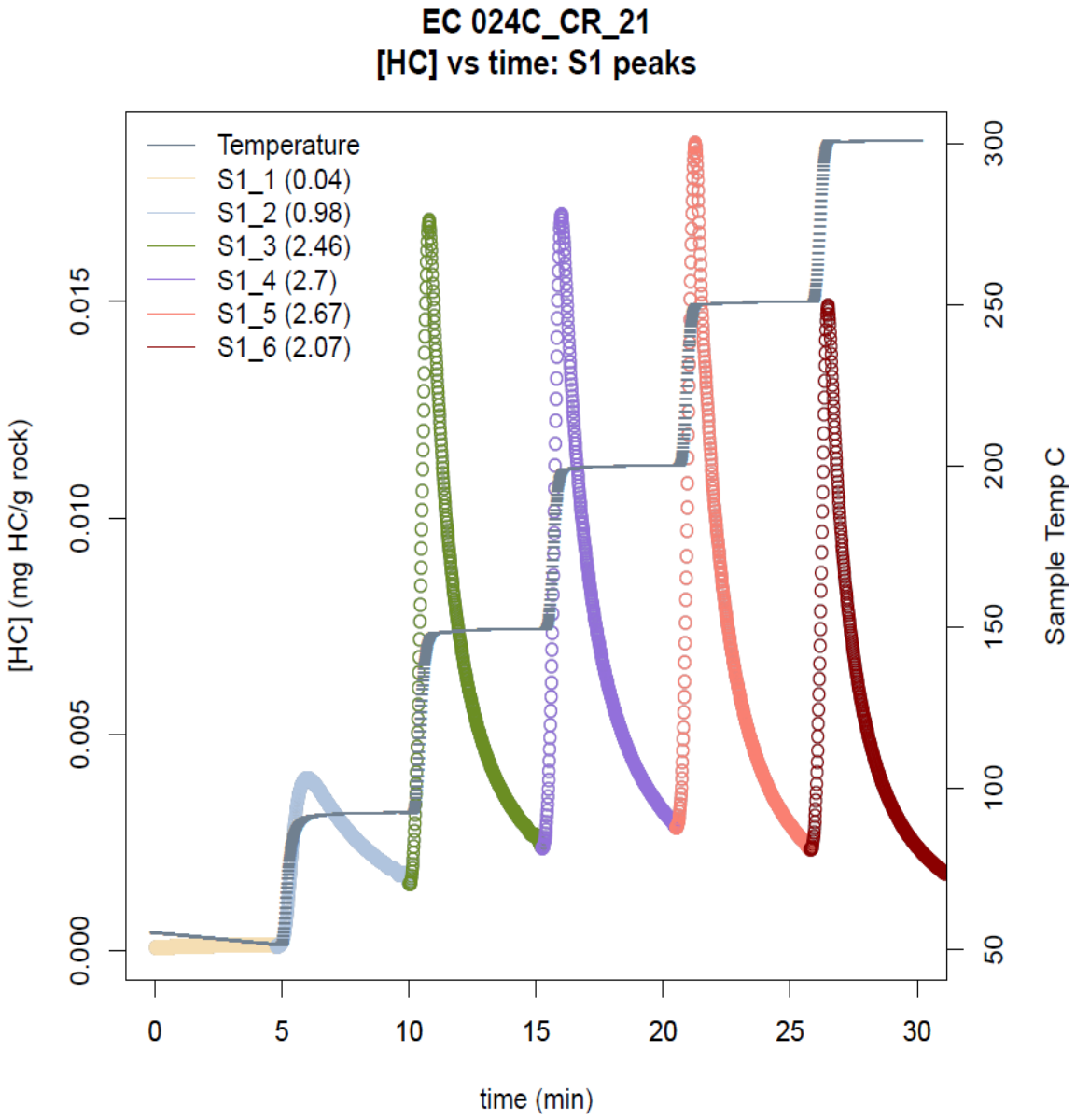

Figure 5.1: Processed FID signal with the area under the curve calculated using the software "R" result of a sample experiment on IS1.

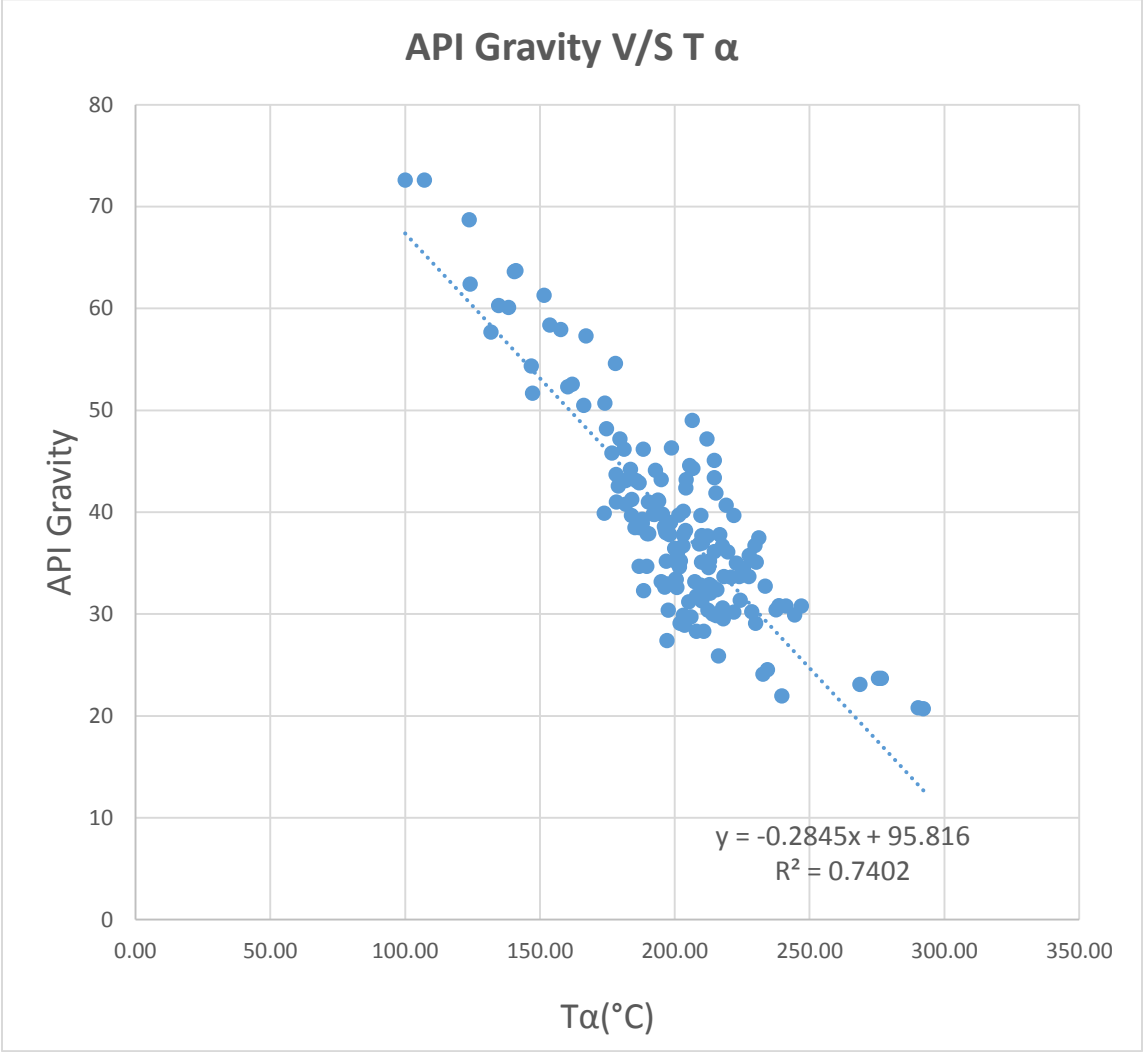

Figure 5.2: A straight line correlation of API gravity versus Tα, showing scatter in the data points between the API gravity values of 30 to 50.

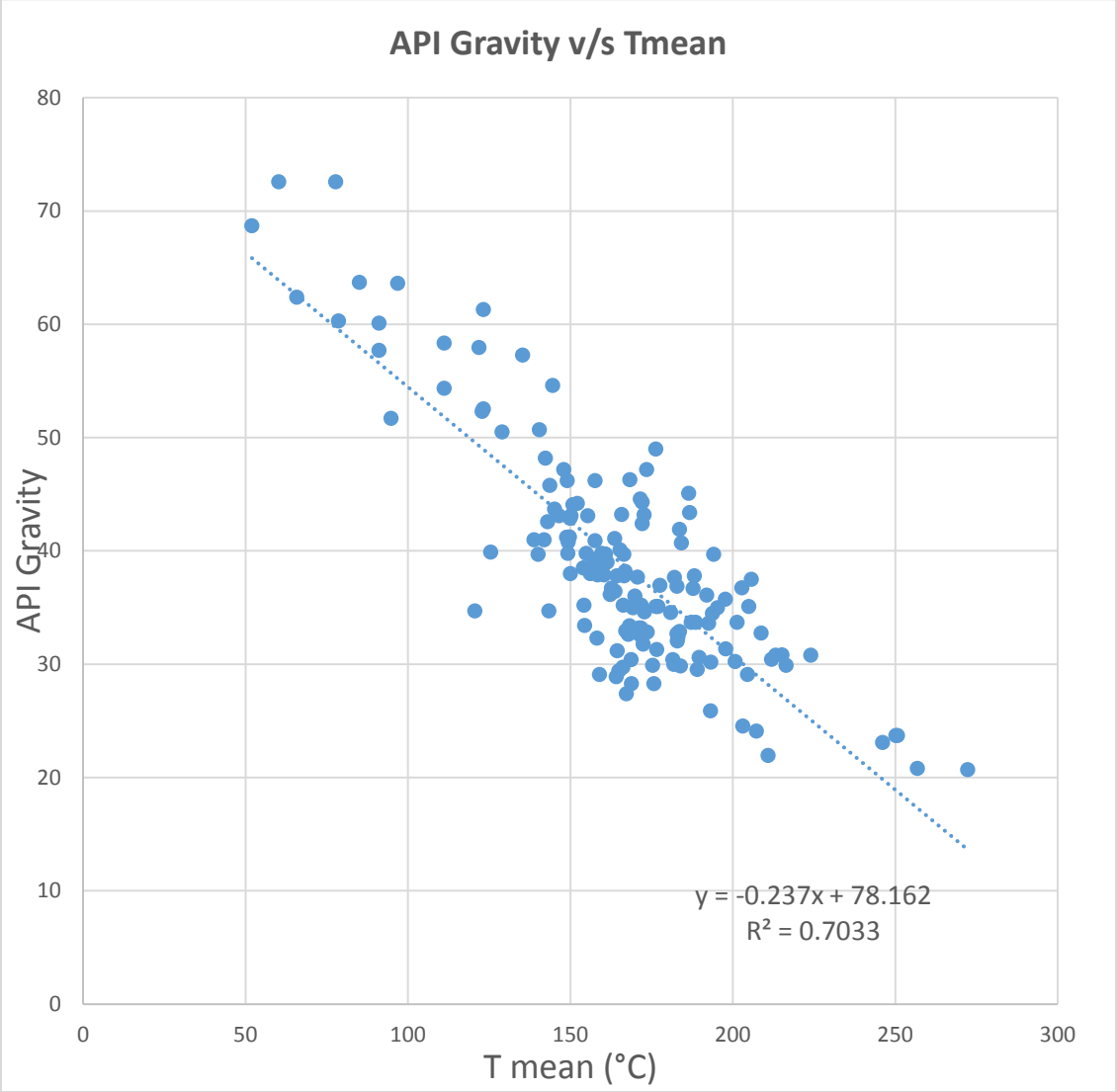

Figure 5.3: A straight line correlation of API gravity versus T mean, showing scatter in the data points between the API gravity values of 30 to 50.

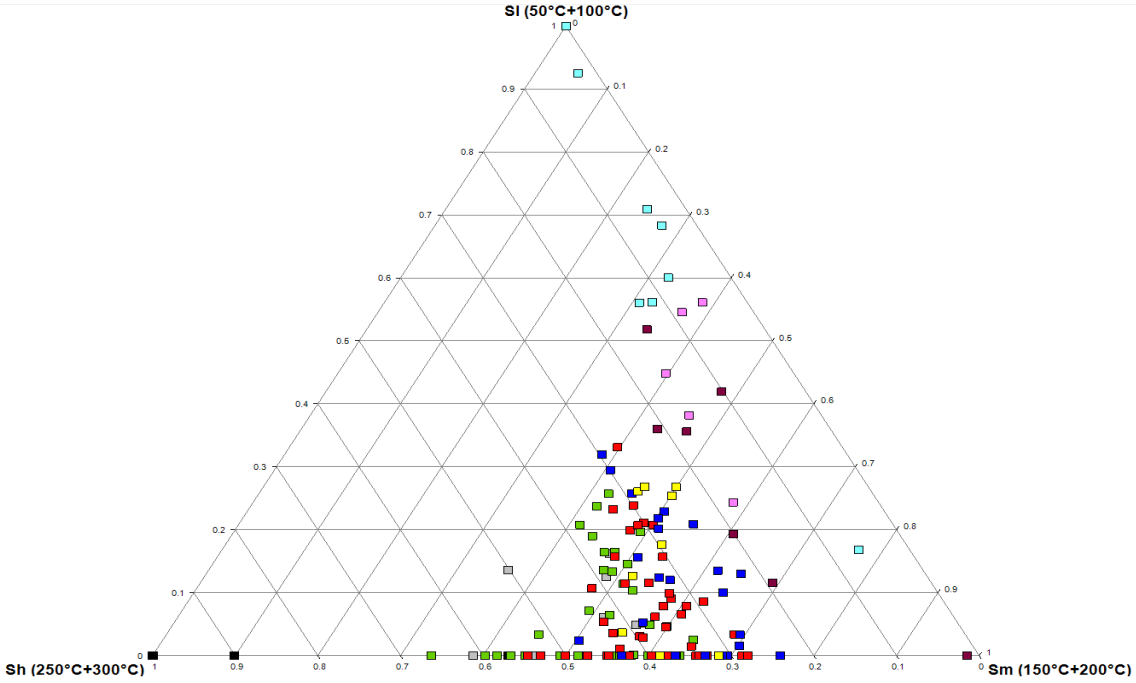

(a)

API Gravity (20-25)	
API Gravity (26-30)	
API Gravity (31-35)	
API Gravity (36-40)	
API Gravity (41-45)	
API Gravity (46-50)	
API Gravity (51-55)	
API Gravity (56-60)	
API Gravity (60+)	

(b)

Figure 5.4: Ternary plot of Sh, Sm, and Sl, showing the fractions of petroleum released at three different temperature ranges of the simulations, (a) Indicating API gravity groups overlapping in one particular area on the ternary plot (labeled in Figure 5.4b) and, (b) Table showing the legends for Figure 5.4a.

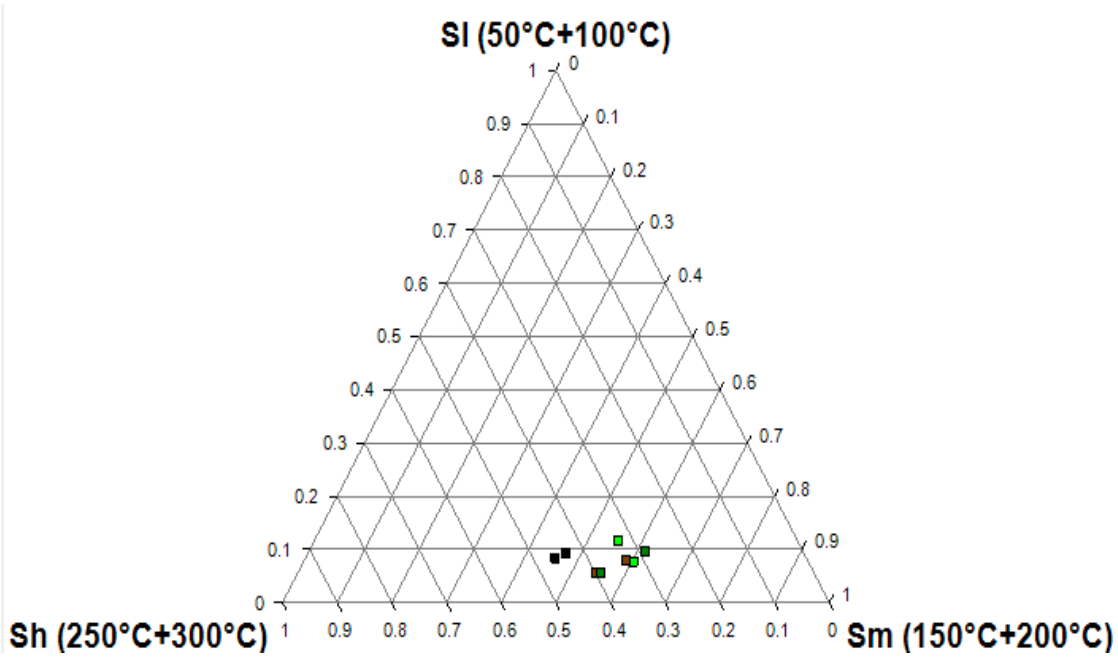

(a)

API Gravity (21)	
API Gravity (31.9)	
API Gravity (40.9)	
API Gravity (53.5)	

(b)

Figure 5.5: Ternary plot of Sh, Sm, and Sl, showing the fractions of petroleum released at three different temperature ranges of the samples experimented on HAWK™ using IS1 method, (a) Indicating the overlap of different API gravity in one nonunique area on the ternary plot (labeled in Figure 5.5b). (b): Legend for Figure 5.5a

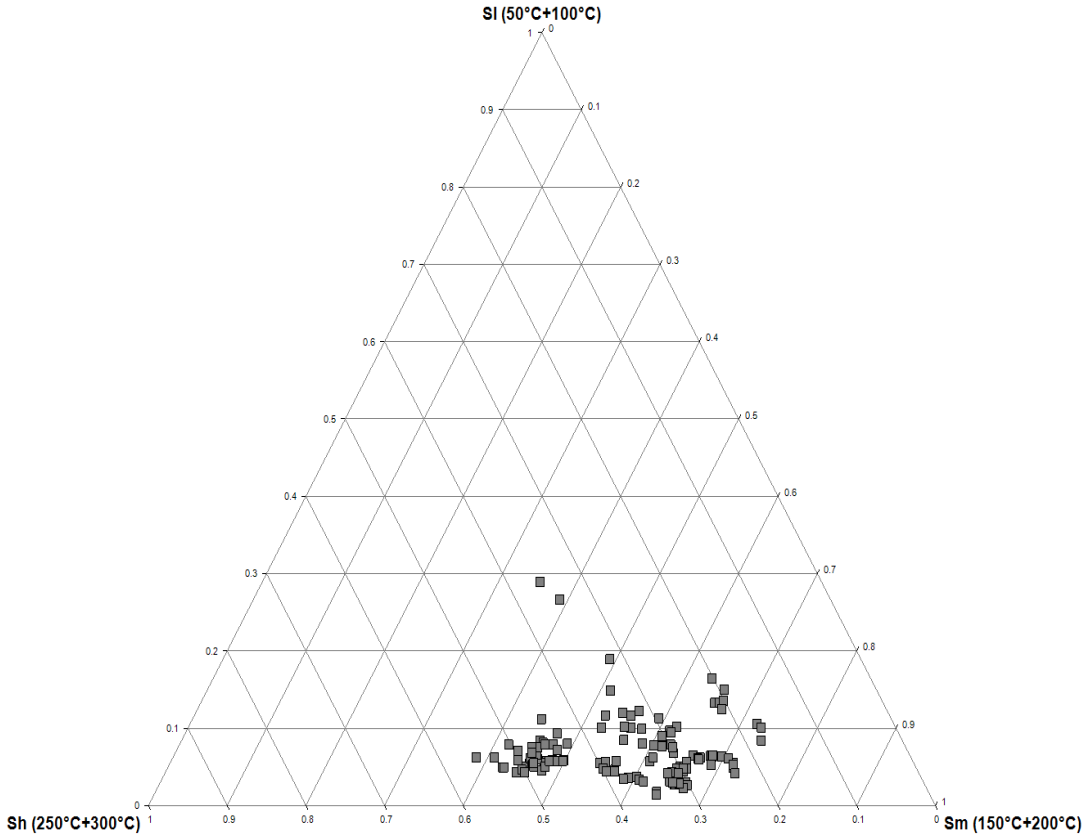

Figure 5.6: Ternary plot of Sh, Sm and Sl, showing the fractions of petroleum released at three different temperature ranges of samples experimented on HAWK™ using IS1 method, indicating the experimental results falling in a not unique API gravity range.

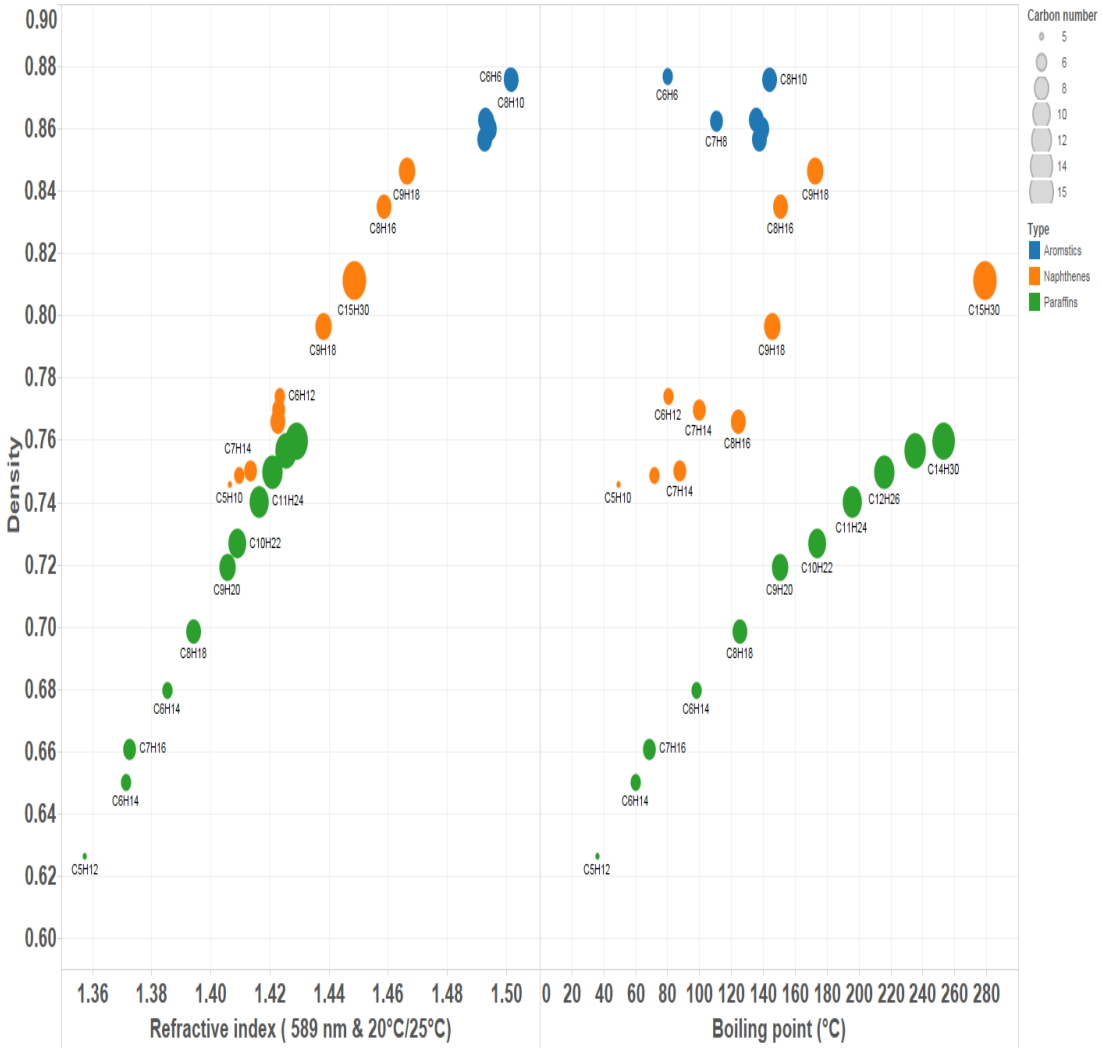

Figure 5.7: Commonly found hydrocarbons molecules plotted with Density versus refractive index and boiling points, showing a direct correlation between density and refractive index, and direct correlation of density and boiling points of the carbon numbers of a hydrocarbon molecules.

Table 5.1: List of real-world samples used to experiment on the HAWK.

Well API#	Basin	Location Name	Sample Type	location_type	avg_depth	depth_unit	Geologic_unit	Remarks	Country
4301950019	Paradox	Fidelity CCU #26-3	Core	Well	7397.9	ft	Cane Creek Shale Unit A	Anhydrate; Grand County	United States
4301950019	Paradox	Fidelity CCU #26-3	Core	Well	7399.5	ft	Cane Creek Shale Unit A	Silty Dolomite Shale; Grand County	United States
4301950019	Paradox	Fidelity CCU #26-3	Core	Well	7400.2	ft	Cane Creek Shale Unit A	Silty Dolomite; Grand County	United States
4301950019	Paradox	Fidelity CCU #26-3	Core	Well	7402.5	ft	Cane Creek Shale Unit A	Silty Dolomite with Anhydrate ; Grand County	United States
4301950019	Paradox	Fidelity CCU #26-3	Core	Well	7406.5	ft	Cane Creek Shale Unit A	Silty Dolomite Shale; Grand County	United States
4301950019	Paradox	Fidelity CCU #26-3	Core	Well	7415.5	ft	Cane Creek Shale Unit B	Silty Dolomite; Grand County	United States
4301950019	Paradox	Fidelity CCU #26-3	Core	Well	7417.1	ft	Cane Creek Shale Unit B	Silty Dolomite; Grand County	United States
4301950019	Paradox	Fidelity CCU #26-3	Core	Well	7418.8	ft	Cane Creek Shale Unit B	Silty Dolomite; Grand County	United States
4301950019	Paradox	Fidelity CCU #26-3	Core	Well	7412.1	ft	Cane Creek Shale Unit B	Silty Dolomite; Grand County	United States

Table 5.1 Continued

Well API#	Basin	Location Name	Sample Type	location_type	avg_depth	depth_unit	Geologic_unit	Remarks	Country
43 0195 0019	Paradox	Fidelity CCU #26-3	Core	Well	7424.5	ft	Cane Creek Shale Unit B	Silty Dolomite; Grand County	United States
43 037 30165	Paradox	Texaco Aneth Unit #E418	Core	Well	5957.2	ft	Gothic Shale	San Juan County	United States
43 037 30165	Paradox	Texaco Aneth Unit #E418	Core	Well	5958.9	ft	Gothic Shale	San Juan County	United States
43 037 30165	Paradox	Texaco Aneth Unit #E418	Core	Well	5961.5	ft	Gothic Shale	San Juan County	United States
43 037 30165	Paradox	Texaco Aneth Unit #E418	Core	Well	5962.5	ft	Gothic Shale	San Juan County	United States
43 037 30165	Paradox	Texaco Aneth Unit #E418	Core	Well	5963.1	ft	Gothic Shale	San Juan County	United States
43 037 0165	Paradox	Texaco Aneth Unit #E418	Core	Well	5966.2	ft	Gothic Shale	San Juan County	United States
43 0373 0165	Paradox	Texaco Aneth Unit #E418	Core	Well	6023.3	ft	Desert Creek fm.	San Juan County	United States
43 037 30165	Paradox	Texaco Aneth Unit #E418	Core	Well	6025.3	ft	Desert Creek fm.	San Juan County	United States
43 0373 0165	Paradox	Texaco Aneth Unit#E418	Core	Well	6026.5	ft	Desert Creek fm.	San Juan County	United States

Table 5.1 Continued

Well API#	Basin	Location Name	Sample Type	location_type	avg_depth	depth_unit	Geologic_unit	Remarks	Country
4303730165	Paradox	Texaco Aneth Unit #E418	Core	Well	6027.3	ft	Desert Creek fm.	San Juan County	United States
4303730165	Paradox	Texaco Aneth Unit #E418	Core	Well	6028.7	ft	Desert Creek fm.	San Juan County	United States
4303730165	Paradox	Texaco Aneth Unit #E418	Core	Well	6030.2	ft	Desert Creek fm.	San Juan County	United States
4303730165	Paradox	Texaco Aneth Unit #E418	Core	Well	6031.2	ft	Desert Creek fm.	San Juan County	United States
4303730165	Paradox	Texaco Aneth Unit #E418	Core	Well	6032.7	ft	Desert Creek fm.	San Juan County	United States
4303730165	Paradox	Texaco Aneth Unit #E418	Core	Well	6038	ft	Desert Creek fm.	San Juan County	United States
4304130036	Utah Hingeline	Wolverine O&G Fed #17-3	Core	Well	6657.9	ft	Upper Navajo SS.	Sevier County	United States
4304130036	Utah Hingeline	Wolverine O&G Fed #17-3	Core	Well	6660.9	ft	Upper Navajo SS.	Sevier County	United States
4304130036	Utah Hingeline	Wolverine O&G Fed #17-3	Core	Well	6674.3	ft	Upper Navajo SS.	Sevier County	United States

Table 5.1 Continued

Well API#	Basin	Location Name	Sample Type	location_type	avg_depth	depth_unit	Geologic_unit	Remarks	Country
43 0430 036	Utah Hingeli	Wolverine O&G Fed #17-3	Core	Well	6679	ft	Upper Navajo SS.	Sevier County	United States
43 041 3003 6	Utah Hingeli ne	Wolverine O&G Fed #17-3	Core	Well	6813 .1	ft	Upper Navajo SS.	Sevier County	United States
43 041 3003 6	Utah Hingeli ne	Wolverine O&G Fed #17-3	Core	Well	6831 .9	ft	Upper Navajo SS.	Sevier County	United States

Table 5.2 : List of artificial samples used on to experiment on the HAWK.

Sample Name	Rock	Oil Added	API gravity
EC 024C_CR_21	Niobrara Chalk	EC 024C	21
EC 024C_SS_21	Sandstone	EC 024C	21
EC 037C_CR_53.5	Niobrara Chalk	EC 037C	53.3
EC 037C_SS_53.5	Sandstone	EC 037C	53.3
EC 038C_CR_31.9	Niobrara Chalk	EC 038C	31.9
EC 038C_SS_31.9	Sandstone	EC 038C	31.9
EC 049C_CR_40.9	Niobrara Chalk	EC 049C	40.9
EC 049C_SS_40.9	Sandstone	EC 049C	40.9

CHAPTER 6

APPLICATIONS

The ability to determine the API gravity of oil residing within the rock (source or reservoir rock) with a simple, fast, and economically viable method will widen the scope of knowledge for understanding the reservoir like never before. This is primarily because, there is no such existing technique in the industry today. This technology provides greater insight that characterizes oil experimentally, without putting the well into production. Consequently, there are a number of practical applications of this technology in petroleum engineering and petroleum geology, which are listed below.

6.1. Applications in petroleum engineering and in petroleum geology

- Understanding the quantity and quality oil in different formations in-situ.
- Identification of producible zones for perforations.
- Better correlation of well logs and understanding lateral extent of producing formations.
- Identification of pressure patterns in the formations by understanding the chemical composition of the oil in the rock.
- Predicting the in-situ location of the bubble point line.
- Predicting mobile and immobile zones in-situ by understanding the viscosity of the petroleum at reservoir conditions.
- Petroleum compositional modeling of a basin.

- Predicting the maturity of the source rock in comparison with the maturity of the oil produced.
- Understanding the source - oil correlations to better understand migration pathways.
- Sweet spot identification in exploration of both conventional and unconventional plays.
- Understanding the mobile hydrocarbon generation potential of a source rock.

CHAPTER 7

CONCLUSIONS

From the work done in this research, it can be stated that HAWK™ can be used to perform partial distillation oil in the rock, and that it is possible to experimentally predict the API gravity of oil residing in the rock (core, cutting, or outcrops). After analysis of results from HAWK experimentation on varying temperature rates, it can be stated that the change in the temperature rate from 25°C per minute to 50°C per minute makes little or no difference in the magnitude of the S2 peak in the HAWK pyrolysis. The TGA-MS experiments provide evidence that the molecules evaporating at Incremental S1 temperatures are petroleum. From the ProMax simulations and HAWK results, it can be stated that separation of pure petroleum can be achieved by altering the temperatures in pyrolysis of a rock. It can also be stated that the organic molecules evaporating at temperatures lower than or equal to 300°C in the HAWK are strictly petroleum compounds. Consequently, the simulations on ProMax and reservoir rock pyrolysis using the IS1 method prove that organic molecules vaporizing at temperatures higher than 300°C in any conventional pyrolysis instruments may include heavy petroleum molecules, bitumen, and kerogen. From the different attempts to interpret API gravity through boiling points in Chapter 5, it can be stated that while there is some correlation, prediction of API gravity of oil by strictly using boiling points of hydrocarbon molecules is not possible. From the explanations provided in Chapter 5, it can be concluded that using refractive index as another interpretative parameter is the most feasible and practical solution to bridge the gap between boiling points and density of petroleum. In conclusion,

the API gravity of a rock containing petroleum can be predicted by experimental results of HAWK and FTIR.

APPENDIX A

DATA COMPARING TEMPERATURE RATES

Table A.1. Pyrolysis data from Hawk with 50°C/min temperature rate.

Sample ID	Weight @ 50°C/min	S1 @ 50°C/min	S2 @ 50°C/min	S3 @ 50°C/min	Tmax @ 50°C/min	PI @ 50°C/min	Analysis date	Time	Calibration Name	Method	S1+S2 @ 50°C/min
1-Peterson i	75	0.64	8.51	0.41	435	0.07	30-Nov-15	3:27:59	11/27/2015 6:00	PyroS3 650_50 C/min	9.15
1-Peterson ii	76	0.6	8.21	0.37	435	0.07	30-Nov-15	3:47:42	11/27/2015 6:00	PyroS3 650_50 C/min	8.81
511/139/140 i	74.7	0.35	23.55	2.06	420	0.01	30-Nov-15	9:02:56	11/27/2015 6:00	PyroS3 650_50 C/min	23.9
511/139/140 ii	77.8	0.32	21.88	2.51	421	0.01	30-Nov-15	9:22:38	11/27/2015 6:00	PyroS3 650_50 C/min	22.2
EGI.Nov.2015.00038 i	77.1	2.33	1.32	0.24	477	0.64	1-Dec-15	3:35:02	11/27/2015 6:00	PyroS3 650_50 C/min	3.65
EGI.Nov.2015.00038 ii	74.1	2.37	1.33	0.21	477	0.64	1-Dec-15	3:54:41	11/27/2015 6:00	PyroS3 650_50 C/min	3.7
ELMOLINO1_2 i	72.6	0.03	0.28	0.33	441	0.09	1-Dec-15	2:01:55	11/27/2015 6:00	PyroS3 650_50 C/min	0.31
ELMOLINO1_2 ii	75.7	0.03	0.29	0.43	442	0.09	1-Dec-15	2:21:39	11/27/2015 6:00	PyroS3 650_50 C/min	0.32
O3 i	76.3	0.64	0.84	0.24	468	0.43	30-Nov-15	6:33:32	11/27/2015 6:00	PyroS3 650_50 C/min	1.48

Table A.1 Continued

Sample ID	Weight @ 50°C/min	S1 @ 50°C/min	S2 @ 50°C/min	S3 @ 50°C/min	Tmax @ 50°C/min	PI @ 50°C/min	Analysis date	Time	Calibration Name	Method	S1+S2 @ 50°C/min
O3 ii	77	0.64	0.87	0.29	467	0.42	30-Nov-15	6:53:12	11/27/2015 6:00	PyroS3 650_50 C/min	1.51
W2A i	76.5	3.03	6.15	0.33	455	0.33	30-Nov-15	10:35:46	11/27/2015 6:00	PyroS3 650_50 C/min	9.18
W2A ii	77.7	2.96	6.03	0.18	453	0.33	30-Nov-15	10:55:27	11/27/2015 6:00	PyroS3 650_50 C/min	8.99
WT i	74.5	0.22	8.04	0.43	417	0.03	30-Nov-15	5:00:50	11/27/2015 6:00	PyroS3 650_50 C/min	8.26
WT ii	76.9	0.21	8.17	0.36	418	0.02	30-Nov-15	5:20:29	11/27/2015 6:00	PyroS3 650_50 C/min	8.38

Table A.2. Pyrolysis data from Hawk with 25°C/min temperature rate.

Sample ID	Weight @ 25°C/min	S1 @ 50°C/min	S2 @ 25°C/min	S3 @ 25°C/min	Tmax @ 25°C/min	PI @ 25°C/min	Analysis date	Time	Calibration Name	Method	S1+S2 @ 25°C/min
1-Peterson i	76.4	0.73	8.91	0.36	433	0.08	30-Nov-15	3:01:16	11/27/2015 5:14	PyroS3 650	9.64
1-Peterson ii	76.5	0.74	9.73	0.36	434	0.07	30-Nov-15	2:34:33	11/27/2015 5:14	PyroS3 650	10.47
511/139/140 i	74	0.38	25.22	1.85	421	0.01	30-Nov-15	8:36:13	11/27/2015 5:14	PyroS3 650	25.6
511/139/140 ii	77.1	0.36	22.94	2.18	421	0.02	30-Nov-15	7:12:52	11/27/2015 5:14	PyroS3 650	23.3
EGI.Nov.2015.00038 i	70	2.77	1.48	0.27	479	0.65	1-Dec-15	3:08:06	11/27/2015 5:14	PyroS3 650	4.25
EGI.Nov.2015.00038 ii	75.9	2.65	1.56	0.3	479	0.63	1-Dec-15	2:41:21	11/27/2015 5:14	PyroS3 650	4.21

Table A.2 Continued

Sample ID	Weight @ 25°C/min	S1 @ 50°C/min	S2 @ 25°C/min	S3 @ 25°C/min	Tmax @ 25°C/min	PI @ 25°C/min	Analysis date	Time	Calibration Name	Method	S1+S2 @ 25°C/min
ELMOLINO1_2 i	76.1	0.05	0.39	0.36	437	0.12	30-Nov-15	11:41:53	11/27/2015 5:14	PyroS3 650	0.44
ELMOLINO1_2 ii	77.8	0.05	0.34	0.27	440	0.13	30-Nov-15	11:15:08	11/27/2015 5:14	PyroS3 650	0.39
O3 i	76.4	0.74	1	0.27	467	0.43	30-Nov-15	6:06:51	11/27/2015 5:14	PyroS3 650	1.74
O3 ii	73.8	0.7	0.92	0.23	467	0.43	30-Nov-15	5:40:09	11/27/2015 5:14	PyroS3 650	1.62
W2A i	77.6	3.35	6.65	0.29	452	0.33	30-Nov-15	10:09:01	11/27/2015 5:14	PyroS3 650	10
W2A ii	74	3.13	6.48	0.28	453	0.33	30-Nov-15	9:42:16	11/27/2015 5:14	PyroS3 650	9.61
WT i	76.4	0.24	8.49	0.36	417	0.03	30-Nov-15	4:34:08	11/27/2015 5:14	PyroS3 650	8.73
WT ii	75.3	0.23	8.39	0.44	417	0.03	30-Nov-15	4:07:23	11/27/2015 5:14	PyroS3 650	8.62

APPENDIX B

LIST OF WORLD OIL LIBRARY

Table B.1. List of world oil library with API gravity

Crude Oil Name	API
Aasgard Blend	50.7
Abu Blend	37.6
Agbami	47.2
Akpo Blend	46.2
Al Jurf	30.24
Alaskan North Slope	32.3
Alba	19.4
Algerian Condensate	68.7
Alvheim Blend	36.9
Anasuria	39.7
Angsi	40.17
Arabian Heavy	27.4
Arabian Light	33.4
Ardjuna	38
Asgard Blend	50.5
Azeri BTC	36.7
Azeri Light	35
Badak	39
Badin	44.6
Barrow Island	37.7
Bayu Undan Condensate	63.7
Beatrice	37.8
Bekapai	43.21
Belida	45.1
Benchamas	42.4
Beryl	38.6
Bintulu	37.67
Bonga	29.1
Bonny Light	33.61
Bontang	72.8
Brass River	34.56
Brent Blend	38.5

Table B.1 Continued	
Crude Oil Name	API
Bunga Kekwa	37.6
Cabinda	32.61
Cakerawala Condensate	52.55
Calypso	30.84
Captain	19.1
Cendor	41.7
Chinguetti	28.3
Cinta	31.1
Clair	23.7
Coco	30.4
Cold Lake Blend	19.6
Condensate NFC II	57.95
Cooper Basin	44.6
Cossack	48.2
CPC Blend	44.2
Cupiaga	43.11
Curlew	42.9
Cusiana	42.57
Dalia	23.1
Dansk Underground Consortium (DUC)	34.7
Dar Blend	25
Diyarbekir	31.99
Djeno	27.36
Doba Blend	21
Draugen	39.9
Dubai	30.4
Dulang	37.2
Duri	20.8
EA	35.09
Ekofisk	37.9
El Sharara	43.11
Eocene	18.4
Erha	33.7
Es Sider	36.71
Escalante	24.1
Escravos	33.7
Espo	34.62
F3FB Condensate	63.62
Flotta	34.7
Foinaven	26.8
Forcados	30.43
Forozan	29.73
Forties Blend	39.8
Frade	18
Galeota	42.4
Geragai Crude	43.1

Table B.1 Continued	
Crude Oil Name	API
Gimboa	23.7
Gippsland Blend	52.32
Girassol	30.2
Glinte	32.9
Grane	19.4
Griffin	54.6
Gulf of Suez	31.3
Gullfaks Blend	37.8
Hamaca	25.9
Handil	41.25
Harding	20.7
Heidrun	25
Hibernia Blend	35
Hidra	51.7
Hondo	19.4
Hondo Sandstone	35.2
Hoops Blend	31.2
Hungo Blend	28.3
Hydra	37.5
Isthmus	32.9
Jotun Blend	41
Kidurong	38.2
Kikeh	36.74
Kissanje Blend	29.84
Kole	32.06
Kuito	21.96
Kumkol	42.5
Kutubu	44.1
Labuan	29.92
Lavan	35.22
Legendre	43.2
Lokele	20.2
Lower Zakum	39.8
Mandji	29.54
Marib Light	43.7
Marine Light	34.5
Mars	28.9
Masa	44.3
Masila	31.36
Maya	21.5
Medanito	35.1
Minas	35
Miri Light	30.79
Mondo	29.9
Murban	39.73
Mutineer-Exeter	43.4

Table B.1 Continued	
Crude Oil Name	API
Nanhai Light	39.7
Nemba	39.79
Nile Blend	32.76
Njord	45.8
Nkossa Blend	41.1
Norne	30.8
North West Shelf	60.3
Olmeca	38.9
Oman	32.95
Ormen Lange	57.3
Oseberg	38.5
Oso Condensate	46.2
Pagerungan	61.3
Palanca	36.97
Penara Blend	37.7
Pennington	33.7
Pierce	37.8
Plutonio	33.2
Poseidon	29.1
Qatar Marine	32.65
Qua Iboe	35.22
Rabi Light	35.1
Ratawi	24.6
Rincon de los Sauces	36.1
Ruby	35.75
Sable Island Condensate	57.7
Saxi Batuque	32.83
Schiehallion Blend	25.5
Senipah Condensate	54.37
Seria Light	36.15
Sharjah	64.8
Siberian Light	37.8
Sirri	33.43
Skua	41.9
Sleipner Condensate	62.4
Snohvit Condensate	60.1
Sokol	39.7
Souedie	23.12
South Pars Condensate	58.36
Southern Green Canyon	29.4
Stag	18.3
Statfjord Blend	39.3
Syrian Light	38.24
Tantawan	42.4
Tapis	46.3
Tempa Rossa	20.4

Table B.1 Continued	
Crude Oil Name	API
Tengiz	47.2
Terengganu	72.6
Terra Nova	33.2
Thevenard Island	40.7
Thunder Horse	32.7
Triton Blend	36.03
Troll Blend	32.4
Umm Shaiff	36.45
Upper Zakum	34
Ural	31.78
Varg	37.9
Vasconia	24.55
Volve	30
West Seno	38
West Texas Intermediate	40.8
Western Desert	41
Woollybutt	49
Wytch Farm	41.2
Xikomba	34.7
Yoho	40.1
Zafiro Blend	30.6
Zakhum Lower	40.91

APPENDIX C

PLOTS OF MOLAR FLOW VERSUS IS1 TEMPERATURE OF DIFFERENT SET OF API GRAVITY (PROMAX SIMULATION RESULTS)

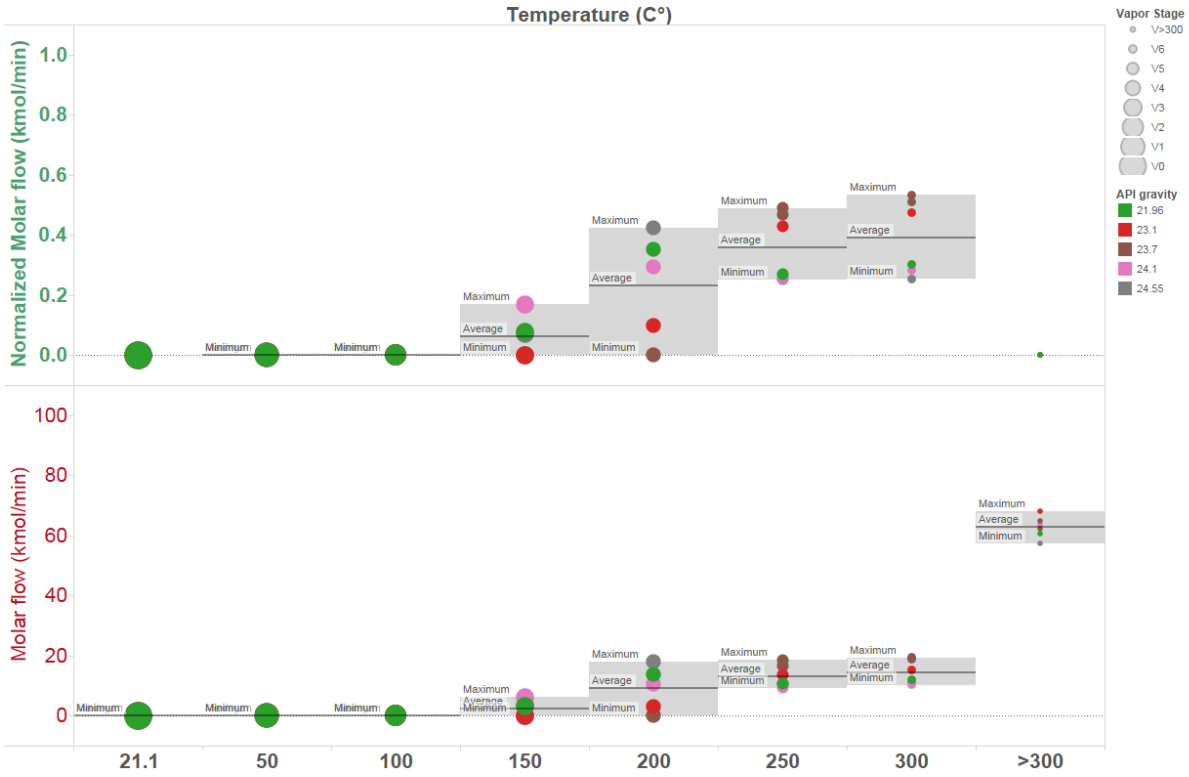

Figure C.1: Molar flow and normalized molar flow (kmol/min) of vapor phase versus temperature (°C) of oils with API gravity ranging from 20 to 25.

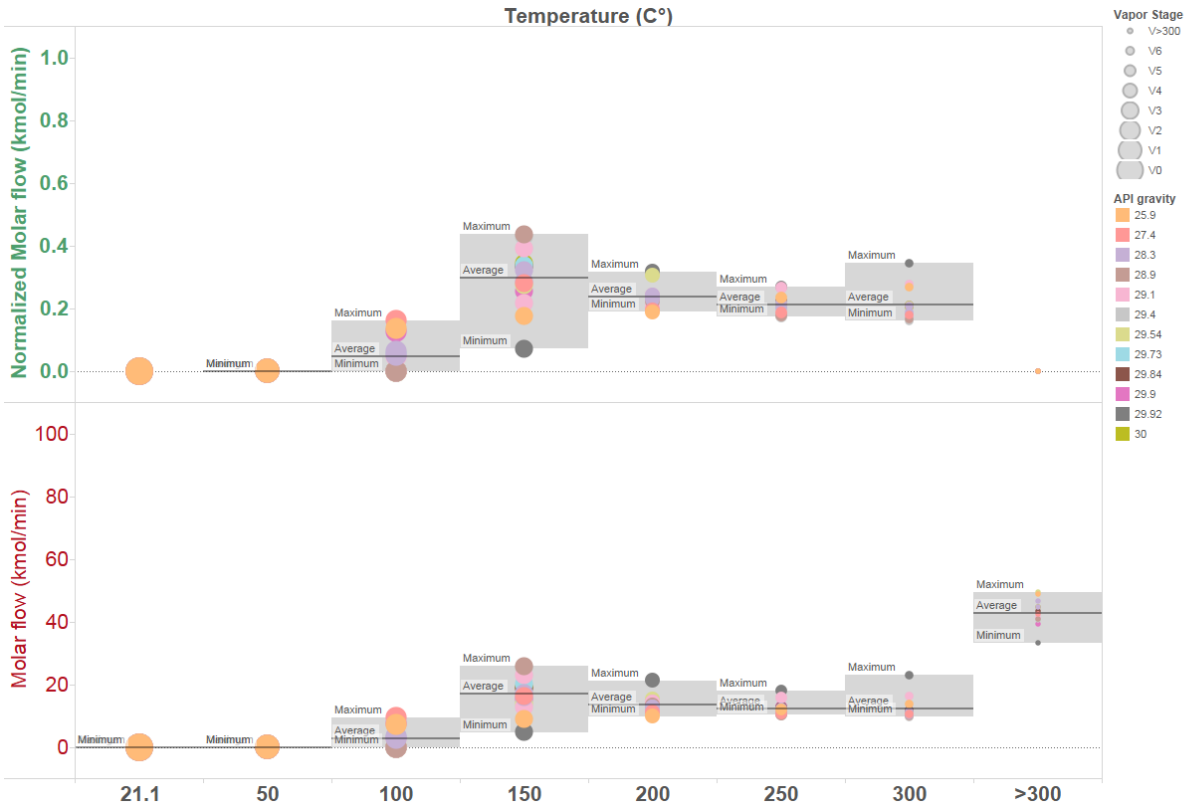

Figure C.2**:** Molar flow and normalized molar flow (kmol/min) of vapor phase versus temperature (°C) of oils with API gravity ranging from 26 to 30.

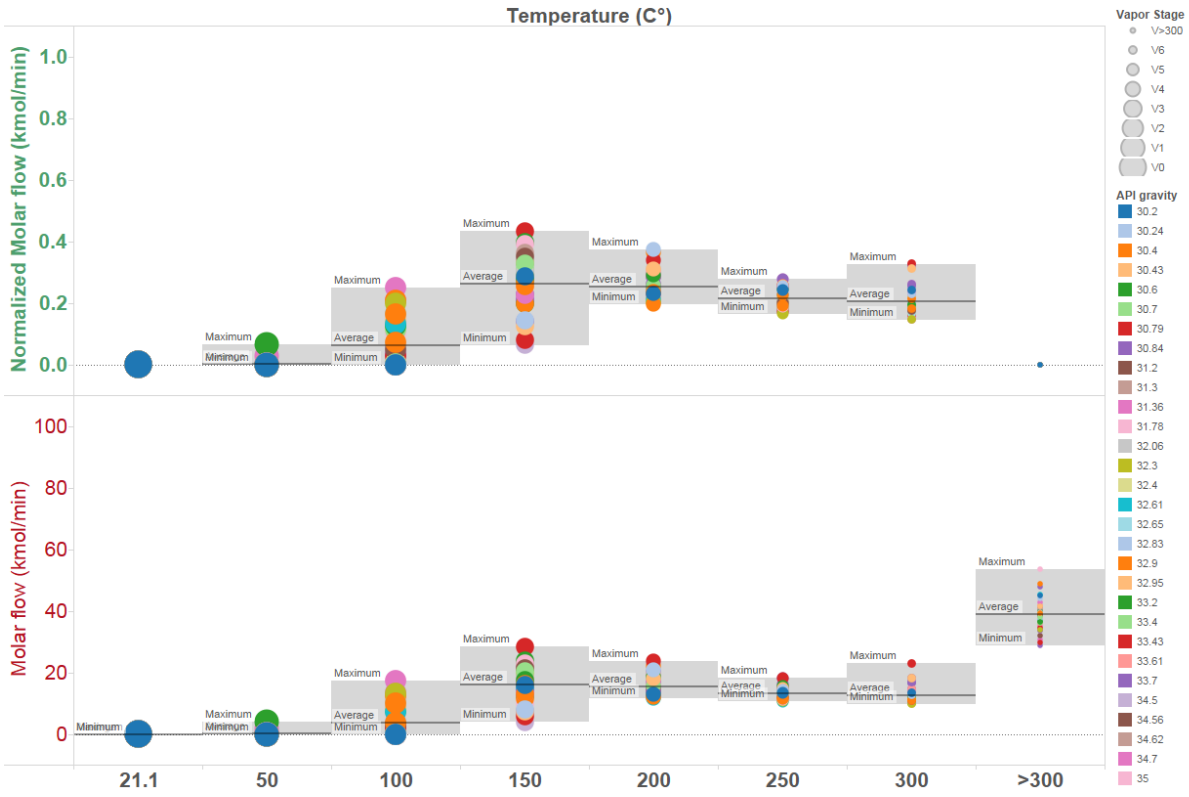

Figure C.3: Molar flow and normalized molar flow (kmol/min) of vapor phase versus temperature (°C) of oils with API gravity ranging from 31 to 35.

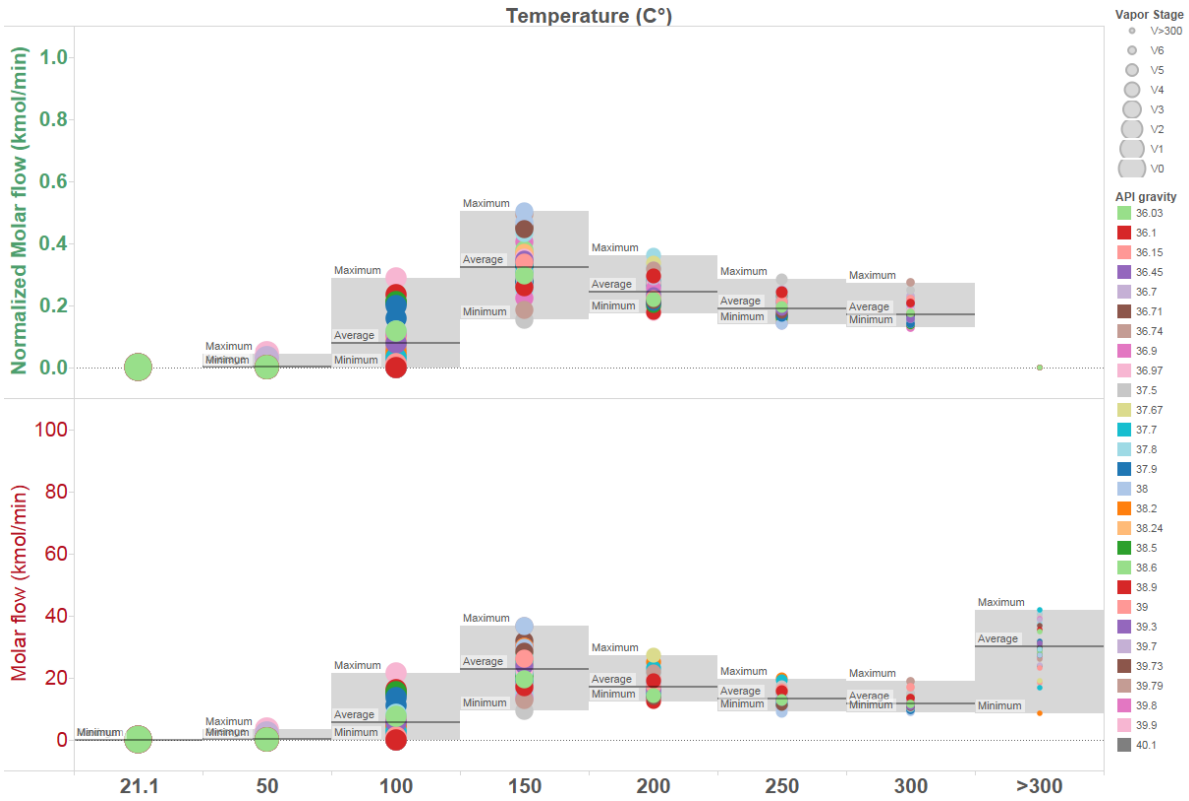

Figure C.4: Molar flow and normalized molar flow (kmol/min) of vapor phase versus temperature (°C) of oils with API gravity ranging from 36 to 40.

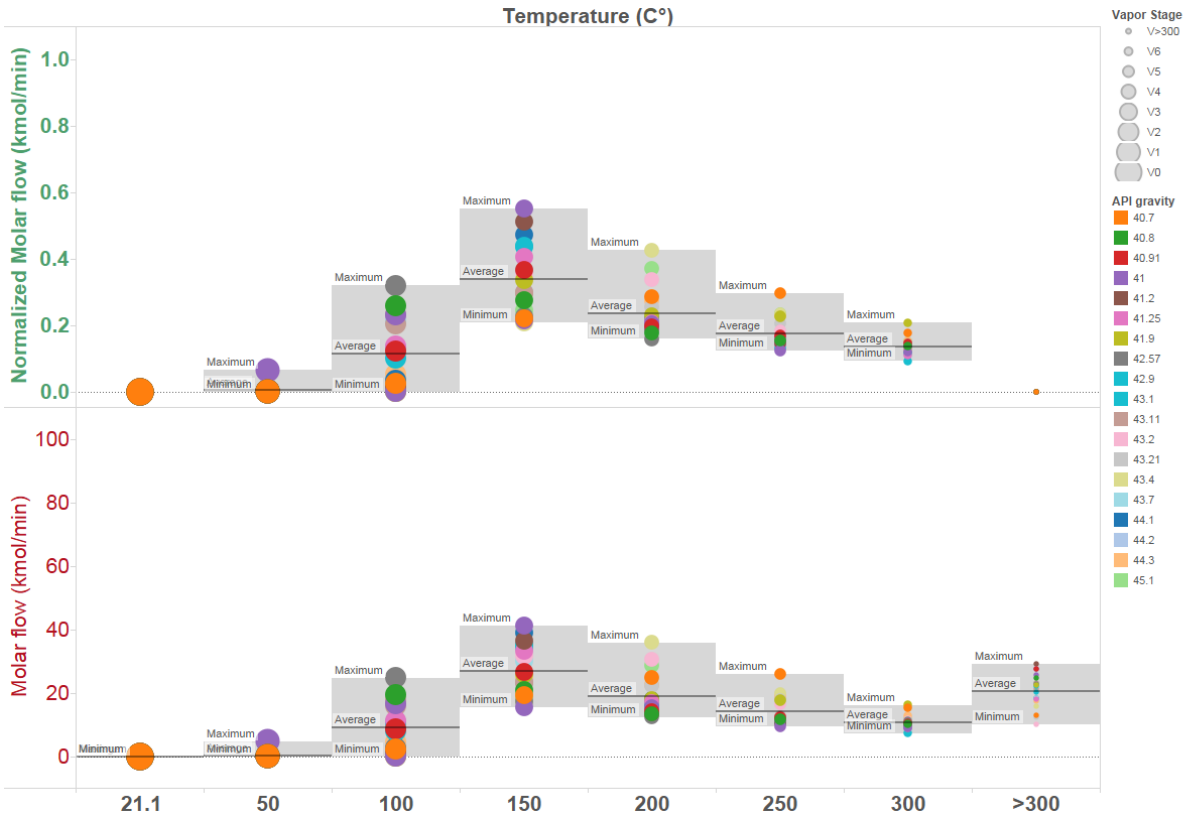

Figure C.5: Molar flow and normalized molar flow (kmol/min) of vapor phase versus temperature (°C) of oils with API gravity ranging from 41 to 45.

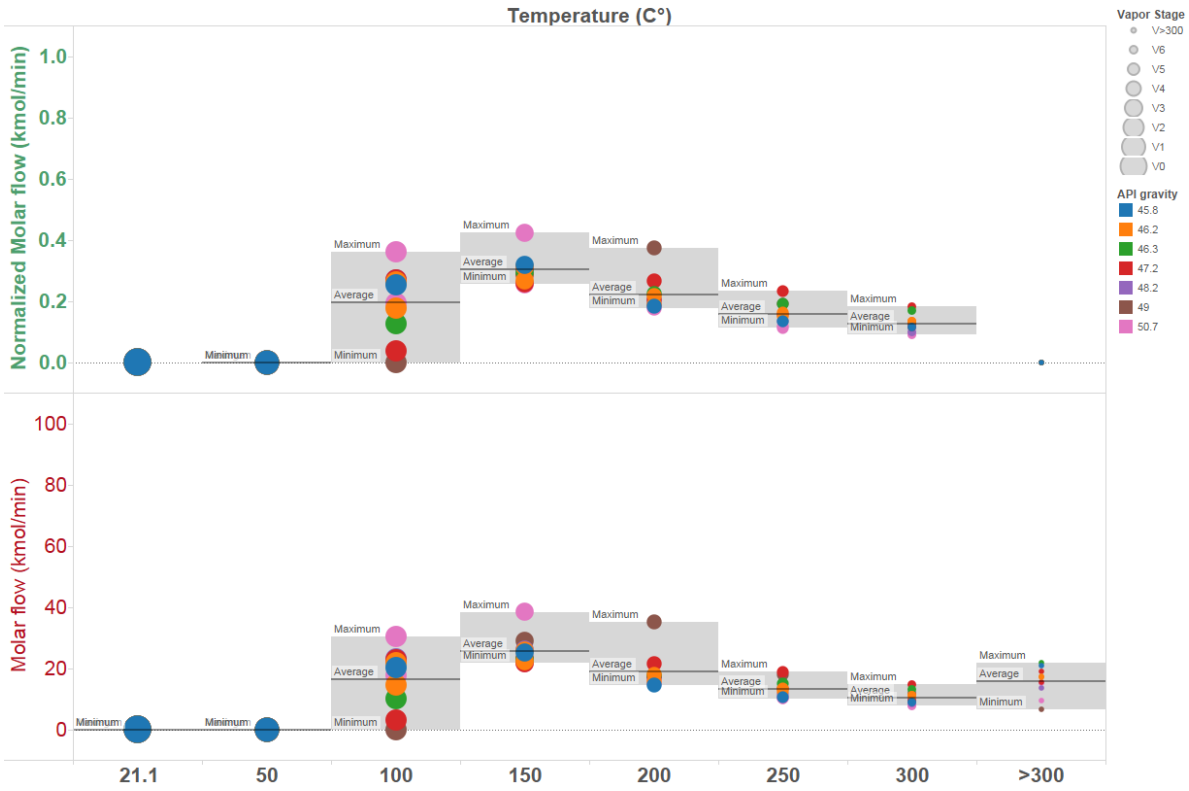

Figure C.6: Molar flow and normalized molar flow (kmol/min) versus temperature (°C) of oils with API gravity ranging from 46 to 50.

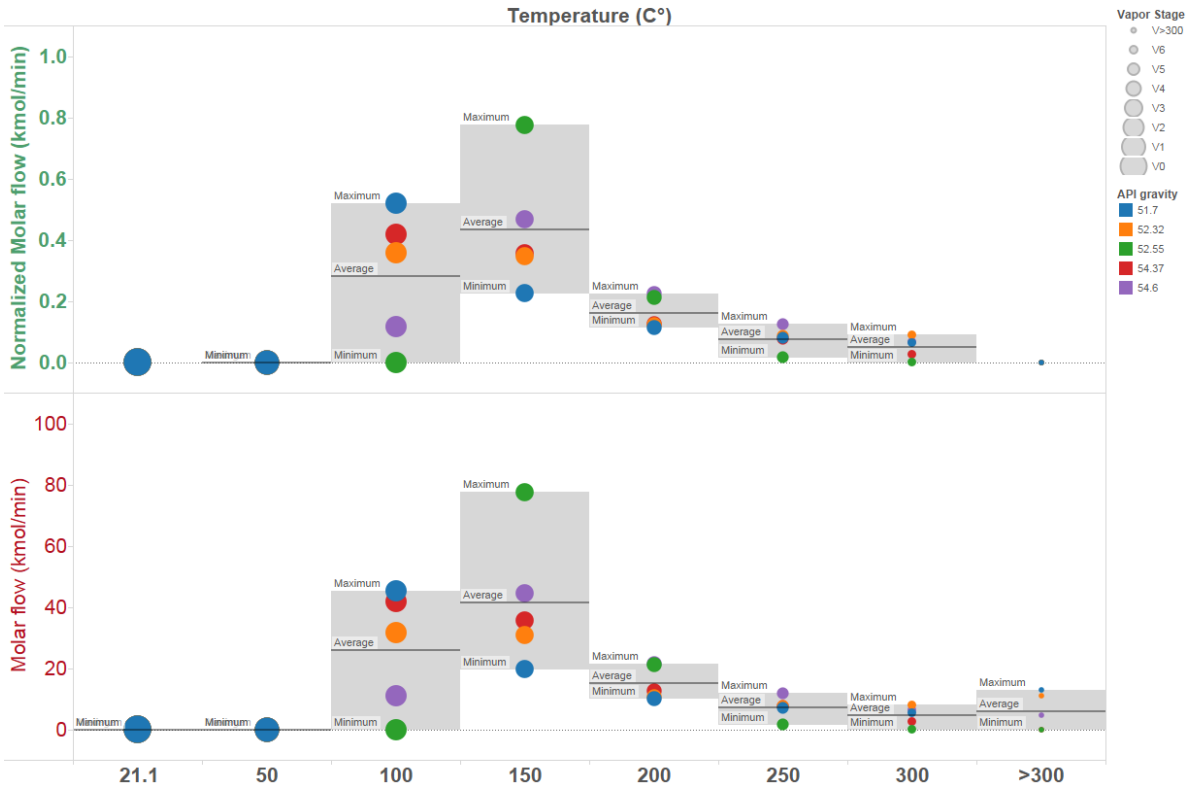

Figure C.7: Molar flow and normalized molar flow (kmol/min) of vapor phase versus temperature (°C) of oils with API gravity ranging from 51 to 55.

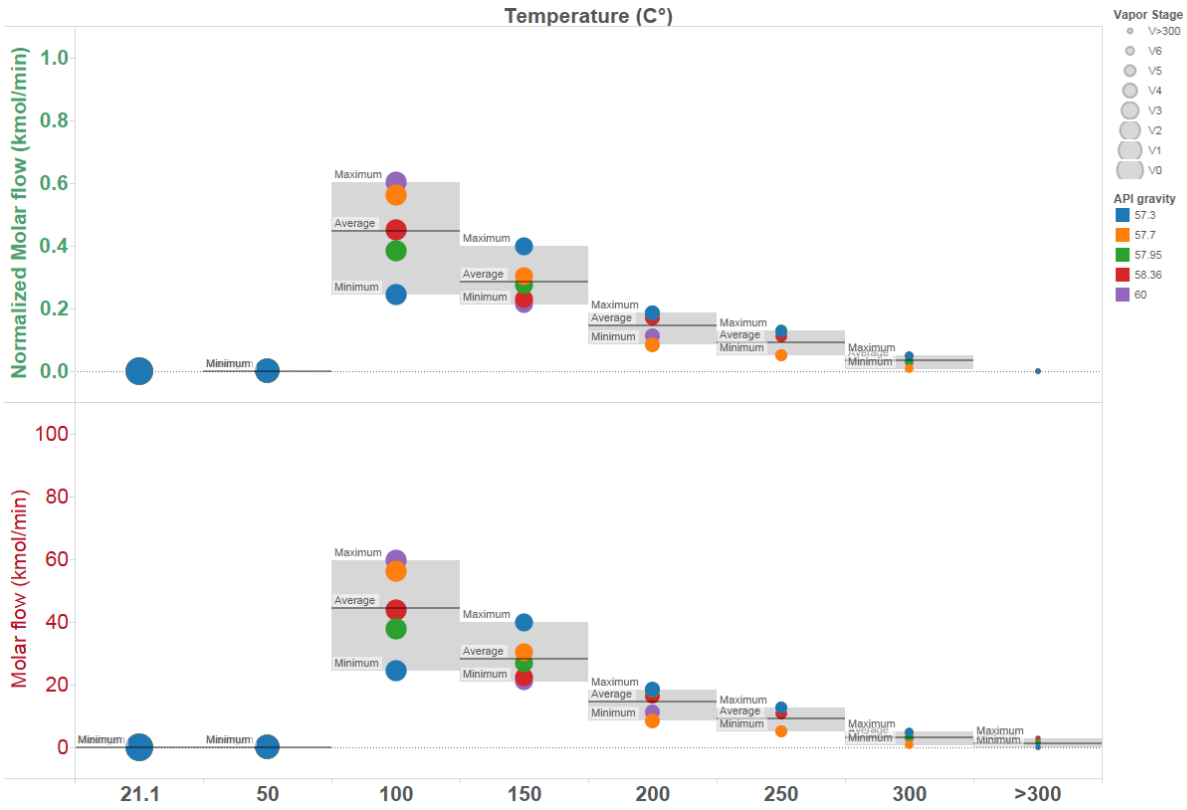

Figure C.8: Molar flow and normalized molar flow (kmol/min) of vapor phase versus temperature (°C) of oils with API gravity ranging from 56 to 60.

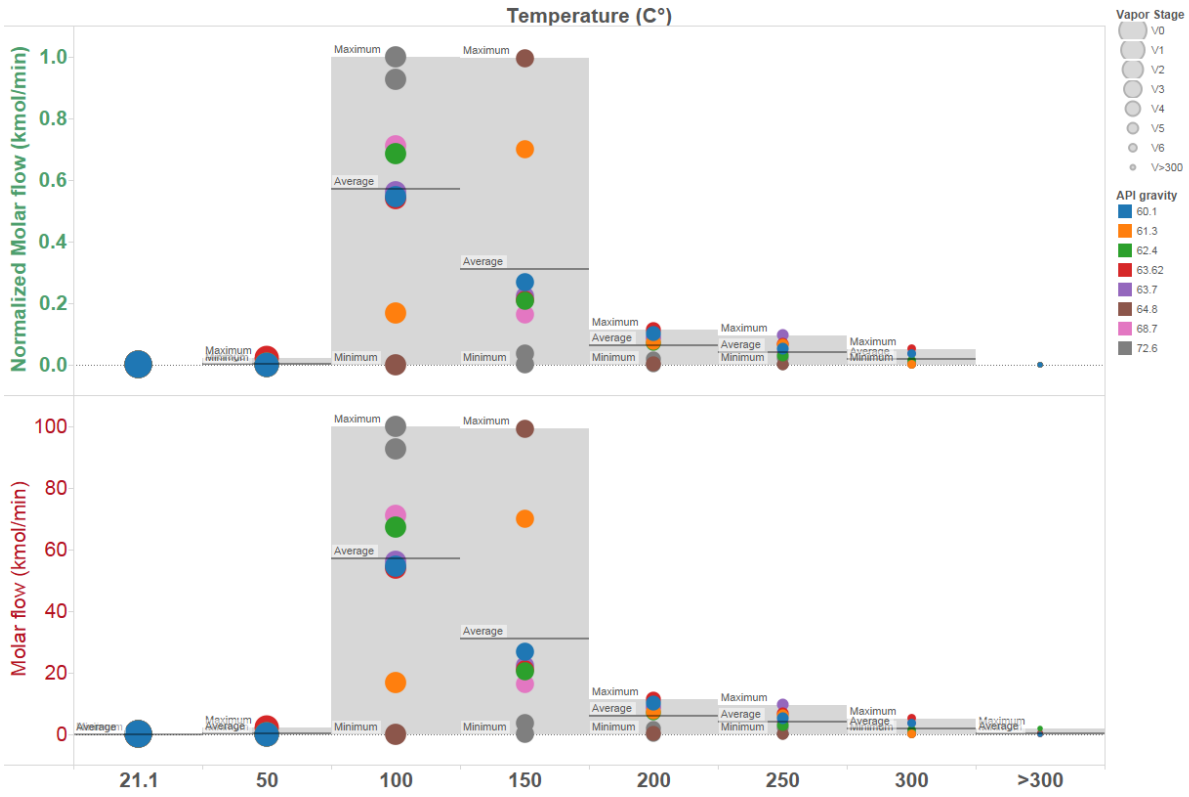

Figure C.9: Molar flow and normalized molar flow (kmol/min) of vapor phase versus temperature (°C) of oils with API gravity above 60.

Table C.1: Simulations results in normalized molar flow of vapor phase at IS1 temperatures (50°C to 300°C) of different oils.

Sample ID	API gravity	Molar flow (Kmol/min) 50°C	Molar flow (Kmol/min) 100°C	Molar flow (Kmol/min) 150°C	Molar flow (Kmol/min) 200°C	Molar flow (Kmol/min) 250°C	Molar flow (Kmol/min) 300°C
		V_1	V_2	V_3	V_4	V_5	V_6
Oil 106_Harding_20.7	20.7	0	0	0	0.001	0.16	0.84
Oil 77_Duri_20.8	20.8	0	0	0	0	0.194	0.806
Oil 121_Kuito_21.96	21.96	0	0	0.077	0.353	0.269	0.301
Oil 68_Dalia_23.1	23.1	0	0	0	0.099	0.428	0.473
Oil 58_Clair_23.7	23.7	0	0	0	0	0.466	0.534
Oil 96_Gimdoa_23.7	23.7	0	0	0	0	0.489	0.511
Oil84_Escalante_24.1	24.1	0	0	0.168	0.293	0.256	0.283
Oil 198_Vasconia_24.55	24.55	0	0	0.072	0.422	0.252	0.254
Oil 104_Hamaca_25.9	25.9	0	0.136	0.173	0.189	0.234	0.268

Table C.1 Continued							
Sample ID	API gravity	Molar flow (Kmol/min) 50°C	Molar flow (Kmol/min) 100°C	Molar flow (Kmol/min) 150°C	Molar flow (Kmol/min) 200°C	Molar flow (Kmol/min) 250°C	Molar flow (Kmol/min) 300°C
		V_1	V_2	V_3	V_4	V_5	V_6
Oil 29_Arabian Heavy_27.4	27.4	0	0.162	0.279	0.193	0.187	0.179
Oil 56_chinguetti_28.3	28.3	0	0.049	0.32	0.24	0.203	0.188
Oil 113_Hungo Blend_28.3	28.3	0	0.061	0.286	0.229	0.218	0.205
Oil 132_Mars_28.9	28.9	0	0	0.435	0.223	0.176	0.166
Oil 45_Bonga_29.1	29.1	0	0	0.217	0.242	0.265	0.276
Oil 160_Poseidon_29.1	29.1	0	0.047	0.39	0.208	0.18	0.174
Oil 181_Southern Green Canyon_29.4	29.4	0	0	0.428	0.237	0.174	0.16
Oil 129_Mandji_29.54	29.54	0	0	0.273	0.303	0.215	0.209
Oil 91_Forozan_29.73	29.73	0	0.051	0.337	0.231	0.202	0.179

Table C.1 Continued							
Sample ID	API gravity	Molar flow (Kmol/min) 50°C	Molar flow (Kmol/min) 100°C	Molar flow (Kmol/min) 150°C	Molar flow (Kmol/min) 200°C	Molar flow (Kmol/min) 250°C	Molar flow (Kmol/min) 300°C
		V_1	V_2	V_3	V_4	V_5	V_6
Oil 119_Kissanja Blend_29.84	29.84	0	0	0.332	0.237	0.221	0.21
Oil 139_Mondo_29.9	29.9	0	0.125	0.253	0.233	0.211	0.178
Oil 124_Labuan_29.92	29.92	0	0	0.071	0.317	0.269	0.344
Oil 199_Voive_30	30	0	0	0.343	0.236	0.218	0.203
Oil 98_Girassol_30.2	30.2	0	0	0.286	0.231	0.242	0.241
Oil 22_Al Jurf_30.24	30.24	0	0	0.144	0.374	0.254	0.229
Oil 59_Coco_30.4	30.4	0	0.071	0.255	0.237	0.224	0.212
Oil 75_Dubai_30.4	30.4	0	0.164	0.268	0.196	0.19	0.181
Oil 90_Forcados_30.43	30.43	0	0	0.124	0.309	0.257	0.31

Table C.1 Continued							
Sample ID	API gravity	Molar flow (Kmol/min) 50°C	Molar flow (Kmol/min) 100°C	Molar flow (Kmol/min) 150°C	Molar flow (Kmol/min) 200°C	Molar flow (Kmol/min) 250°C	Molar flow (Kmol/min) 300°C
		V_1	V_2	V_3	V_4	V_5	V_6
Oil 207_Zafiro Blend_30.6	30.6	0	0	0.272	0.289	0.245	0.193
Oil 138_Miri Light_30.79	30.79	0	0	0.079	0.337	0.257	0.326
Oil 147_Norne_30.8	30.8	0	0	0.091	0.246	0.296	0.367
Oil53_Calypso_30.84	30.84	0	0	0.14	0.262	0.277	0.32
Oil 112_Hoops Blend_31.2	31.2	0	0.049	0.348	0.229	0.199	0.175
Oil 102_Gulf of Suez_31.3	31.3	0	0	0.361	0.26	0.196	0.183
Oil 134_Masila_31.36	31.36	0	0	0.225	0.291	0.251	0.232
Oil 196_Ural_31.7	31.78	0	0	0.39	0.241	0.187	0.182
Oil 120_Kole_32.06	32.06	0	0	0.303	0.312	0.203	0.182
Oil 23_Alaskan North Slope_32.3	32.3	0	0.197	0.29	0.201	0.164	0.147

Table C.1 Continued							
Sample ID	API gravity	Molar flow (Kmol/min) 50°C	Molar flow (Kmol/min) 100°C	Molar flow (Kmol/min) 150°C	Molar flow (Kmol/min) 200°C	Molar flow (Kmol/min) 250°C	Molar flow (Kmol/min) 300°C
		V_1	V_2	V_3	V_4	V_5	V_6
Oil 194_Troll Blend_32.4	32.4	0	0.003941	0.33	0.233	0.215	0.218
Oil 51_Cabinda_32.61	32.61	0	0.133	0.277	0.212	0.191	0.186
Oil 161_Qatar Marine_32.65	32.65	0	0.165	0.264	0.212	0.192	0.166
Oil 192_Thunder Horse_32.7	32.7	0	0.001614	0.326	0.255	0.225	0.192
Oil 144_Nile Blend_32.76	32.76	0	0	0.16	0.29	0.263	0.286
Oil 168_Saxi Batuque_32.83	32.83	0	0.065	0.297	0.224	0.213	0.202
Oil 99_Glinte_32.9	32.9	0	0.208	0.197	0.216	0.197	0.182
Oil 115_Isthmus_32.9	32.9	0	0	0.272	0.362	0.202	0.164
Oil150_Oman_32.95	32.95	0	0.146	0.287	0.215	0.184	0.168

Table C.1 Continued							
Sample ID	API gravity	Molar flow (Kmol/min) 50°C	Molar flow (Kmol/min) 100°C	Molar flow (Kmol/min) 150°C	Molar flow (Kmol/min) 200°C	Molar flow (Kmol/min) 250°C	Molar flow (Kmol/min) 300°C
		V_1	V_2	V_3	V_4	V_5	V_6
Oil159_Plutonio_33.2	33.2	0	0	0.396	0.242	0.184	0.179
Oil 190_Terra Nova_33.2	33.2	0.065	0.125	0.197	0.24	0.204	0.169
Oil 30_Arabian Light_33.4	33.4	0	0.114	0.311	0.201	0.192	0.181
Oil 174_Sirri_33.43	33.43	0	0.025	0.433	0.208	0.172	0.161
Oil 46_Bonny Light_33.61	33.61	0	0	0.254	0.303	0.215	0.228
Oil 82_Erha_33.7	33.7	0	0.034	0.229	0.221	0.255	0.261
Oil 85_Escravos_33.7	33.7	0	0	0.299	0.256	0.227	0.218
Oil 157_Penningt on_33.7	33.7	0	0	0.21	0.283	0.254	0.253
Oil 131_Marine Light_34.5	34.5	0	0	0.062	0.537	0.229	0.172

Table C.1 Continued							
Sample ID	API gravity	Molar flow (Kmol/min) 50°C	Molar flow (Kmol/min) 100°C	Molar flow (Kmol/min) 150°C	Molar flow (Kmol/min) 200°C	Molar flow (Kmol/min) 250°C	Molar flow (Kmol/min) 300°C
		V_1	V_2	V_3	V_4	V_5	V_6
Oil 48_Brass River_34.56	34.56	0	0	0.329	0.285	0.193	0.193
Oil 86_Espo_34.62	34.62	0	0.136	0.266	0.212	0.199	0.187
Oil 69_DUC_34.7	34.7	0.006349	0.251	0.209	0.214	0.175	0.145
Oil 205_Xikomba_34.7	34.7	0.028	0.209	0.204	0.214	0.186	0.158
Oil 34_Azeri Light_35	35	0	0	0.261	0.254	0.251	0.234
Oil 108_ Hibernia Blend_35	35	0	0.104	0.304	0.224	0.197	0.17
Oil 78_EA_ 35.09	35.09	0	0	0.215	0.239	0.272	0.274
Oil 136_Medanito_35.1	35.1	0	0	0.353	0.274	0.2	0.174
Oil 163_Rabi Light_35.1	35.1	0	0.054	0.281	0.238	0.225	0.203
Oil 111_Hondo Sandstone_35.2	35.2	0	0.157	0.291	0.19	0.182	0.18

Table C.1 Continued							
Sample ID	API gravity	Molar flow (Kmol/min) 50°C	Molar flow (Kmol/min) 100°C	Molar flow (Kmol/min) 150°C	Molar flow (Kmol/min) 200°C	Molar flow (Kmol/min) 250°C	Molar flow (Kmol/min) 300°C
		V_1	V_2	V_3	V_4	V_5	V_6
Oil 125_Lavan_35.22	35.22	0	0.015	0.434	0.21	0.176	0.165
Oil 162_Qua Iboe_35.22	35.22	0	0.036	0.298	0.242	0.226	0.199
Oil166_Ruby_35.75	35.75	0	0	0.108	0.442	0.239	0.211
OIL 193_Triton Blend_36.03	36.03	0	0.115	0.296	0.218	0.195	0.176
Oil 165_Rincon de los Sauces_36.1	36.1	0	0	0.258	0.293	0.241	0.207
Oil 171_Seria Light_36.15	36.15	0	0.011	0.337	0.223	0.211	0.219
Oil 195_Umm Shaiff_36.45	36.45	0	0.079	0.346	0.233	0.186	0.157
Oil 33_Azeri BTC_36.7	36.7	0	0	0.289	0.288	0.21	0.214
Oil 83_Es Sider_36.71	36.71	0	0	0.445	0.212	0.174	0.168
Oil 118_kikeh_36.74	36.74	0	0	0.183	0.317	0.228	0.273

Table C.1 Continued							
Sample ID	API gravity	Molar flow (Kmol/min) 50°C	Molar flow (Kmol/min) 100°C	Molar flow (Kmol/min) 150°C	Molar flow (Kmol/min) 200°C	Molar flow (Kmol/min) 250°C	Molar flow (Kmol/min) 300°C
		V_1	V_2	V_3	V_4	V_5	V_6
Oil 26_Alvheim Blend_36.9	36.9	0	0.107	0.221	0.257	0.212	0.203
Oil 155_Palanca_36.97	36.97	0	0	0.352	0.27	0.197	0.181
Oil 114_Hydra_37.5	37.5	0	0	0.154	0.315	0.283	0.248
Oil 44_Bintulul_37.67	37.67	0	0	0.297	0.336	0.193	0.174
Oil 37_Barrow_37.7	37.7	0	0.031	0.297	0.277	0.23	0.165
Oil 103_Gullfaks Blend_37.8	37.8	0	0.116	0.307	0.236	0.187	0.155
Oil 158_Pierce_37.8	37.8	0	0	0.433	0.228	0.176	0.162
Oil 173_Siberian Light_37.8	37.8	0	0	0.244	0.359	0.215	0.182
Oil 79_Ekofisk_37.9	37.9	0	0.157	0.328	0.21	0.166	0.138

Table C.1 Continued							
Sample ID	API gravity	Molar flow (Kmol/min) 50°C	Molar flow (Kmol/min) 100°C	Molar flow (Kmol/min) 150°C	Molar flow (Kmol/min) 200°C	Molar flow (Kmol/min) 250°C	Molar flow (Kmol/min) 300°C
		V_1	V_2	V_3	V_4	V_5	V_6
Oil 197_Varg_37.9	37.9	0	0.199	0.273	0.205	0.168	0.155
Oil 31_Ardjuna_38	38	0	0	0.502	0.212	0.141	0.146
Oil 200_West Seno_38	38	0	0	0.468	0.252	0.141	0.139
Oil 117_Kiouroung_38.2	38.2	0	0.046	0.326	0.272	0.214	0.142
Oil 184_Syran Light_38.24	38.24	0	0.091	0.369	0.213	0.173	0.154
Oil 49_Brent Blend_38.5	38.5	0	0.208	0.304	0.198	0.155	0.135
Oil 152_Oseberg_38.5	38.5	0	0.211	0.281	0.208	0.162	0.138
Oil 43_Beryl_38.6	38.6	0	0.079	0.379	0.228	0.173	0.142
Oil 149_Olmeca_38.9	38.9	0	0.232	0.263	0.178	0.168	0.159
Oil 35_Badak_39	39	0	0.066	0.364	0.243	0.189	0.138

Table C.1 Continued							
Sample ID	API gravity	Molar flow (Kmol/min) 50°C	Molar flow (Kmol/min) 100°C	Molar flow (Kmol/min) 150°C	Molar flow (Kmol/min) 200°C	Molar flow (Kmol/min) 250°C	Molar flow (Kmol/min) 300°C
		V_1	V_2	V_3	V_4	V_5	V_6
Oil 183_Sttfiord Blend_39.3	39.3	0	0.207	0.276	0.208	0.167	0.142
Oil 27_Anasuria_ 39.7	39.7	0.028	0.211	0.249	0.213	0.163	0.136
Oil142_Nanhai Light_39.7	39.7	0	0	0.264	0.262	0.245	0.229
Oil 178_Sokol_39.7	39.7	0	0.029	0.325	0.254	0.206	0.186
Oil 140_Murban_39.73	39.73	0	0	0.451	0.22	0.176	0.153
Oil 143_Nemba_ 39.79	39.79	0	0.034	0.494	0.193	0.147	0.132
Oil 92_Forties Blend_39.8	39.8	0	0.086	0.405	0.218	0.164	0.127
Oil 128_Lower Zakum_39.8	39.8	0	0.099	0.366	0.21	0.177	0.148
Oil 74_Draugen_ 39.9	39.9	0.043	0.288	0.223	0.174	0.138	0.134
Oil206_Yoho_40.1	40.1	0	0.062	0.341	0.236	0.194	0.167

Table C.1 Continued							
Sample ID	API gravity	Molar flow (Kmol/min) 50°C	Molar flow (Kmol/min) 100°C	Molar flow (Kmol/min) 150°C	Molar flow (Kmol/min) 200°C	Molar flow (Kmol/min) 250°C	Molar flow (Kmol/min) 300°C
		V_1	V_2	V_3	V_4	V_5	V_6
Oil 191_Thevenard Island_40.7	40.7	0	0.024	0.219	0.285	0.295	0.177
Oil 201_West Texas Intermediate_40.8	40.8	0	0.258	0.276	0.175	0.154	0.137
Oil 208_Zakhum Lower_40.91	40.91	0	0.12	0.367	0.199	0.168	0.146
Oil 116_jotun Blend_41	41	0.065	0.23	0.213	0.193	0.162	0.137
Oil 202_ Western Desert_41	41	0	0	0.552	0.207	0.124	0.117
Oil 146_Nkossa Blend_41.1	41.1	0	0.156	0.298	0.211	0.178	0.157
Oil 204_Wytch Farm_41.2	41.2	0	0.016	0.512	0.19	0.145	0.137
Oil 105_Handil_41.25	41.25	0	0.135	0.406	0.21	0.141	0.108
Oil 175_Skua_41.9	41.9	0	0	0.335	0.232	0.226	0.207

Table C.1 Continued							
Sample ID	API gravity	Molar flow (Kmol/min) 50°C	Molar flow (Kmol/min) 100°C	Molar flow (Kmol/min) 150°C	Molar flow (Kmol/min) 200°C	Molar flow (Kmol/min) 250°C	Molar flow (Kmol/min) 300°C
		V_1	V_2	V_3	V_4	V_5	V_6
Oil 94_Galeota_42.4	42.4	0	0	0.353	0.342	0.175	0.13
Oil 67_Cusiana_42.57	42.57	0	0.32	0.225	0.159	0.152	0.145
Oil 66_Curlew_42.9	42.9	0	0.1	0.437	0.203	0.146	0.114
Oil 95_Geragai Crude_43.1	43.1	0	0.13	0.437	0.209	0.132	0.091
Oil 65_Cupiaga_43.11	43.11	0	0.229	0.299	0.206	0.144	0.123
Oil 80_El Sharana_43.11	43.11	0	0.202	0.295	0.216	0.161	0.126
Oil 126_Legende_43.2	43.2	0	0	0.351	0.337	0.183	0.128
Oil 40_Bekpai_43.21	43.21	0	0.124	0.297	0.254	0.205	0.12
Oil 141_Mutineer-Exeeter_43.4	43.4	0	0	0.207	0.425	0.235	0.133

Table C.1 Continued							
Sample ID	API gravity	Molar flow (Kmol/min) 50°C	Molar flow (Kmol/min) 100°C	Molar flow (Kmol/min) 150°C	Molar flow (Kmol/min) 200°C	Molar flow (Kmol/min) 250°C	Molar flow (Kmol/min) 300°C
		V_1	V_2	V_3	V_4	V_5	V_6
Oil 130_Marib Light_43.7	43.7	0	0.209	0.367	0.183	0.132	0.109
Oil 123_Kutubu_44.1	44.1	0	0.033	0.473	0.221	0.149	0.124
Oil 64_CPC Blend_44.2	44.2	0	0.219	0.3	0.203	0.153	0.126
Oil 133_Msa_44.3	44.3	0	0.053	0.295	0.272	0.229	0.152
Oil 36_Badin_44.6	44.6	0	0	0.377	0.292	0.173	0.158
Oil 41_Belida_45.1	45.1	0	0	0.245	0.369	0.234	0.152
Oil 145_Njord_45.8	45.8	0	0.254	0.319	0.183	0.132	0.113
Oil 21_Akpo Blend_46.2	46.2	0	0.176	0.311	0.217	0.163	0.133
Oil 153_Oso Condensate_46.2	46.2	0	0.261	0.268	0.189	0.149	0.133
Oil 186_Tapis_46.3	46.3	0	0.127	0.293	0.224	0.189	0.167

Table C.1 Continued							
Sample ID	API gravity	Molar flow (Kmol/min) 50°C	Molar flow (Kmol/min) 100°C	Molar flow (Kmol/min) 150°C	Molar flow (Kmol/min) 200°C	Molar flow (Kmol/min) 250°C	Molar flow (Kmol/min) 300°C
		V_1	V_2	V_3	V_4	V_5	V_6
Oil 20_Agbami_47.2	47.2	0	0.037	0.286	0.264	0.233	0.181
Oil188_Tenigiz_47.2	47.2	0	0.268	0.256	0.205	0.157	0.114
Oil 63_Cossack_48.2	48.2	0	0.268	0.302	0.197	0.134	0.099
Oil 203_Wollybutt_49	49	0	0	0.311	0.374	0.19	0.125
Oil 32_Asgard Blend_50.7	50.5	0	0.36	0.255	0.176	0.118	0.091
Oil 18_Aasgard Blend_50.7	50.7	0	0.193	0.423	0.183	0.112	0.089
Oil 109_Hadra_51.7	51.7	0	0.518	0.225	0.114	0.08	0.063
Oil 97_Gippsland Blend_52.32	52.32	0	0.356	0.347	0.121	0.086	0.09
Oil 52_Cakerawala Condensate_52.55	52.55	0	0	0.775	0.21	0.015	0

Table C.1 Continued							
Sample ID	API gravity	Molar flow (Kmol/min) 50°C	Molar flow (Kmol/min) 100°C	Molar flow (Kmol/min) 150°C	Molar flow (Kmol/min) 200°C	Molar flow (Kmol/min) 250°C	Molar flow (Kmol/min) 300°C
		V_1	V_2	V_3	V_4	V_5	V_6
Oil 170_Senipah Condensate_ 54.37	54.37	0	0.419	0.354	0.125	0.076	0.026
Oil 101_Griffin_ 54.6	54.6	0	0.116	0.467	0.225	0.124	0.068
Oil 151_Oman Lange_57.3	57.3	0	0.244	0.398	0.183	0.127	0.049
Oil 167_Sable IslandCondensate_57.7	57.7	0	0.561	0.302	0.083	0.049	0.005401
Oil 61_Condensate NFCII_57.95	57.95	0	0.382	0.273	0.185	0.128	0.032
Oil 180_South Pars Condensate_ 58.36	58.36	0	0.448	0.229	0.167	0.108	0.047
Oil 177_Snohvit Condensate_ 60.1	60.1	0	0.546	0.268	0.1	0.051	0.036
Oil 148 _North West Shelf_60	60.3	0	0.601	0.212	0.112	0.049	0.027

Table C.1 Continued							
Sample ID	API gravity	Molar flow (Kmol/min) 50°C	Molar flow (Kmol/min) 100°C	Molar flow (Kmol/min) 150°C	Molar flow (Kmol/min) 200°C	Molar flow (Kmol/min) 250°C	Molar flow (Kmol/min) 300°C
		V_1	V_2	V_3	V_4	V_5	V_6
Oil 154_Pagerugan_61.3	61.3	0	0.168	0.699	0.072	0.062	0
Oil 176_Sieipner Condensate_62.4	62.4	0	0.684	0.206	0.069	0.03	0.012
Oil 89_F3FB Condensate_63.62	63.62	0.022	0.539	0.21	0.114	0.065	0.05
Oil 38_Bayau Undan Condensate_63.7	63.7	0	0.56	0.221	0.087	0.095	0.036
Oil 25_Algerian Condensate_68.7	68.7	0	0.709	0.161	0.083	0.038	0.008802
Oil 47_Bontang_72.6	72.6	0	1	0	0	0	0
OIL 189_Terengganu_72.6	72.6	0	0.926	0.035	0.017	0.019	0.003801

APPENDIX D

RAW RESULTS OF HAWK EXPERIMENTS

Table D.1. Raw results of HAWK experiments using the IS1 method

Sample_id	mgHC.conc.S1_1	mgHC.conc.S1_2	mgHC.conc.S1_3	mgHC.conc.S1_4	mgHC.conc.S1_5	mgHC.conc.S1_6	mgHC.conc.S2
1 Peterson	0.028914878	0.072405741	0.190038386	0.348616278	0.339797126	0.307943685	8.350615734
Beebe Draw	0.024831547	0.073000091	0.287858607	0.523171165	0.471642503	0.317930131	2.680282344
EC 024C_CR_21	0.035784935	0.982001603	2.461346562	2.699571738	2.67075854	2.074330967	7.362546504
EC 024C_SS_21	0.042995008	2.368142861	6.145235239	6.900223883	7.416048369	5.74794855	16.97836979
EC 037C_CR_53.5	0.004712217	0.223389728	0.612427513	0.479663768	0.369530425	0.278448251	0.531359867
EC 037C_SS_53.5	0.005846334	0.368312835	1.320095779	1.585028793	1.036182127	0.498310424	0.989857169
EC 038C_CR_31.9	0.027235177	0.904645119	3.043036386	3.805873614	2.6340197	1.241387835	2.226617838
EC 038C_SS_31.9	0.043779711	1.323740384	5.862578579	7.612532625	6.583028836	3.27745752	3.344544997
EC 049C_CR_40.9	0.039455683	1.01405267	3.07059518	3.608142873	2.22878956	0.921002023	1.861836461
EC 049C_SS_40.9	0.026221566	1.031960671	4.133023715	6.175819612	5.281461688	2.017067608	2.665459973
EGI.Sep.2015.00032	0.005191585	0.033352123	0.091857432	0.056766794	0.028838171	0.018397496	0.116843603
EGI.Sep.2015.00033	0.005932215	0.095446199	0.621832955	0.494743722	0.229953931	0.153745473	0.482758736
EGI.Sep.2015.00034	0.007535479	0.203280859	1.708537961	1.750890082	1.147422678	0.928026805	5.627948667

Table D.1 Continued

Sample_id	mgHC.conc.S1_1	mgHC.conc.S1_2	mgHC.conc.S1_3	mgHC.conc.S1_4	mgHC.conc.S1_5	mgHC.conc.S1_6	mgHC.conc.S2
EGI.Sep.2015.00035	0.006137203	0.077220087	0.249855319	0.187734112	0.136163677	0.081542658	0.404656576
EGI.Sep.2015.00036	0.006882148	0.478237223	1.467894996	0.916804794	0.471658036	0.309379711	3.604985848
EGI.Sep.2015.00037	0.005291852	0.018474052	0.133047515	0.119212745	0.05689792	0.036815574	0.184540967
EGI.Sep.2015.00038	0.007812979	0.074139388	0.826791586	0.995449525	0.514354091	0.309423897	2.220005608
EGI.Sep.2015.00039	0.005737205	0.073702278	0.553308916	0.481089104	0.215680396	0.115653388	0.6178801 5
EGI.Sep.2015.00040	0.005703035	0.028447367	0.210441063	0.157062383	0.079719605	0.055505841	0.183429064
EGI.Sep.2015.00041	0.008594604	0.1927666	0.862131969	0.512703523	0.197904858	0.134429629	0.365643041
EGI.Sep.2015.00042	0.006058506	0.097642485	0.363443454	0.525982831	0.570328785	0.527528941	5.564065961
EGI.Sep.2015.00043	0.004980638	0.117907302	0.451539034	0.59115917	0.588483241	0.526066394	6.203083654
EGI.Sep.2015.00044	0.004812884	0.114880992	0.386746413	0.513220531	0.518941282	0.439077178	5.688215075
EGI.Sep.2015.00045	0.006647892	0.090654734	0.363801007	0.503606091	0.517534996	0.4396778	4.736720056
EGI.Sep.2015.00046	0.004913455	0.104511016	0.41989441	0.533097442	0.509106074	0.431907198	4.556731146
EGI.Sep.2015.00047	0.006267924	0.08188841	0.38404238	0.530029291	0.556993018	0.492163449	7.233249082
EGI.Sep.2015.00048	0.006434719	0.018796582	0.190372629	0.220248713	0.172364226	0.085670186	0.275762033
EGI.Sep.2015.00049	0.007099257	0.009335722	0.032190328	0.066200035	0.061235121	0.031363031	0.128625695
EGI.Sep.2015.00050	0.007132062	0.008690773	0.046770046	0.087573593	0.079238589	0.039995985	0.120853747
EGI.Sep.2015.00051	0.006202118	0.007820267	0.033764853	0.069995146	0.076126913	0.034546208	0.151556121
EGI.Sep.2015.00052	0.005847298	0.053001394	0.590628424	0.573867732	0.387107743	0.168325739	0.371572255
EGI.Sep.2015.00053	0.0055095	0.12060029	0.653476767	0.632847542	0.38073913	0.15797771	0.2856714

Table D.1 Continued

Sample_id	mgHC.conc.S1_1	mgHC.conc.S1_2	mgHC.conc.S1_3	mgHC.conc.S1_4	mgHC.conc.S1_5	mgHC.conc.S1_6	mgHC.conc.S2
EGI.Sep.2015.00054	0.006106522	0.143315606	1.158055918	1.224356649	0.790630965	0.382384239	0.567616297
EGI.Sep.2015.00	0.138135886	0.324232529	1.376800582	1.323177996	0.983119525	0.529245446	0.936323838
EGI.Sep.2015.00056	0.005955168	0.007972615	0.032593107	0.060474657	0.069415972	0.026843971	0.124145123
EGI.Sep.2015.00057	0.005481785	0.149948882	1.00337149	0.992949115	0.634449344	0.2836577	0.476497684
EGI.Sep.2015.00058	0.005016994	0.168406386	1.17216915	1.103588698	0.701486338	0.320879709	0.533438119
EGI.Sep.2015.00059	0.131772902	0.494723817	2.224977087	2.000868502	1.360594491	0.738805182	1.237412594
EGI.Sep.2015.00060	0.437476934	0.635653907	1.398176194	1.392157853	1.050491269	0.759800236	1.557902236
EGI.Sep.2015.00061	0.005165288	0.06825972	1.106832509	1.558826608	0.973643072	0.473600833	0.958225939
EGI.Sep.2015.00062	0.00549546	0.128836898	1.218455136	1.279577938	0.791114075	0.445137181	0.957057324
i1 Peterson	0.034547245	0.029748708	0.129180498	0.295647161	0.294050585	0.256452238	7.250870121
iBeebe Draw	0.125751032	0.110063844	0.336608236	0.598403153	0.53896867	0.399444613	2.31632283
iEC 024C_CR_21	0.013209681	0.887413132	2.709907926	2.842460868	2.725334166	2.105210602	7.619949531
iEC 024C_SS_21	0.044429201	2.182187467	6.025465069	6.662024841	7.065707118	5.542101744	17.13784828
iEC 037C_CR_53.5	0.006753355	0.190661863	0.618386539	0.488313372	0.377171096	0.285647039	0.541311046
iEC 037C_SS_53.5	0.006886768	0.24881946	1.207296635	1.50978283	0.99810258	0.492853483	0.983785306
iEC 038C_CR_31.9	0.014510162	0.910270494	3.507983717	3.948922889	2.56079086	1.18935597	2.036983667
iEC 038C_SS_31.9	0.013172207	1.169393027	5.935454513	7.652612286	6.531475233	3.243991879	3.325446853
iEC 049C_CR_40.9	0.009036225	0.699844993	3.012593459	3.57700695	2.193198028	0.922753137	1.868268416
iEC 049C_SS_40.9	0.013695889	0.826533302	4.177014021	6.184092007	5.065519512	1.926315512	2.592386865

Table D.1 Continued

Sample_id	mgHC.conc.S1_1	mgHC.conc.S1_2	mgHC.conc.S1_3	mgHC.conc.S1_4	mgHC.conc.S1_5	mgHC.conc.S1_6	mgHC.conc.S2
ii1 Peterson	0.03628429	0.031665862	0.12400749	0.298003557	0.315825646	0.28958364	8.518319471
iiBeebe Draw	0.034265843	0.045263019	0.312261924	0.527532795	0.484094567	0.355515435	2.277260256
iiEC 024C_CR_21	0.014011438	0.839576147	2.71042211	3.027194974	2.960412165	2.321944561	8.348623817
iiEC 024C_SS_21	0.030473124	1.675672427	6.203012479	7.190888732	7.551038756	6.142433959	19.650917 2
iiEC 037C_CR_53.5	0.005529857	0.150780869	0.560003196	0.476220725	0.373100956	0.279728435	0.548443992
iiEC 037C_SS_53.5	0.005833 96	0.272931056	1.231531258	1.520735236	0.991089937	0.489724289	1.014876832
iiEC 038C_CR_31.9	0.014465 91	0.980790884	3.846655025	4.063429344	2.574720283	1.191440463	2.008040751
iiEC 038C_SS_31.9	0.018949439	1.0629317	5.945159863	7.724715846	6.432289329	3.258709527	3.575072309
iiEC 049C_CR_40.9	0.011353833	0.798072037	3.133066135	3.653485267	2.255726748	0.93955142	1.884752789
iiEC 049C_SS_40.9	0.013100798	0.76274472	4.053618354	6.090306601	4.984735902	1.882633503	2.561846212
iiEGI.Sep.2015.00032	0.006885601	0.033135175	0.107447889	0.068013979	0.03208878	0.019513983	0.135497444
iiEGI.Sep.2015.00033	0.006617289	0.088903268	0.623545214	0.490961844	0.221106721	0.145662941	0.463540404
iiEGI.Sep.2015.00034	0.006342423	0.181807218	1.701094727	1.764677735	1.138997392	0.917240344	5.568686241
iiEGI.Sep.2015.00035	0.005039549	0.070915735	0.264291947	0.197839906	0.135293747	0.07187737	0.403110738
iiEGI.Sep.2015.00036	0.005553539	0.439062019	1.357047398	0.853265764	0.427838787	0.270095908	3.234632022
iiEGI.Sep.2015.00037	0.005572138	0.019184685	0.134570133	0.133063652	0.066634676	0.040379518	0.200540936
iiEGI.Sep.2015.00038	0.007436957	0.062738752	0.8012467	0.961163162	0.505460371	0.28755129	2.093947174
iiEGI.Sep.2015.00039	0.006500946	0.06490028	0.552588044	0.494470659	0.220741857	0.117001724	0.617143398
iiEGI.Sep.2015.00040	0.007902438	0.028154343	0.216294809	0.165228257	0.082292725	0.057324608	0.190976309

Table D.1 Continued

Sample_id	mgHC.conc.S1_1	mgHC.conc.S1_2	mgHC.conc.S1_3	mgHC.conc.S1_4	mgHC.conc.S1_5	mgHC.conc.S1_6	mgHC.conc.S2
iiEGI.Sep.2015.00041	0.009121429	0.191868268	0.901191006	0.545132282	0.204925685	0.134338948	0.371742824
iiEGI.Sep.2015.00042	0.006018058	0.091146215	0.338984679	0.498017688	0.537043011	0.489280877	5.353189138
iiEGI.Sep.2015.00043	3.100292139	3.946135325	4.308035829	4.297085091	4.377150354	4.327138744	14.55936472
iiEGI.Sep.2015.00044	0.007544867	0.120517987	0.390007131	0.504043011	0.502751215	0.416931399	5.474759898
iiEGI.Sep.2015.00045	0.005569552	0.092324481	0.37077699	0.503742555	0.504218758	0.418575481	4.584821123
iiEGI.Sep.2015.00046	0.008640181	0.10830962	0.43291628	0.538889635	0.503391976	0.415536766	4.479680576
iiEGI.Sep.2015.00047	0.007171117	0.087707693	0.388174103	0.537977996	0.554949602	0.476521665	7.074562527
iiEGI.Sep.2015.00048	0.015885482	0.025540129	0.184262493	0.224710829	0.18090016	0.092147413	0.302598681
iiEGI.Sep.2015.00049	0.006640912	0.007229466	0.024789087	0.058827499	0.05714764	0.028307318	0.092646233
iiEGI.Sep.2015.00050	0.006512888	0.008522918	0.043768333	0.085063871	0.079962323	0.039090776	0.12253691
iiEGI.Sep.2015.00051	0.007660257	0.008738237	0.03271326	0.068743329	0.078602583	0.037081878	0.171044226
iiEGI.Sep.2015.00052	0.00468528	0.042015363	0.538291115	0.553343193	0.371210142	0.160457753	0.355938406
iiEGI.Sep.2015.00053	0.005534551	0.11147185	0.658811208	0.632335133	0.376170745	0.149358424	0.270541554
iiEGI.Sep.2015.00054	0.006310626	0.126553893	1.130408279	1.229237823	0.789854238	0.378071026	0.544923584
iiEGI.Sep.2015.00055	0.34747735	0.595172273	1.623940989	1.619974666	1.289695896	0.852787572	1.588334655
iiEGI.Sep.2015.00056	0.007317806	0.008200638	0.033280876	0.058807079	0.071756684	0.025540838	0.126302541
iiEGI.Sep.2015.00057	0.006676644	0.121184625	0.96285123	0.940356601	0.598464511	0.265314178	0.455226008
iiEGI.Sep.2015.00058	0.007877041	0.170643336	1.134309482	1.063874569	0.66825659	0.30131976	0.514703757
iiEGI.Sep.2015.00059	0.005855295	0.307033348	1.936368795	1.709279663	1.085895325	0.517250964	0.83723359

Table D.1 Continued

Sample_id	mgHC.conc.S1_1	mgHC.conc.S1_2	mgHC.conc.S1_3	mgHC.conc.S1_4	mgHC.conc.S1_5	mgHC.conc.S1_6	mgHC.conc.S2
iiEGI.Sep.2015.00060	0.005320631	0.196988862	1.369435102	1.348543419	0.864732087	0.411658569	0.681419328
iiEGI.Sep.2015.00061	3.290016688	3.999021601	5.075632469	5.560929945	4.936085605	4.477521732	9.822580204
iiEGI.Sep.2015.00062	0.005092844	0.119039955	1.253882479	1.317014535	0.815663459	0.465233344	1.000786637
iiiEGI.Sep.2015.00032	0.005233872	0.024914521	0.088811397	0.059185786	0.02807449	0.017016526	0.121984064
iiiEGI.Sep.2015.00033	0.006217634	0.075466468	0.612266765	0.494561163	0.216628683	0.138430327	0.448273553
iiiEGI.Sep.2015.00034	0.003263542	0.17432749	1.705561585	1.757134229	1.114634886	0.891985887	5.384624337
iiiEGI.Sep.2015.00035	0.005344457	0.05721742	0.231043601	0.178003885	0.122980194	0.068164559	0.367897887
iiiEGI.Sep.2015.00036	0.005587704	0.399453353	1.326707778	0.828725181	0.416621063	0.25988753	3.025161336
iiiEGI.Sep.2015.00037	0.006296599	0.015220385	0.120008279	0.122178949	0.060363229	0.037840237	0.187221876
iiiEGI.Sep.2015.00038	0.005104543	0.052929305	0.775294983	0.959538195	0.509735805	0.291042111	2.088534116
iiiEGI.Sep.2015.00039	0.004809477	0.055094127	0.546725163	0.504176641	0.22455374	0.114640567	0.610255764
iiiEGI.Sep.2015.00040	0.005528733	0.022269985	0.201599482	0.165320404	0.081845468	0.056342264	0.183351975
iiiEGI.Sep.2015.00041	0.005137175	0.156033794	0.87788373	0.536256459	0.206315625	0.137336251	0.366213197
iiiEGI.Sep.2015.00042	0.004836008	0.110314566	0.433569296	0.578548082	0.570600484	0.491982658	5.086238214
iiiEGI.Sep.2015.00043	0.004629494	0.105151804	0.44007682	0.57087226	0.563855551	0.492224494	5.913355041
iiiEGI.Sep.2015.00044	0.004613827	0.096504799	0.427914852	0.539479937	0.509307715	0.44355296	5.730025806
iiiEGI.Sep.2015.00045	0.005001442	0.094251436	0.360879995	0.481055008	0.484141245	0.395020125	4.28430481
iiiEGI.Sep.2015.00046	0.006867986	0.102656705	0.428978688	0.516952473	0.470090888	0.376225151	4.213964522
iiiEGI.Sep.2015.00047	0.005183754	0.078073464	0.370279233	0.512737801	0.526490482	0.443890873	6.917591878

Table D.1 Continued

Sample_id	mgHC.conc.S1_1	mgHC.conc.S1_2	mgHC.conc.S1_3	mgHC.conc.S1_4	mgHC.conc.S1_5	mgHC.conc.S1_6	mgHC.conc.S2
iiiEGI.Sep.2015.00048	0.005415705	0.017397627	0.172081992	0.220765456	0.17285716	0.081558184	0.285740992
iiiEGI.Sep.2015.00049	0.00540311	0.005886952	0.022032589	0.053729837	0.054346727	0.025527892	0.088485377
iiiEGI.Sep.2015.00050	0.005704648	0.008936878	0.040154434	0.081515979	0.078446386	0.038545125	0.118391307
iiiEGI.Sep.2015.00051	0.005849921	0.006829969	0.030703542	0.06491935	0.076874959	0.032124843	0.145775886
iiiEGI.Sep.2015.00052	0.006055737	0.038702537	0.540165557	0.552016319	0.371146223	0.158066818	0.349287397
iiiEGI.Sep.2015.00053	0.004802692	0.052627083	0.638350298	0.674370961	0.422207219	0.196216882	0.390738136
iiiEGI.Sep.2015.00054	0.004493733	0.147630724	1.080898716	1.191011824	0.758300157	0.347793927	0.491420966
iiiEGI.Sep.2015.00055	0.00491448	0.149015455	1.212448646	1.162526235	0.820283776	0.369449591	0.570918596
iiiEGI.Sep.2015.00056	0.006723709	0.006560425	0.027208726	0.050943143	0.058421619	0.018343952	0.099994937
iiiEGI.Sep.2015.00057	0.004927239	0.11736125	0.995675329	0.995742436	0.642446474	0.291467954	0.562520381
iiiEGI.Sep.2015.00058	0.004816299	0.154414133	1.12918894	1.060197608	0.668302318	0.302561984	0.496836623
iiiEGI.Sep.2015.00059	0.00400935	0.276385496	2.057856003	1.833876304	1.191487018	0.56533664	0.887714044
iiiEGI.Sep.2015.00060	0.004230966	0.164107177	1.306900963	1.296288997	0.827777219	0.394296379	0.651581618
iiiEGI.Sep.2015.00061	0.002866285	0.058466545	1.132987983	1.617730628	1.013077559	0.487188843	0.993250495
iiiEGI.Sep.2015.00062	0.003357638	0.099687228	1.127081627	1.170285292	0.71938484	0.406071532	0.888297392
iiT-HB_2157	0.031254595	0.511442914	1.573594145	1.368601066	0.994811739	0.835276524	63.0065059
iiTORC_2303.3	0.0345826	0.799818959	2.227623056	2.119200201	1.696579263	1.401755834	105.5016536
iT-HB_2157	0.048181607	0.633918182	1.755918035	1.380080462	0.983916354	0.777044791	59.06260146
iTORC_2303.3	NA	0.945271101	2.172766324	1.935758312	1.341201267	0.979444781	96.26509332

Table D.1 Continued

Sample_id	mgHC.conc.S1_1	mgHC.conc.S1_2	mgHC.conc.S1_3	mgHC.conc.S1_4	mgHC.conc.S1_5	mgHC.conc.S1_6	mgHC.conc.S2
T-HB_2157	0.018153983	0.616836739	1.578464602	1.291210928	0.971440605	0.811020939	61.42443609
TORC_2303.3	0.010511187	0.956628483	2.255695015	2.074343959	1.653228222	1.343500778	104.23975

APPENDIX E

PROCESSED RESULTS OF HAWK EXPERIMENTS

Table E.1: Experimental results Normalized FID signal at different IS1 temperatures on the HAWK.

Sample_id	S1_1	S1_2	S1_3	S1_4	S1_5	S1_6
1 Peterson	0.022454	0.056228	0.147578	0.270724	0.263876	0.239139
Beebe Draw	0.01462	0.042981	0.169485	0.308031	0.277693	0.18719
EC 024C_CR_21	0.003276	0.089896	0.22532	0.247128	0.24449	0.189891
EC 024C_SS_21	0.001502	0.082743	0.214714	0.241093	0.259116	0.200833
EC 037C_CR_53.5	0.002394	0.113501	0.311166	0.24371	0.187753	0.141476
EC 037C_SS_53.5	0.001215	0.076512	0.274233	0.329269	0.215253	0.103518
EC 038C_CR_31.9	0.002337	0.077611	0.261066	0.326511	0.225976	0.1065
EC 038C_SS_31.9	0.001772	0.053586	0.237321	0.308161	0.266486	0.132674
EC 049C_CR_40.9	0.003626	0.093186	0.282171	0.331569	0.204814	0.084635
EC 049C_SS_40.9	0.001405	0.055287	0.221425	0.330867	0.282952	0.108064
EGI.Sep.2015.00032	0.022148	0.142285	0.391877	0.242175	0.123028	0.078486
EGI.Sep.2015.00033	0.003704	0.059592	0.388244	0.308895	0.143573	0.095992
EGI.Sep.2015.00034	0.001312	0.03538	0.29736	0.304731	0.199701	0.161517

Table E.1 Continued						
Sample_id	S1_1	S1_2	S1_3	S1_4	S1_5	S1_6
EGI.Sep.2015.00035	0.008309	0.104542	0.338258	0.254157	0.184341	0.110394
EGI.Sep.2015.00036	0.001885	0.130993	0.402069	0.25112	0.129191	0.084742
EGI.Sep.2015.00037	0.014312	0.049965	0.359841	0.322423	0.153886	0.099572
EGI.Sep.2015.00038	0.002864	0.027177	0.303079	0.364905	0.188548	0.113426
EGI.Sep.2015.00039	0.00397	0.050999	0.382867	0.332894	0.149242	0.080027
EGI.Sep.2015.00040	0.010623	0.052987	0.391971	0.292547	0.148487	0.103386
EGI.Sep.2015.00041	0.004503	0.101003	0.451725	0.268638	0.103695	0.070436
EGI.Sep.2015.00042	0.002897	0.046697	0.173814	0.251548	0.272756	0.252287
EGI.Sep.2015.00043	0.002184	0.051711	0.198032	0.259265	0.258091	0.230717
EGI.Sep.2015.00044	0.002434	0.058089	0.195556	0.259506	0.262399	0.222016
EGI.Sep.2015.00045	0.003459	0.047169	0.18929	0.262032	0.26928	0.22877
EGI.Sep.2015.00046	0.002453	0.052166	0.209588	0.266092	0.254117	0.215584
EGI.Sep.2015.00047	0.003055	0.039919	0.187211	0.258376	0.271521	0.239918
EGI.Sep.2015.00048	0.009273	0.027089	0.274357	0.317413	0.248404	0.123464
EGI.Sep.2015.00049	0.034226	0.045008	0.155191	0.319154	0.295218	0.151203

Table E.1 Continued						
Sample_id	S1_1	S1_2	S1_3	S1_4	S1_5	S1_6
EGI.Sep.2015.00050	0.026474	0.03226	0.173608	0.325068	0.294129	0.148463
EGI.Sep.2015.00051	0.027148	0.034231	0.147796	0.306384	0.333224	0.151216
EGI.Sep.2015.00052	0.003287	0.029797	0.332042	0.322619	0.217626	0.09463
EGI.Sep.2015.00053	0.002824	0.06181	0.334919	0.324346	0.195136	0.080966
EGI.Sep.2015.00054	0.001648	0.038683	0.312578	0.330474	0.213404	0.103212
EGI.Sep.2015.00055	0.02955	0.069359	0.294521	0.28305	0.210306	0.113215
EGI.Sep.2015.00056	0.029299	0.039225	0.160355	0.29753	0.341521	0.13207
EGI.Sep.2015.00057	0.001786	0.048846	0.326846	0.323451	0.206671	0.092401
EGI.Sep.2015.00058	0.001445	0.04851	0.33765	0.317895	0.202067	0.092431
EGI.Sep.2015.00059	0.018955	0.071165	0.32006	0.287823	0.19572	0.106276
EGI.Sep.2015.00060	0.077105	0.112034	0.246429	0.245368	0.185149	0.133915
EGI.Sep.2015.00061	0.001234	0.016305	0.264392	0.372361	0.232577	0.11313
EGI.Sep.2015.00062	0.001421	0.033303	0.314959	0.330759	0.204495	0.115064
i1 Peterson	0.03323	0.028615	0.124257	0.284378	0.282843	0.246677
iBeebe Draw	0.059619	0.052182	0.159587	0.283706	0.255527	0.189378
iEC 024C_CR_21	0.001171	0.078647	0.240165	0.251912	0.241532	0.186574
iEC 024C_SS_21	0.001614	0.079289	0.218933	0.242063	0.25673	0.20137

Table E.1 Continued						
Sample_id	S1_1	S1_2	S1_3	S1_4	S1_5	S1_6
iEC 037C_CR_53.5	0.003433	0.096934	0.314391	0.248261	0.191756	0.145225
iEC 037C_SS_53.5	0.001543	0.055742	0.270467	0.338233	0.223602	0.110413
iEC038C_CR_31.9	0.001196	0.075032	0.289155	0.325501	0.21108	0.098036
iEC 038C_SS_31.9	0.000537	0.047641	0.241808	0.311765	0.26609	0.132159
iEC 049C_CR_40.9	0.000868	0.0672	0.289271	0.343466	0.210592	0.088603
iEC 049C_SS_40.9	0.000753	0.045431	0.229592	0.339913	0.27843	0.105881
ii1 Peterson	0.033125	0.028909	0.113211	0.272057	0.288328	0.26437
iiBeebe Draw	0.019481	0.025733	0.177529	0.299916	0.27522	0.20212
iiEC 024C_CR_21	0.00118	0.07071	0.228274	0.254953	0.249328	0.195556
iiEC 024C_SS_21	0.001058	0.058196	0.215431	0.24974	0.262248	0.213327
iiEC 037C_CR_53.5	0.002997	0.081708	0.303465	0.258063	0.202183	0.151584
iiEC 037C_SS_53.5	0.001293	0.060492	0.272955	0.337054	0.219664	0.108542
iiEC 038C_CR_31.9	0.001142	0.077401	0.303567	0.320675	0.20319	0.094025
iiEC 038C_SS_31.9	0.000775	0.043487	0.243228	0.316033	0.263157	0.13332
iiEC 049C_CR_40.9	0.001052	0.073955	0.290334	0.33856	0.209033	0.087066
iiEC 049C_SS_40.9	0.000737	0.042882	0.227896	0.342399	0.280244	0.105842
iiEGI.Sep.2015.00032	0.025781	0.124062	0.402298	0.254653	0.120144	0.073063

Table E.1 Continued						
Sample_id	S1_1	S1_2	S1_3	S1_4	S1_5	S1_6
iiEGI.Sep.2015.00033	0.004197	0.056382	0.39545	0.311366	0.140225	0.092379
iiEGI.Sep.2015.00034	0.001111	0.031839	0.297907	0.309042	0.199469	0.160633
iiEGI.Sep.2015.00035	0.006762	0.095156	0.354631	0.265465	0.181539	0.096446
iiEGI.Sep.2015.00036	0.001656	0.130951	0.404743	0.254489	0.127604	0.080557
iiEGI.Sep.2015.00037	0.013951	0.048033	0.336927	0.333155	0.166835	0.101099
iiEGI.Sep.2015.00038	0.002832	0.023895	0.305167	0.366074	0.192513	0.109518
iiEGI.Sep.2015.00039	0.004464	0.044568	0.379472	0.339562	0.151587	0.080347
iiEGI.Sep.2015.00040	0.014182	0.050529	0.388184	0.296535	0.14769	0.10288
iiEGI.Sep.2015.00041	0.004592	0.096582	0.45364	0.274408	0.103155	0.067623
iiEGI.Sep.2015.00042	0.00307	0.046492	0.172908	0.254027	0.273933	0.249571
iiEGI.Sep.2015.00043	0.127292	0.16202	0.176879	0.176429	0.179717	0.177663
iiEGI.Sep.2015.00044	0.003886	0.062065	0.200849	0.259576	0.25891	0.214714
iiEGI.Sep.2015.00045	0.002939	0.048715	0.195639	0.265798	0.266049	0.22086
iiEGI.Sep.2015.00046	0.004304	0.053948	0.21563	0.268414	0.250733	0.206973
iiEGI.Sep.2015.00047	0.003494	0.042732	0.189122	0.262108	0.270377	0.232166

Table E.1 Continued

Sample_id	S1_1	S1_2	S1_3	S1_4	S1_5	S1_6
iiEGI.Sep.2015.00048	0.021958	0.035303	0.254701	0.310612	0.250053	0.127373
iiEGI.Sep.2015.00049	0.036301	0.039518	0.135502	0.321564	0.312381	0.154734
iiEGI.Sep.2015.00050	0.024771	0.032416	0.166469	0.323534	0.30413	0.148679
iiEGI.Sep.2015.00051	0.032801	0.037417	0.140076	0.294354	0.336571	0.158782
iiEGI.Sep.2015.00052	0.002806	0.025159	0.322329	0.331343	0.222281	0.096082
iiEGI.Sep.2015.00053	0.002862	0.057647	0.340703	0.327011	0.194536	0.07724
iiEGI.Sep.2015.00054	0.001724	0.034573	0.308818	0.335817	0.215781	0.103286
iiEGI.Sep.2015.00055	0.054902	0.094038	0.256585	0.255959	0.203774	0.134742
iiEGI.Sep.2015.00056	0.035713	0.040022	0.162422	0.286998	0.350197	0.124648
iiEGI.Sep.2015.00057	0.002306	0.041862	0.332609	0.324838	0.206734	0.09165
iiEGI.Sep.2015.00058	0.002354	0.050995	0.338976	0.317927	0.199701	0.090046
iiEGI.Sep.2015.00059	0.001053	0.055205	0.348162	0.307331	0.195246	0.093003
iiEGI.Sep.2015.00060	0.001268	0.046939	0.326314	0.321336	0.206052	0.098092
iiEGI.Sep.2015.00061	0.120341	0.146274	0.185654	0.203405	0.18055	0.163777
iiEGI.Sep.2015.00062	0.001281	0.02994	0.315369	0.331247	0.205151	0.117013

Table E.1 Continued						
Sample_id	S1_1	S1_2	S1_3	S1_4	S1_5	S1_6
iiiEGI.Sep.2015.00032	0.023445	0.111606	0.397835	0.265126	0.125761	0.076226
iiiEGI.Sep.2015.00033	0.004028	0.048891	0.396656	0.320401	0.140343	0.089682
iiiEGI.Sep.2015.00034	0.000578	0.030871	0.302035	0.311168	0.197389	0.15796
iiiEGI.Sep.2015.00035	0.008064	0.086333	0.348611	0.268582	0.185559	0.10285
iiiEGI.Sep.2015.00036	0.001726	0.123403	0.409859	0.256018	0.128707	0.080287
iiiEGI.Sep.2015.00037	0.017398	0.042056	0.331599	0.337597	0.166792	0.104558
iiiEGI.Sep.2015.00038	0.001968	0.020407	0.298921	0.369957	0.196533	0.112214
iiiEGI.Sep.2015.00039	0.003317	0.037996	0.377052	0.347708	0.154865	0.079062
iiiEGI.Sep.2015.00040	0.010375	0.04179	0.378302	0.310224	0.153583	0.105726
iiiEGI.Sep.2015.00041	0.002677	0.081312	0.457478	0.279451	0.107514	0.071568
iiiEGI.Sep.2015.00042	0.002208	0.050375	0.19799	0.264195	0.260566	0.224665
iiiEGI.Sep.2015.00043	0.002127	0.048305	0.202166	0.262252	0.259028	0.226122
iiiEGI.Sep.2015.00044	0.002283	0.047742	0.211695	0.266888	0.251961	0.219431
iiiEGI.Sep.2015.00045	0.002748	0.051777	0.198248	0.264265	0.265961	0.217002
iiiEGI.Sep.2015.00046	0.003611	0.05398	0.225568	0.271827	0.247186	0.197829

Table E.1 Continued						
Sample_id	S1_1	S1_2	S1_3	S1_4	S1_5	S1_6
iiiEGI.Sep.2015.00047	0.002677	0.040314	0.191195	0.264754	0.271856	0.229205
iiiEGI.Sep.2015.00048	0.008082	0.025964	0.25681	0.329463	0.257966	0.121715
iiiEGI.Sep.2015.00049	0.032368	0.035267	0.131989	0.321876	0.325572	0.152928
iiiEGI.Sep.2015.00050	0.022521	0.035281	0.158523	0.321812	0.309693	0.15217
iiiEGI.Sep.2015.00051	0.026921	0.031431	0.141294	0.298751	0.353769	0.147835
iiiEGI.Sep.2015.00052	0.003635	0.023229	0.324199	0.331312	0.222756	0.094869
iiiEGI.Sep.2015.00053	0.002415	0.026465	0.321009	0.339123	0.212316	0.098672
iiiEGI.Sep.2015.00054	0.001273	0.04182	0.306192	0.337385	0.214808	0.098522
iiiEGI.Sep.2015.00055	0.001322	0.040073	0.326046	0.312621	0.220587	0.099351
iiiEGI.Sep.2015.00056	0.039974	0.039003	0.161763	0.30287	0.347331	0.109059
iiiEGI.Sep.2015.00057	0.001617	0.038509	0.326706	0.326728	0.210803	0.095638
iiiEGI.Sep.2015.00058	0.001451	0.046518	0.34017	0.319387	0.201327	0.091147
iiiEGI.Sep.2015.00059	0.000676	0.046616	0.347086	0.309309	0.200961	0.095352
iiiEGI.Sep.2015.00060	0.001059	0.041093	0.327249	0.324591	0.207276	0.098732
iiiEGI.Sep.2015.00061	0.000665	0.013558	0.262733	0.375142	0.234926	0.112976

Table E.1 Continued						
Sample_id	S1_1	S1_2	S1_3	S1_4	S1_5	S1_6
iiiEGI.Sep.2015.0 0062	0.000952	0.028273	0.319661	0.331914	0.204031	0.115169
iiT-HB_2157	0.00588	0.096227	0.296068	0.257499	0.187171	0.157155
iiTORC_2303.3	0.004177	0.096602	0.269051	0.255956	0.204912	0.169303
iT-HB_2157	0.008636	0.113625	0.314734	0.247368	0.176359	0.139279
iTORC_2303.3	#VALUE!	0.128182	0.294635	0.262496	0.181872	0.132816
T-HB_2157	0.003434	0.116668	0.298549	0.244218	0.183737	0.153395
TORC_2303.3	0.001267	0.115341	0.27197	0.250105	0.19933	0.161986

APPENDIX F

PROMAX DATA FOR TERNARY PLOT

Table F.1: ProMax simulation results for ternary plots.

Sample ID	API gravity	Sh (250°C+300°C)	Sm (150°C+200°C)	Sl (50°C+100°C)
Oil 106_Harding_20.7	20.7	1	0.001	0
Oil 77_Duri_20.8	20.8	1	0	0
Oil 121_Kuito_21.96	21.96	0.57	0.43	0
Oil 68_Dalia_23.1	23.1	0.901	0.099	0
Oil 58_Clair_23.7	23.7	1	0	0
Oil 96_Gimdoa_23.7	23.7	1	0	0
Oil 84_Escalante_24.1	24.1	0.539	0.461	0
Oil 198_Vasconia_24.55	24.55	0.506	0.494	0
Oil 104_Hamaca_25.9	25.9	0.502	0.362	0.136
Oil 29_Arabian Heavy_27.4	27.4	0.366	0.472	0.162
Oil 56_chinguetti_28.3	28.3	0.391	0.56	0.049
Oil 113_Hungo Blend_28.3	28.3	0.423	0.515	0.061
Oil 132_Mars_28.9	28.9	0.342	0.658	0
Oil 45_Bonga_29.1	29.1	0.541	0.459	0
Oil 160_Poseidon_29.1	29.1	0.354	0.598	0.047
Oil 181_Southern Green Canyon_29.4	29.4	0.334	0.665	0

Table F.1 Continued				
Sample ID	API gravity	Sh (250°C+300°C)	Sm (150°C+200°C)	Sl (50°C+100°C)
Oil 129_Mandji_29.54	29.54	0.424	0.576	0
Oil 91_Forozan_29.73	29.73	0.381	0.568	0.051
Oil 119_Kissanja Blend_29.84	29.84	0.431	0.569	0
Oil 139_Mondo_29.9	29.9	0.389	0.486	0.125
Oil 124_Labuan_29.92	29.92	0.613	0.388	0
Oil 199_Voive_30	30	0.421	0.579	0
Oil 98_Girassol_30.2	30.2	0.483	0.517	0
Oil 22_Al Jurf_30.24	30.24	0.483	0.518	0
Oil 59_Coco_30.4	30.4	0.436	0.492	0.071
Oil 75_Dubai_30.4	30.4	0.371	0.464	0.164
Oil 90_Forcados_30.43	30.43	0.567	0.433	0
Oil 207_Zafiro Blend_30.6	30.6	0.438	0.561	0
Oil 138_Miri Light_30.79	30.79	0.583	0.416	0
Oil 147_Norne_30.8	30.8	0.663	0.337	0
Oil 53_Calypso_30.84	30.84	0.597	0.402	0
Oil 112_Hoops Blend_31.2	31.2	0.374	0.577	0.049
Oil 102_Gulf of Suez_31.3	31.3	0.379	0.621	0
Oil 134_Masila_31.36	31.36	0.483	0.516	0
Oil 196_Ural_31.78	31.78	0.369	0.631	0
Oil 120_Kole_32.06	32.06	0.385	0.615	0
Oil 23_Alaskan North Slope_32.3	32.3	0.311	0.491	0.197
Oil 194_Troll Blend_32.4	32.4	0.433	0.563	0.003941

Table F.1 Continued				
Sample ID	API gravity	Sh (250°C+300°C)	Sm (150°C+200°C)	Sl (50°C+100°C)
Oil 51_Cabinda_32.61	32.61	0.377	0.489	0.133
Oil 161_Qatar Marine_32.65	32.65	0.358	0.476	0.165
Oil 192_Thunder Horse_32.7	32.7	0.417	0.581	0.001614
Oil 144_Nile Blend_32.76	32.76	0.549	0.45	0
Oil 168_Saxi Batuque_32.83	32.83	0.415	0.521	0.065
Oil 99_Glinte_32.9	32.9	0.379	0.413	0.208
Oil 115_Isthmus_32.9	32.9	0.366	0.634	0
Oil 150_Oman_32.95	32.95	0.352	0.502	0.146
Oil 159_Plutonio_33.2	33.2	0.363	0.638	0
Oil 190_Terra Nova_33.2	33.2	0.373	0.437	0.19
Oil 30_Arabian Light_33.4	33.4	0.373	0.512	0.114
Oil 174_Sirri_33.43	33.43	0.333	0.641	0.025
Oil 46_Bonny Light_33.61	33.61	0.443	0.557	0
Oil 82_Erha_33.7	33.7	0.516	0.45	0.034
Oil 85_Escravos_33.7	33.7	0.445	0.555	0
Oil 157_Pennington_33.7	33.7	0.507	0.493	0
Oil 131_Marine Light_34.5	34.5	0.401	0.599	0
Oil 48_Brass River_34.56	34.56	0.386	0.614	0
Oil 86_Espo_34.62	34.62	0.386	0.478	0.136
Oil 69_DUC_34.7	34.7	0.32	0.423	0.257349
Oil 205_Xikomba_34.7	34.7	0.344	0.418	0.237
Oil 34_Azeri Light_35	35	0.485	0.515	0

Table F.1 Continued				
Sample ID	API gravity	Sh (250°C+300°C)	Sm (150°C+200°C)	Sl (50°C+100°C)
Oil 108_ Hibernia Blend_35	35	0.367	0.528	0.104
Oil 78_EA_35.09	35.09	0.546	0.454	0
Oil 136_Medanito_35.1	35.1	0.374	0.627	0
Oil 163_Rabi Light_35.1	35.1	0.428	0.519	0.054
Oil 111_Hondo Sandstone_35.2	35.2	0.362	0.481	0.157
Oil 125_Lavan_35.22	35.22	0.341	0.644	0.015
Oil 162_Qua Iboe_35.22	35.22	0.425	0.54	0.036
Oil 166_Ruby_35.75	35.75	0.45	0.55	0
OIL 193_Triton Blend_36.03	36.03	0.371	0.514	0.115
Oil 165_Rincon de los Sauces_36.1	36.1	0.448	0.551	0
Oil 171_Seria Light_36.15	36.15	0.43	0.56	0.011
Oil 195_Umm Shaiff_36.45	36.45	0.343	0.579	0.079
Oil 33_Azeri BTC_36.7	36.7	0.424	0.577	0
Oil 83_Es Sider_36.71	36.71	0.342	0.657	0
Oil 118_kikeh_36.74	36.74	0.501	0.5	0
Oil 26_Alvheim Blend_36.9	36.9	0.415	0.478	0.107
Oil 155_Palanca_36.97	36.97	0.378	0.622	0
Oil 114_Hydra_37.5	37.5	0.531	0.469	0
Oil 44_Bintulul_37.67	37.67	0.367	0.633	0
Oil 37_Barrow_37.7	37.7	0.395	0.574	0.031
Oil 103_Gullfaks Blend_37.8	37.8	0.342	0.543	0.116
Oil 158_Pierce_37.8	37.8	0.338	0.661	0

Table F.1 Continued				
Sample ID	API gravity	Sh (250°C+300°C)	Sm (150°C+200°C)	Sl (50°C+100°C)
Oil 173_Siberian Light_37.8	37.8	0.397	0.603	0
Oil 79_Ekofisk_37.9	37.9	0.304	0.538	0.157
Oil 197_Varg_37.9	37.9	0.323	0.478	0.199
Oil 31_Ardjuna_38	38	0.287	0.714	0
Oil 200_West Seno_38	38	0.28	0.72	0
Oil 117_Kiourong_38.2	38.2	0.356	0.598	0.046
Oil 184_Syran Light_38.24	38.24	0.327	0.582	0.091
Oil 49_Brent Blend_38.5	38.5	0.29	0.502	0.208
Oil 152_Oseberg_38.5	38.5	0.3	0.489	0.211
Oil 43_Beryl_38.6	38.6	0.315	0.607	0.079
Oil 149_Olmeca_38.9	38.9	0.327	0.441	0.232
Oil 35_Badak_39	39	0.327	0.607	0.066
Oil 183_Sttfiord Blend_39.3	39.3	0.309	0.484	0.207
Oil 27_Anasuria_39.7	39.7	0.299	0.462	0.239
Oil 142_Nanhai Light_39.7	39.7	0.474	0.526	0
Oil 178_Sokol_39.7	39.7	0.392	0.579	0.029
Oil 140_Murban_39.73	39.73	0.329	0.671	0
Oil 143_Nemba_39.79	39.79	0.279	0.687	0.034
Oil 92_Forties Blend_39.8	39.8	0.291	0.623	0.086
Oil 128_Lower Zakum_39.8	39.8	0.325	0.576	0.099
Oil 74_Draugen_39.9	39.9	0.272	0.397	0.331
Oil 206_Yoho_40.1	40.1	0.361	0.577	0.062

Table F.1 Continued				
Sample ID	API gravity	Sh (250°C+300°C)	Sm (150°C+200°C)	Sl (50°C+100°C)
Oil 191_Thevenard Island_40.7	40.7	0.472	0.504	0.024
Oil 201_West Texas Intermediate_40.8	40.8	0.291	0.451	0.258
Oil 208_Zakhum Lower_40.91	40.91	0.314	0.566	0.12
Oil 116_jotun Blend_41	41	0.299	0.406	0.295
Oil 202_ Western Desert_41	41	0.241	0.759	0
Oil 146_Nkossa Blend_41.1	41.1	0.335	0.509	0.156
Oil 204_Wytch Farm_41.2	41.2	0.282	0.702	0.016
Oil 105_Handil_41.25	41.25	0.249	0.616	0.135
Oil 175_Skua_41.9	41.9	0.433	0.567	0
Oil 94_Galeota_42.4	42.4	0.305	0.695	0
Oil 67_Cusiana_42.57	42.57	0.297	0.384	0.32
Oil 66_Curlew_42.9	42.9	0.26	0.64	0.1
Oil 95_Geragai Crude_43.1	43.1	0.223	0.646	0.13
Oil 65_Cupiaga_43.11	43.11	0.267	0.505	0.229
Oil 80_El Sharana_43.11	43.11	0.287	0.511	0.202
Oil 126_Legende_43.2	43.2	0.311	0.688	0
Oil 40_Bekpai_43.21	43.21	0.325	0.551	0.124
Oil 141_Mutineer-Exeeter_43.4	43.4	0.368	0.632	0
Oil 130_Marib Light_43.7	43.7	0.241	0.55	0.209
Oil 123_Kutubu_44.1	44.1	0.273	0.694	0.033
Oil 64_CPC Blend_44.2	44.2	0.279	0.503	0.219
Oil 133_Msa_44.3	44.3	0.381	0.567	0.053

Table F.1 Continued				
Sample ID	API gravity	Sh (250°C+300°C)	Sm (150°C+200°C)	Sl (50°C+100°C)
Oil 36_Badin_44.6	44.6	0.331	0.669	0
Oil 41_Belida_45.1	45.1	0.386	0.614	0
Oil 145_Njord_45.8	45.8	0.245	0.502	0.254
Oil 21_Akpo Blend_46.2	46.2	0.296	0.528	0.176
Oil 153_Oso Condensate_46.2	46.2	0.282	0.457	0.261
Oil 186_Tapis_46.3	46.3	0.356	0.517	0.127
Oil 20_Agbami_47.2	47.2	0.414	0.55	0.037
Oil 188_Tenigiz_47.2	47.2	0.271	0.461	0.268
Oil 63_Cossack_48.2	48.2	0.233	0.499	0.268
Oil 203_Wollybutt_49	49	0.315	0.685	0
Oil 32_Asgard Blend_50.7	50.5	0.209	0.431	0.36
Oil 18_Aasgard Blend_50.7	50.7	0.201	0.606	0.193
Oil 109_Hadra_51.7	51.7	0.143	0.339	0.518
Oil 97_Gippsland Blend_52.32	52.32	0.176	0.468	0.356
Oil 52_Cakerawala Condensate_52.55	52.55	0.015	0.985	0
Oil 170_Senipah Condensate_54.37	54.37	0.102	0.479	0.419
Oil 101_Griffin_54.6	54.6	0.192	0.692	0.116
Oil 151_Oman Lange_57.3	57.3	0.176	0.581	0.244
Oil 167_Sable Island Condensate_57.7	57.7	0.054401	0.385	0.561
Oil 61_Condensate NFCII_57.95	57.95	0.16	0.458	0.382
Oil 180_South Pars Condensate_58.36	58.36	0.155	0.396	0.448
Oil 177_Snohvit Condensate_60.1	60.1	0.087	0.368	0.546

Table F.1 Continued				
Sample ID	API gravity	Sh (250°C+300°C)	Sm (150°C+200°C)	Sl (50°C+100°C)
Oil 148_North West Shelf_60	60.3	0.076	0.324	0.601
Oil 154_Pagerugan_61.3	61.3	0.062	0.771	0.168
Oil 176_Sieipner Condensate_62.4	62.4	0.042	0.275	0.684
Oil 89_F3FB Condensate_63.62	63.62	0.115	0.324	0.561
Oil 38_Bayau Undan Condensate_63.7	63.7	0.131	0.308	0.56
Oil 25_Algerian Condensate_68.7	68.7	0.046802	0.244	0.709
Oil 47_Bontang_72.6	72.6	0	0	1
OIL 189_Terengganu_72.6	72.6	0.022801	0.052	0.926

APPENDIX G

HAWK™ DATA FOR TERNARY PLOT

Table G.1: IS1 experimental for ternary plot

Sample_id	Sh (250°C+300°C)	Sm (150°C+200°C)	Sl (50°C+100°C)
1 Peterson	0.496984768	1.369411606	0.503015233
Beebe Draw	0.535117283	1.076998713	0.464882717
EC 024C_CR_21	0.565618927	0.837006539	0.434381073
EC 024C_SS_21	0.540051581	0.832289552	0.459948419
EC 037C_CR_53.5	0.670771301	0.541812462	0.3292287
EC 037C_SS_53.5	0.681228945	0.489329237	0.318771056
EC 038C_CR_31.9	0.66752387	0.492862746	0.332476129
EC 038C_SS_31.9	0.600840408	0.518404643	0.399159592
EC 049C_CR_40.9	0.710551315	0.435545264	0.289448685
EC 049C_SS_40.9	0.608984069	0.515972938	0.391015931
EGI.Sep.2015.00032	0.798485747	0.53416773	0.201514254
EGI.Sep.2015.00033	0.760435595	0.471168545	0.239564404
EGI.Sep.2015.00034	0.638781749	0.856042019	0.36121825
EGI.Sep.2015.00035	0.705265776	0.648668596	0.294734224
EGI.Sep.2015.00036	0.786067281	0.710771746	0.21393272
EGI.Sep.2015.00037	0.746541946	0.586395847	0.253458055

Table G.1 Continued			
Sample_id	Sh (250°C+300°C)	Sm (150°C+200°C)	Sl (50°C+100°C)
EGI.Sep.2015.00038	0.698025438	0.750643902	0.301974562
EGI.Sep.2015.00039	0.770730441	0.528767739	0.229269559
EGI.Sep.2015.00040	0.748126912	0.506526616	0.251873089
EGI.Sep.2015.00041	0.825868978	0.334911599	0.174131023
EGI.Sep.2015.00042	0.474956671	1.251892306	0.525043329
EGI.Sep.2015.00043	0.511191551	1.220026557	0.48880845
EGI.Sep.2015.00044	0.515584519	1.226431326	0.484415481
EGI.Sep.2015.00045	0.501950371	1.209413844	0.498049628
EGI.Sep.2015.00046	0.530298806	1.164307824	0.469701194
EGI.Sep.2015.00047	0.488561759	1.290494198	0.511438241
EGI.Sep.2015.00048	0.62813197	0.65626167	0.371868031
EGI.Sep.2015.00049	0.553579248	0.829179287	0.446420752
EGI.Sep.2015.00050	0.557408646	0.752270436	0.442591353
EGI.Sep.2015.00051	0.515559405	0.883260292	0.484440596
EGI.Sep.2015.00052	0.687744407	0.485051721	0.312255593
EGI.Sep.2015.00053	0.723897904	0.403815103	0.276102096
EGI.Sep.2015.00054	0.683383879	0.449470606	0.316616121
EGI.Sep.2015.00055	0.676479539	0.490392303	0.323520461
EGI.Sep.2015.00056	0.526409136	0.852775014	0.473590864
EGI.Sep.2015.00057	0.700928528	0.433434091	0.299071471
EGI.Sep.2015.00058	0.705501332	0.427692192	0.294498668
EGI.Sep.2015.00059	0.698003799	0.453100028	0.301996201
EGI.Sep.2015.00060	0.680935983	0.534492083	0.319064017

Table G.1 Continued			
Sample_id	Sh (250°C+300°C)	Sm (150°C+200°C)	Sl (50°C+100°C)
EGI.Sep.2015.00061	0.65429276	0.531967495	0.345707239
EGI.Sep.2015.00062	0.680441006	0.517885138	0.319558993
i1 Peterson	0.470480161	1.40412006	0.529519839
iBeebe Draw	0.555094023	0.968302246	0.444905978
iEC 024C_CR_21	0.571894431	0.831203156	0.42810557
iEC 024C_SS_21	0.541899295	0.84184318	0.458100705
iEC 037C_CR_53.5	0.66301951	0.552793218	0.33698049
iEC 037C_SS_53.5	0.665985143	0.514607866	0.334014857
iEC 038C_CR_31.9	0.690883769	0.452881484	0.309116231
iEC 038C_SS_31.9	0.601750687	0.517562638	0.398249312
iEC 049C_CR_40.9	0.700804525	0.451301137	0.299195474
iEC 049C_SS_40.9	0.615689023	0.509031563	0.384310977
ii1 Peterson	0.447301808	1.438759581	0.552698192
iiBeebe Draw	0.522659634	1.0415502	0.477340366
iiEC 024C_CR_21	0.555116064	0.857728726	0.444883936
iiEC 024C_SS_21	0.524425186	0.881213079	0.475574815
iiEC 037C_CR_53.5	0.646232733	0.582876696	0.353767267
iiEC 037C_SS_53.5	0.671794137	0.511836726	0.328205864
iiEC 038C_CR_31.9	0.702784976	0.434006803	0.297215024
iiEC 038C_SS_31.9	0.603522657	0.524077253	0.396477344
iiEC 049C_CR_40.9	0.703901164	0.444785454	0.296098836
iiEC 049C_SS_40.9	0.613913791	0.51198173	0.386086209
iiEGI.Sep.2015.00032	0.806793028	0.529777306	0.193206973

Table G.1 Continued			
Sample_id	Sh (250°C+300°C)	Sm (150°C+200°C)	Sl (50°C+100°C)
iiEGI.Sep.2015.00033	0.767395806	0.459792277	0.232604195
iiEGI.Sep.2015.00034	0.639898392	0.853829973	0.360101607
iiEGI.Sep.2015.00035	0.722014328	0.629014603	0.277985673
iiEGI.Sep.2015.00036	0.79183921	0.699186863	0.208160789
iiEGI.Sep.2015.00037	0.732065831	0.602199293	0.26793417
iiEGI.Sep.2015.00038	0.697969037	0.745706664	0.302030963
iiEGI.Sep.2015.00039	0.768065673	0.529589966	0.231934327
iiEGI.Sep.2015.00040	0.749429219	0.505827499	0.250570781
iiEGI.Sep.2015.00041	0.829221557	0.328408771	0.170778443
iiEGI.Sep.2015.00042	0.47649638	1.255445595	0.52350362
iiEGI.Sep.2015.00043	0.642620004	0.731510513	0.357379996
iiEGI.Sep.2015.00044	0.526375171	1.211805767	0.473624829
iiEGI.Sep.2015.00045	0.513090729	1.194440238	0.48690927
iiEGI.Sep.2015.00046	0.54229424	1.148229657	0.457705761
iiEGI.Sep.2015.00047	0.497456688	1.277662446	0.502543312
iiEGI.Sep.2015.00048	0.622573928	0.672343571	0.377426072
iiEGI.Sep.2015.00049	0.532884773	0.803291621	0.467115227
iiEGI.Sep.2015.00050	0.547190795	0.770708701	0.452809206
iiEGI.Sep.2015.00051	0.504647227	0.918118685	0.495352774
iiEGI.Sep.2015.00052	0.681636534	0.494053855	0.318363466
iiEGI.Sep.2015.00053	0.728223564	0.394514247	0.271776438
iiEGI.Sep.2015.00054	0.680932736	0.448645625	0.319067265
iiEGI.Sep.2015.00055	0.661484126	0.539129457	0.338515874

Table G.1 Continued			
Sample_id	Sh (250°C+300°C)	Sm (150°C+200°C)	Sl (50°C+100°C)
iiEGI.Sep.2015.00056	0.525155392	0.856185418	0.474844608
iiEGI.Sep.2015.00057	0.70161516	0.434270205	0.298384838
iiEGI.Sep.2015.00058	0.710252542	0.423056399	0.289747459
iiEGI.Sep.2015.00059	0.711751609	0.41908828	0.288248391
iiEGI.Sep.2015.00060	0.695856948	0.443832604	0.304143051
iiEGI.Sep.2015.00061	0.655673738	0.608645627	0.344326263
iiEGI.Sep.2015.00062	0.67783691	0.523256982	0.32216309
iiiEGI.Sep.2015.00032	0.79801243	0.555338568	0.201987569
iiiEGI.Sep.2015.00033	0.769975595	0.455078887	0.230024405
iiiEGI.Sep.2015.00034	0.64465139	0.84346072	0.35534861
iiiEGI.Sep.2015.00035	0.711590245	0.645366212	0.288409756
iiiEGI.Sep.2015.00036	0.791006418	0.692080744	0.208993582
iiiEGI.Sep.2015.00037	0.728650496	0.612292506	0.271349503
iiiEGI.Sep.2015.00038	0.691253839	0.754806443	0.30874616
iiiEGI.Sep.2015.00039	0.766072846	0.53013108	0.233927153
iiiEGI.Sep.2015.00040	0.740690394	0.515295432	0.259309606
iiiEGI.Sep.2015.00041	0.820917928	0.33933807	0.179082072
iiiEGI.Sep.2015.00042	0.514769241	1.184265358	0.48523076
iiiEGI.Sep.2015.00043	0.514849786	1.2160815	0.485150215
iiiEGI.Sep.2015.00044	0.528607456	1.210617186	0.471392545
iiiEGI.Sep.2015.00045	0.517036982	1.184772617	0.482963019
iiiEGI.Sep.2015.00046	0.554985515	1.134050807	0.445014485
iiiEGI.Sep.2015.00047	0.498939639	1.282334195	0.501060361

Table G.1 Continued			
Sample_id	Sh (250°C+300°C)	Sm (150°C+200°C)	Sl (50°C+100°C)
iiiEGI.Sep.2015.00048	0.620318744	0.678630695	0.379681255
iiiEGI.Sep.2015.00049	0.521500009	0.824941072	0.478499991
iiiEGI.Sep.2015.00050	0.538136925	0.780380635	0.461863076
iiiEGI.Sep.2015.00051	0.498396199	0.903103472	0.501603802
iiiEGI.Sep.2015.00052	0.68237432	0.490931408	0.317625681
iiiEGI.Sep.2015.00053	0.689011449	0.475211625	0.310988552
iiiEGI.Sep.2015.00054	0.686670358	0.435526547	0.313329643
iiiEGI.Sep.2015.00055	0.68006208	0.453032929	0.319937921
iiiEGI.Sep.2015.00056	0.543609674	0.829232375	0.456390326
iiiEGI.Sep.2015.00057	0.693559493	0.462257238	0.306440507
iiiEGI.Sep.2015.00058	0.707525297	0.422662134	0.292474703
iiiEGI.Sep.2015.00059	0.703687261	0.426539774	0.29631274
iiiEGI.Sep.2015.00060	0.693992119	0.44627826	0.306007882
iiiEGI.Sep.2015.00061	0.652097443	0.535111623	0.347902557
iiiEGI.Sep.2015.00062	0.680800212	0.520437686	0.319199789
iiT-HB_2157	0.655673602	1.266532703	0.344326399
iiTORC_2303.3	0.62578505	1.301447577	0.374214949
iT-HB_2157	0.684362361	1.22933015	0.315637639
iTORC_2303.3	#VALUE!	1.243532973	0.31468769
T-HB_2157	0.662867702	1.257878755	0.337132298
TORC_2303.3	0.638683099	1.287615326	0.3613169

REFERENCES

Bordenave, M.L. ed. 1993. *Applied Petroleum Geochemistry*, Paris: Editions Technip.

Dake, L. P. (1978). *Fundamentals of Reservoir Engineering*. Amsterdam: Elsevier.

Espitalié J., Deroo G., Marquis F. 1985. La pyrolyse RockEval et ses applications. Partie 1. Revue de l'Institut français du pétrole 40 (5): 563–579. http://dx.doi.org/10.2516/ogst:1985035

Espitalié J., Deroo G., Marquis F. 1985. La pyrolyse RockEval et ses applications. Deuxième partie Revue de l'Institut français du pétrole 40 (6): 755-784. http://dx.doi.org/10.2516/ogst:1985045

Espitalié J., Deroo G., Marquis F. 1986. La pyrolyse RockEval et ses applications.Troisième partieRevue de l'Institut français du pétrole 41 (1): 73-89. http://dx.doi.org/10.2516/ogst:1986003

Espitalié J., Laporte J.L., Madec M., et al. 1977. Méthode rapide de caractérisation des roches mères, de leur potential pétrolier et de leur degré d'evolution. Revue de l'Institut français du pétrole 32 (1): 23–42. http://dx.doi.org/10.2516/ogst:1977002

Hawk Eye, Version 5402. 2015. Humble, Texas: Wildcat Technologies.

Haynes W. M. ed. 2014. *CRC Handbook of Chemistry and Physics*, 95 Edition, Boca Raton, FL:CRC Press/Taylor and Francis.

Jarvie, D. M., Baker, D. 1984. Application of the Rock Eval III Oil Show Analyzer to the Study of Gaseous Hydrocarbon in an Oklahoma Gas Well. Worldwide Geochemistry, http://www.wwgeochem.com/resources/ (accessed 7 January 2016).

James, G .S. 2006. *The Chemistry and Technology of Petroleum*, Fourth Edition. Laramie, WY: CRC Press.

Jones, P.J., Al-Shafei, E.N., Halpern, H.I. et al. 2004. Pyrolytic oil-productivity index method for predicting reservoir rock and oil characteristics. US Patent No. US 6823298 B1.

Jones, P.J., Mark H. Tobey, M.H. 1999. Pyrolytic oil-productivity index method for characterizing reservoir rock. US Patent No. US 5866814 A.

Jones, P.J., Halpern, H.I. 2008. Compositional modeling and pyrolysis data analysis methods. US Patent No. US 7363206 B2.

Jones, P.J., Halpern, H.I. 2009. Method for determining volume of organic matter in reservoir

rock. US Patent No.US 20100057409 A1.

Jones, P.J., Halpern, H.I. 2014. Method for reconstructing the total organic carbon content from compositional modeling analysis. US Patent No.US 20140114627 A1.

Lafargue, E., Marquis, F., Pillot, D. 1998 Rock-Eval 6 Applications in Hydrocarbon Exploration, Production, and Soil Contamination Studies. Revue de l'Institut français du pétrole 53 (4): 421-437.http://dx.doi.org/10.2516/ogst:1998036

Magoon, L.B., Dow, W.G. 1994. The Petroleum System—From Source to Trap: AAPG Memoir 60.

R Core Team (2015). R: A language and environment for statistical computing. R Foundation for Statistical Computing, Vienna, Austria. URL http://www.R-project.org/

Schlumberger. 2011. *Basic Petroleum Geochemistry for Source Rock Evaluation*, Schlumberger Massachusetts, USA.

Sparkman O.D., Penton Z., Kitson F. G. 2011. *Gas Chromatography and Mass Spectrometry*, 2nd Edition. Oxford, UK:Elsevier Inc.

TA Instruments. 2016. Q600-TGA. Our products Q600-TGA , http://www.tainstruments.com/product.aspx?siteid=11&id=22&n=3 (accessed date 27 january 2016)

Tissot, B., Demaison, G., Masson, P. et al. 1980. Paleoenvironment and petroleum potential of middle Cretaceous black shales in Atlantic basins: Am. Assoc. Petrol. Geol. Bull., 64 (11) :2051-2063 DOI:0149-1423/80/B012-0O01.

Tissot, B. P., Welte, D. H. (1978). *Petroleum Formation and Occurrence: A New Approach to Oil and Gas Exploration*. Berlin: Springer-Verlag